Metamagnetic Phase Transition and Anomalous Hysteresis in $FeCl_2 \cdot 2H_2O$

by Koichi KATSUMATA

Contents

Abstract

Magnetization in metamagnetic $FeCl_2 \cdot 2H_2O$ has been studied in detail under both a pulsed and a static magnetic fields at temperatures between 1.5K$\sim$14K. At high temperatures($T \sim 8K$ for the pulsed field and $T \sim 4K$ for the static field), a transition from the antiferromagnetic (A.F.) to the ferrimagnetic($M_s/3$) states at H_{c1} and that from the $M_s/3$ to the ferromagnetic(M_s) states at H_{c2} are observed. A large hysteresis at H_{c1} even under a slowly varying field, while at H_{c2}, little hysteresis have been observed. As the temperature is lowered($4.5K<T<7.5K$ for the pulsed field and $3.25K<T<3.86K$ for the static field), a transition from the A.F. to a $M_s/2$ states followed by that from the $M_s/2$ to the $M_s/3$ states accompanying with that from the $M_s/3$ to the M_s states takes place in an increasing field. The $M_s/2$ state which is a high energy state in this salt becomes stable with decreasing temperature. Below 2.24K, a large hysteresis at H_{c2} is observed even under a slowly varying field.

The anomalously large hysteresis and the appearance of a new metamagnetic phase($M_s/2$ state) in $FeCl_2 \cdot 2H_2O$ are explained by using a localized excitation model of Fe^{2+} spin(S=2). Main origin of the large hysteresis comes from the energetic barrier due to a strong single ion anisotropy energy in this salt which prevents a spin from reversing. The appearance of a new phase arises from the fact that a $M_s/2$ state is constructed by a simple reversal of down spins in the A.F. state, while the $M_s/3$ state by a complicated rearrangement of up and down spins in the A.F. state.

Effects of Co^{2+} impurity on the phase transition and the hysteresis are also discussed.

§1. Introduction

Phase transitions in antiferromagnetic substances under an external magnetic field have been studied by many researchers both theoretically and experimentally. In an antiferromagnet where the antiferromagnetic exchange energy is larger than the anisotropy energy, spin-flop transition[1,2] occurs when the external magnetic field applied along the easy axis comes to a critical value. On the other hand, when the anisotropy energy is comparable with or larger than the exchange energy, metamagnetic transition[3] i.e., a transition of the antiferromagnetic(A.F.) state to a state of high net moment and low differential susceptibility takes place instead of spin-flop transition. Often spin-flop and metamagnetic transitions are of first kinds at low temperatures in the sense that the magnetizations change discontinuously with respect to the magnetic field and are associated with hysteresises.

Hysteresis of spin-flop transition is in many cases small. For example, in $CuCl_2 \cdot 2H_2O$(T_N=4.33K, H_c=6.56kOe) Date and Nagata[4] have reported the figure to be 2.4Oe at T=1.4K in a static field (theoretical prediction by the same authors is 13Oe), and in MnF_2 (T_N=67.7K, H_c=92.4kOe) Jacobs[5] has not observed a hysteresis within the experimental error($\sim$1kOe) in a pulsed magnetic field. Recently, an attempt to explain small hysteresis in spin-flop transition is made by Keffer and Chow[6] by considering a surface spin-flop state which has originally been studied by Mills[7]; a surface spin

wave becomes soft at a lower field than the critical field of a bulk(H_c). The surface spin-flop(SSF) regions at first grow slowly with increasing field and as $H \to H_c$, the SSF regions catastrophically expand into three dimensions.

Some metamagnetic substances which show hysteresis have been reported. For example, Motokawa and Date[8] have observed a considerable amount of hysteresis in $CoCl_2 \cdot 2H_2O$(T_N=17.2K) which has two metamagnetic transitions from the A.F. to the $M_s/3$ states(M_s the magnetization at the ferromagnetic state) at H_{c1}=31.6kOe followed by that from the $M_s/3$ to the M_s states at H_{c2}=46.0kOe[9]. In a pulsed magnetic field with a duration time of ∿5msec, they have observed a hysteresis at H_{c1}: the transition occurs at 35kOe and at 28kOe in an increasing and a decreasing fields, respectively at T=4.2K. They have observed no hysteresis at H_{c2}. Jacobs and Lawrence[10] have reported in anhydrous $FeCl_2$(T_N=23.5K, H_c=10.6kOe[11]), a hysteresis of ∿3kOe at T=4.2K in a pulsed field with a sweep rate of dH/dt=2.5 $\times 10^7$Oe/sec. Ball, Wolf and Wyatt[12] have observed no hysteresis in a static field at the metamagnetic transition of dysprosium aluminum garnet(DAG)(T_N=2.53K, H_c=3.8kOe[13]). Rado[14], in his magneto-electric experiment in $DyPO_4$(T_N=3.40K, H_c=5.20kOe[15]) has pointed out that repeated cycling of the external magnetic field causes the hysteresis of the metamagnetic transition to become negligibly small.

We have observed anomalously large hysteresises at the metamagnetic transition points in $FeCl_2 \cdot 2H_2O$ and also observed an appear-

ance of a new metamagnetic phase. To report the detailed experimental results and the analysis of the hysteretic behavior is the purpose of this paper. $FeCl_2 \cdot 2H_2O$(T_N=23K[16]), H_{c1}=36.2kOe, H_{c2}=46.7kOe) has two metamagnetic transitions as in $CoCl_2 \cdot 2H_2O$. In an increasing pulsed field($dH/dt \sim 4 \times 10^7$Oe/sec) two metamagnetic transitions occur at 40kOe and 47kOe at T=4.2K. Hysteresis at the lower critical field becomes large with decreasing temperature and at T=1.4K, the transition occurs at 57kOe. Under a very slowly varying field(dH/dt=60 Oe/sec) we have also observed considerable amounts of hysteresises at H_{c1} and H_{c2} at low temperatures. More interesting is an observation of a new metamagnetic phase: when the hysteresis at H_{c1} becomes large and a critical field denoted by H_c' is met in an increasing field, a transition from the A.F. to a $M_s/2$ states takes place. The $M_s/2$ state is not the lowest energy state in $FeCl_2 \cdot 2H_2O$ in the whole region of the external field. This is the first observation of a metamagnetic phase change which includes a transition to a high energy state.

The crystal of $FeCl_2 \cdot 2H_2O$ consists of $-FeCl_2-$ linear chains running along the c-axis which are linked together by weak hydrogen bonds. The exchange interaction J_0 between Fe^{2+} spins within the same chain is ferromagnetic and much stronger than the antiferromagnetic interactions between chains as in $CoCl_2 \cdot 2H_2O$. The magnetization in $FeCl_2 \cdot 2H_2O$ was first studied by Narath[16] in a static field and showed two sharp transitions at H_{c1}=39±1kOe and H_{c2}=46±1kOe at T=4.0K(there is no mention of hysteresis). The corresponding

magnetic moments are $M_1=1.4\pm0.1\mu_B/Fe^{2+}$ and $M_2=4.25\pm0.05\mu_B/Fe^{2+}$, respectively. The study of far-infrared excitations in this salt has been reported by Hay and Torrance[17]. They have observed spin-wave excitations in the A.F., Ferri. and F. states and the obtained parameters are, g-value along the easy axis $g_{//}=2.23\pm0.02$, spin quantum number S=2 and the single ion anisotropy($-DS_z^2$ type) constant D=9.58 $\pm0.05cm^{-1}$. A coexistence of the antiferromagnetic and the ferrimagnetic resonance lines near H_{c1} has also been reported by the same authors and the hysteresis of the magnetization at H_{c1} has been inferred from the relative intensity of the A.F. and the Ferri. absorption lines.

Tinkham[18] has discussed the dynamics of the metamagnetic transitions in $CoCl_2\cdot2H_2O$ from a microscopic point of view. In $CoCl_2\cdot2H_2O$, Co^{2+} spin is well approximated by an Ising spin with S=1/2[19] at low temperatures and in such the Ising spin system, elementary excitation becomes localized and is described in terms of the spin-cluster excitation[20,21] instead of a conventional spin wave excitation. By using the spin-cluster model, Tinkham has shown that the nucleation rate for the transition at H_{c2} is far faster than that at H_{c1} and explained the presence and the absence of hysteresises at H_{c1} and H_{c2}, respectively. In the model proposed by Tinkham, the effect of surfaces and the internal defects on the nucleation is also important(especially at low temperatures) as in the case of spin-flop transition. At the surfaces, the exchange bond is half of that in a bulk, so that the activation energy(energy necessary to reverse

a spin) is half of that in the interior sites. At low temperatures, the nucleation at surfaces becomes dominant although the number of spins at surfaces is much smaller than that in the bulk. In the case of $FeCl_2 \cdot 2H_2O$, as is mentioned previously, S=2 and the five-fold degeneracy is split by the $-DS_z^2$ term into two doubly degenerate states ($S_z=\pm 1, \pm 2$) and a singlet($S_z=0$). The energy difference between the ground state($S_z=\pm 2$) and the next higher state($S_z=\pm 1$) is $3D \sim 29 cm^{-1}$ which is large compared with $kT_N \sim 16 cm^{-1}$. So, at low temperatures, Fe^{2+} spin in $FeCl_2 \cdot 2H_2O$ behaves as a near Ising spin($S_z=\pm 2$). In this case, elementary excitations become nearly localized as in the case of $CoCl_2 \cdot 2H_2O$. Then, a question arises why n-fold spin cluster excitations(or multiple-magnon bound states) which have been observed in $CoCl_2 \cdot 2H_2O$[21] are not seen in $FeCl_2 \cdot 2H_2O$[17]. This is due to the fact that the matrix element which couples the magnon-bound states with the ground state depends on the transverse anisotropy in the exchange interaction which is very small in the case of $FeCl_2 \cdot 2H_2O$[17,21] We use in the following the localized excitation model to describe the dynamics of the metamagnetic transition in $FeCl_2 \cdot 2H_2O$. Although Fe^{2+} spin is approximated by a near Ising spin, a spin at $S_z=-2$ state for example, does not make a direct transition to $S_z=+2$ state when a spin reversal occurs at a critical field. Instead, a transition of $S_z=-2 \rightarrow S_z=-1 \rightarrow S_z=0 \rightarrow S_z=+1 \rightarrow S_z=+2$ takes place. This is contrasted with the case of $CoCl_2 \cdot 2H_2O$ where an $S_z=-1/2 \rightarrow S_z=+1/2$ transition is enough to reverse a spin. In this model, spin reversals in $CoCl_2 \cdot 2H_2O$ occur far faster than

those in $FeCl_2 \cdot 2H_2O$. Consequently, much larger hysteresis is expected in $FeCl_2 \cdot 2H_2O$ than in $CoCl_2 \cdot 2H_2O$. In the case of $FeCl_2 \cdot 2H_2O$, the energetic barrier which prevents a spin from reversing is mainly determined by the D term(of course the exchange term is not negligible) and the D-value at the surfaces is not half of that in the interior sites, rather may be larger. So that the nucleation at surfaces may be less significant in the case of $FeCl_2 \cdot 2H_2O$ than in $CoCl_2 \cdot 2H_2O$. It is worthwhile here to consider the case of anhydrous $FeCl_2$. The energy level scheme of Fe^{2+} in $FeCl_2$ at low temperatures is described by a fictitious spin with S=1 and a single ion anisotropy ($-DS_z^2$ type with $D=8.8cm^{-1}$)[22]. In this case, Fe^{2+} spin is not approximated by an Ising spin in a temperature range of interest. However, if we assume a localized excitation in $FeCl_2$, spin reversal will occur in $FeCl_2$ more easily than in $FeCl_2 \cdot 2H_2O$ but less easily than in $CoCl_2 \cdot 2H_2O$. Experimental results seem to confirm the assumption.

In §2, the crystallographic and magnetic properties of $FeCl_2 \cdot 2H_2O$ are described. The experimental procedures are presented in §3. The experimental results are described in §4. In §5, origin of the large hysteresis and mechanism of metamagnetic phase transition in $FeCl_2 \cdot 2H_2O$ are discussed. Effect of Co^{2+} impurity on the metamagnetic transition in $FeCl_2 \cdot 2H_2O$ is discussed in §6.

§2. Crystallographic and Magnetic Properties of $FeCl_2 \cdot 2H_2O$

The crystal structure of $FeCl_2 \cdot 2H_2O$ has been determined by Morosin and Graeber[23] using X-ray diffraction techniques. The crystal structure is monoclinic(space group C2/m) and contains two formula units. However, these are related by the lattice centering operation and thus equivalent.. The lattice parameters are, a_0=7.355A, b_0=8.548A, c_0=3.637A and β=98.18°. The crystal consists of $-FeCl_2-$ linear chains running along the c-axis which are linked together by weak hydrogen bonds as is shown in Fig.1.

From the susceptibility measurements[16], $FeCl_2 \cdot 2H_2O$ is antiferromagnetic below 23K with the sublattice magnetizations directed along the α-axis shown in Fig.2. The susceptibility data are analyzed[16] by using a Curie-Weiss relation with S=2, g_α =2.4, g_β =g_γ=1.9, θ_α=+12K and θ_β=θ_γ=+5K where θ's are the Weiss constants. $FeCl_2 \cdot 2H_2O$ has two metamagnetic transitions at H_{c1}=36.2kOe and H_{c2} =46.7kOe at low temperatures. The transition at H_{c1} is from the A.F. to the ferrimagnetic array with a net moment which is one-third of that in the ferromagnetic state above H_{c2}. The spin structure in the A.F. state has been determined by Narath[16] from the proton NMR which is shown in Fig.3(a). We assume the spin structure in the intermediate state($M_s/3$) to be the same as that of isomorphic $CoCl_2 \cdot 2H_2O$(Fig.3(b)). As magnetic moments lie in the ac-plane and directed parallel or antiparallel to the α-axis, Fig.3 shows the projection of the moments on the ab-plane.

§3. Experimental Procedures

(3-1) Preparation of the Specimen

Single crystals of $FeCl_2 \cdot 2H_2O$ used in the experiment were grown by slowly evaporating saturated aqueous solution of reagent grade $FeCl_2 \cdot nH_2O$ in a thermostated water bath. The temperature of the bath was kept constant within ±0.5°C. Good single crystals up to 1×1×5cm in size were obtained at temperatures between 75~85°C. Cares are taken to avoid the oxidation of Fe^{2+} to Fe^{3+} by atmospheric oxygen.

(3-2) Magnetization Measurement

The magnetization in $FeCl_2 \cdot 2H_2O$ was measured in a pulsed field by using the same technique described by Motokawa and Date[24]. In the pulsed experiment, we observe the derivative of a magnetization with respect to the external magnetic field, dM/dH. The field sweep rate is about 4×10^7Oe/sec in the vicinity of 40kOe.

The technique of magnetization measurement in a static field used in the experiment has been developed by the present author and is described below. A static high field is produced in an 90kOe superconducting solenoid wound with Nb_3Sn superconductive ribbon. The solenoid has a winding length of 150mm and a bore size of 18mm. The field deviation along the coil axis is less than 1% at the distance of 20mm from the center as is seen from Fig.4.

Magnetic fields are monitored by using a copper magneto-resistor as was done by Scott, Springford and Stockton[25]; a constant current with a stability of 10^{-5}/day is supplied to the magneto-resistor and the voltage across the resistor is measured by a digital voltmeter. The accuracy of the field measurement is better than 0.5%. The voltage vs. field relation was determined by using a search coil and independently by ESR of DPPH at millimeter wavelengths. When a measurement was made again after a year, no change of the calibrated curve was detected. A schematic diagram of the magnetization measurement system is shown in Fig.5. A sample is driven mechanically between two series-opposing coils as were done by Strnat and Bartimay[26] and by Foner and McNiff[27]. The A.C. signal from the pickup coils with a frequency of 5Hz is amplified and converted to a D.C. signal proportional to the magnetization of a sample. By sweeping the external field, we can display an M-H curve directly on a recorder as is exemplified in Fig.6 by this system. The absolute accuracy of the magnitude of the observed magnetization depends mainly on the accuracy of the A.C. to D.C. converter and estimated within 5%. Dependence of the recorder output signal on sample weight has been measured by using single crystals of $FeCl_2 \cdot 2H_2O$ in the ferromagnetic state. The result shows a linear dependence of the output on sample weight as is seen in Fig.7.

Below 4.2K, specimens were always immersed in the liquid helium bath, and above 4.2K, a temperature control system similar to that described by Okuda and Date[28] was used.

§4. Experimental Results

(4-1) Pulsed Field Experiment[29)]

In the pulsed field experiment, as was described in §3, we observe dM/dH. In the case of $FeCl_2 \cdot 2H_2O$, we have observed sharp peaks corresponding to the step wise changes of M as H. Typical examples of the photographs of memoriscope traces of dM/dH signals obtained in an increasing field are shown in Fig.8. In the photographs, the spikes correspond to the dM/dH signals and the smooth curves represent the variations of the magnetic field as time. The magnetic fields corresponding to the peak positions of the dM/dH signals are plotted in Figs.9 and 10 as functions of temperature in the increasing field case. When we measure the areas of dM/dH signals, we can estimate the magnitudes of the magnetization changes at the critical fields. At T=8.0K the ratio of the estimated magnetization changes at the lower critical field to that at the higher critical field is about 1.0:1.9 indicating that a transition from the A.F. to the $M_s/3$ states followed by a transition from the $M_s/3$ to the M_s(F.) states takes place. With decreasing temperature, a curious behaviour has been observed as is seen in Fig.8(b); between the lower and the upper critical fields, there exists a transition field associated with a decrease in magnetization. Between T=4.5K and 7.5K, three peaks overlap and an estimation of the magnitude of the magnetization changes is difficult. However, roughly speaking, the ratio is 1.0:(-)0.2:1.5

from the lower to the higher critical fields. At T=4.2K the ratio is about 1.0:1.0 indicating the occurrence of a transition from the A.F. to a $M_s/2$ states followed by that from the $M_s/2$ to the F. states. A small magnetization change is observed in the intermediate region (Fig.8(c)). Which is also observed in a static field and is discussed later. On cooling the specimen below 4.2K, the magnetization change at 40kOe becomes small rapidly as is shown in Fig.11 and the delay at the transition field becomes pronounced with decreasing temperature(Fig.9). Below 2.5K, a transition from the A.F. to the F. states is observed. Under a decreasing field, the dM/dH signal shows a complicated behaviour which depends on field sweep rate and on temperature. In Fig.12, examples of the photographs of memoriscope traces of dM/dH signals obtained in a duration of a pulsed field are shown. The critical fields are plotted in Figs.13, 14 and 15 versus maximum fields produced in the pulsed field coil at representative temperatures.

We have examined temperature dependences of H_c's in three single crystals which were grown under different conditions to check whether Fe^{3+} impurity ion affects the $H_c(T)$ or not; sample 1 was grown from aqueous solution of $FeCl_2 \cdot nH_2O$ only, sample 2 from $FeCl_2 \cdot nH_2O$ aqueous solution containing $\sim$2% of aqueous HCl and iron blocks(in this solution, $2Fe^{3+}+Fe \rightarrow 3Fe^{2+}$) and sample 3 from $FeCl_2 \cdot nH_2O$ aqueous solution with small amount of $SnCl_2 \cdot 2H_2O$ which is a strong deoxidizer. No appreciable change of $H_c(T)$ was observed in the three specimens as is shown in Fig.16.

(4-2) Static Field Experiment

Examples of recorder traces of M-H curve obtained in a slowly increasing field(dH/dt=60 Oe/sec) are shown in Fig.17 at various temperatures, and those of decreasing field case in Fig.18. At T=4.22K, a transition from the A.F. to the $M_s/3$ states followed by that from the $M_s/3$ to the F. states takes place. No appreciable hysteresis is observed at the upper critical field, while a considerable amount of hysteresis is observed at the lower critical field. With decreasing temperature, a curious transition is observed in an increasing field; the A.F. state flips to an intermediate state whose magnetization is larger than $M_s/3$. Then the intermediate state decays to the $M_s/3$ state. Below 3.00K, a transition from the A.F. to a $M_s/2$ states followed by a transition of the $M_s/2$ to the F. states is seen in an increasing field. Delays at these transition points become pronounced below 2.24K. The value of the transition point of the $M_s/3$ to the A.F. states under a decreasing field becomes small with decreasing temperature. In a decreasing field, no abrupt change of magnetization is observed below 2.00K.

Dependence of the transition from the A.F. to the $M_s/3$ states on a process of field sweep was investigated at T=4.22K and the results are shown in Figs. 19 and 20. When the external field is increased in a virgin state of antiferromagnetic $FeCl_2 \cdot 2H_2O$(1st run), the value of the critical field is lower than that of a 2nd run and a small change in magnetization is observed at 39.5kOe. Once the ferro-

magnetic state is experienced, the value is not influenced by field sweep rates. The hysteresis at the lower critical field is smaller in the case when the external field is decreased from the ferromagnetic state than decreased from the $M_s/3$ state(Fig.20). At 3.00K(Fig.21), the value of the lower critical field was not varied in a 1st and a 2nd runs, while the magnitude of the magnetization in the intermediate state is smaller in the 1st run than in the 2nd run and a pronounced dip was observed at H=43kOe in the 1st run. Fig.22 shows how the magnetization changes when the external field is decreased in the intermediate state. At 2.00K, the $M_s/2$ state makes a transition to the A.F. state at 38.1kOe(at 41.5kOe in an increasing case). The transition at 3.00K is more complicated. The initial value of the magnetization in the intermediate state is shown by the line in the right side of Fig.22. The magnetization decreased in a fixed external field to the value shown by a dotted arrow in the figure in about ten minutes. When the external field is decreased in that state, a transition occurs at 39.5kOe which is the same value as that of the transition from the A.F. to the $M_s/2$ states in an increasing field at 3.00K. This phenomenon can be explained if we assume that the intermediate state at 3.00K is a mixing of the $M_s/2$ and the $M_s/3$ states and that the decay time of the $M_s/2$ to the A.F. states is faster than that of the $M_s/3$ to the A.F. states. It is noted that at 2.00K, the intermediate state shown in Fig.22 is a pure $M_s/2$ state. Fig.23 shows a detail of the M-H curve at 2.24K obtained in a decreasing field.

The intermediate state has a magnetization larger than $M_s/3$ and small magnetization changes are seen at about 43kOe and 40kOe.

Temperature dependences of the critical fields and of the magnitudes of the magnetizations at the intermediate and the ferromagnetic states are shown in Figs.24 and 25, respectively. Some of the outstanding features of the experimental results shown in Figs.24 and 25 are: (1)temperature dependent critical fields and (2)appearance of a new intermediate phase($M_s/2$ state). As we have observed the $M_s/3$ state in the intermediate region at T=4.22K, the appearance of the $M_s/2$ state at low temperatures may come from a variation of exchange interactions with temperature. To eliminate this possibility, we have investigated temperature dependence of the magnetization in the $M_s/3$ state under a fixed external field(the $M_s/3$ state was realized at 4.22K). The result is shown in Fig.25(H=43.1kOe) and exhibits no change of magnetization between 4.22K and 1.48K when the external field is fixed. So, we can conclude that the $M_s/3$ state is the lowest energy state in the intermediate region of $FeCl_2 \cdot 2H_2O$. The appearance of the $M_s/2$ state can be explained if we assume that the transition from the A.F. to the $M_s/2$ states takes place more easily than that of the A.F. to the $M_s/3$ states, i.e., the rise time of the A.F. to the $M_s/2$ states is shorter than that of the A.F. to the $M_s/3$ states when the external field is increased. As the $M_s/2$ state is a high energy state, it goes to the $M_s/3$ state as is observed experimentally(Figs.17 and 25).

However, if the decay time of the $M_s/2$ to the $M_s/3$ states becomes long with decreasing temperature, the $M_s/2$ state will remain unchanged. Which is observed experimentally as is shown in Figs.17 and 25. The presence of the delays at the transitions from the A.F. to the $M_s/2$ states and from the $M_s/2$ to the F. states at low temperatures can also be explained if we assume the rise times become long with decreasing temperature compared with the field sweep rate.

To assure the above assumptions, we have investigated time dependences of magnetizations under fixed temperature and external field. Typical examples of time dependences of magnetizations are shown in Fig.26. Magnetization decays(or rises) as exponentially, and from a best fit curve to the experimental points, the decay(or rise) time is obtained at the given temperature and external field. The rise time of the A.F. to the $M_s/3$ states and the decay time of the $M_s/2$ to the $M_s/3$ states is long compared with the rise time of the A.F. to the $M_s/2$ states as is exemplified in Fig.26. Temperature dependences of the rise time of the A.F. to the $M_s/2$ states at H=39.6kOe and of the decay time of the $M_s/2$ to the $M_s/3$ states at H=44.3kOe are shown in Fig.27. From Fig.27, we see that the decay or rise time τ varies with temperature as $\tau \propto \exp(E/kT)$. The value of the activation energy(E) at the transition from the A.F. to the $M_s/2$ states at H=39.6kOe is determined to be $E=(4.0\pm0.4)\times10^{-15}$erg (or $20\pm2 cm^{-1}$).

Dependence of τ on the external field was investigated and the results are shown in Fig.28. In the case of the transition from

the A.F. to the $M_s/2$ states, τ depends strongly on H, whereas the dependence is weak in the transition from the $M_s/2$ to the $M_s/3$ states. It is shown above that τ depends both on temperature and external field. Then we can obtain the dependence of τ on H from the observed M-H curve at a given temperature. Experimental evidence tells us that under a fixed field which is equal to or larger than a critical field, magnetization increases with time approximately as,

$$M(t)=M_1 - (M_1-M_0)\exp[-t/\tau(H,T)], \qquad (1)$$

where M_0 and M_1 are the magnetizations at t=0 and t=∞, respectively. When the external field is swept in a slow speed, the magnetization changes as eq.(1) where τ depends on H(t). Then M-H curve in a slowly increasing field is expressed as,

$$M(H(t))=M_1 - (M_1-M_0)\exp[-t/\tau\{H(t),T\}]. \qquad (2)$$

From eq.(2) together with the observed M-H curve, we can obtain $\tau(H,T)$ and these are plotted in Figs.29 and 30. In Fig.29, we have also plotted the data obtained under a fixed external field and those obtained in a pulsed field(in the case of the pulsed field experiment, the delay time is plotted). The field independent parts in Fig.30 come from an ambiguity in determining the M(H(t)) from the observed broad M-H curve at low temperatures. In the case of a decreasing field, we can obtain also $\tau(H,T)$ in a similar

manner. We assume that magnetization decays with time in a fixed field as,

$$M(t)=M_1+(M_0-M_1)\exp[-t/\tau(H,T)], \tag{3}$$

where M_0 and M_1 are the same as those in eq.(1). This assumption is verified in the transition from the $M_s/2$ to the $M_s/3$ states where magnetization decreases with time as eq.(3). Similarly to the preceding argument, we obtain the relation between M(H(t)) and H(t) as,

$$M(H(t))=M_1+(M_0-M_1)\exp[-t/\tau\{H(t),T\}]. \tag{4}$$

From eq.(4) with the experiment, we obtain $\tau(H,T)$ which is shown in Fig.31 in the case of the transition from the $M_s/3$ to the A.F. states.

Finally, let us compare the data obtained in the pulsed experiment with those in the static experiment. As was described previously, the transition from the A.F. to the $M_s/3$ states followed by that from the $M_s/3$ to the F. states takes place in the pulsed field at 8.0K and this corresponds to the case of the static experiment at 4.22K. Between 3.86K and 3.25K we have observed a transition associated with a decrease in magnetization in a slowly increasing field(the transition from the $M_s/2$ to the $M_s/3$ states), and this corresponds to the case of the pulsed experiment at $4.5K<T<7.5K$. In this case, the ratio of the magnetization changes from the lower

to the higher critical fields must be 1.00:(-)0.33:1.33 and the observed ratio in the pulsed field is near to this value.
The transition from the A.F. to the $M_s/2$ states followed by that from the $M_s/2$ to the F. states observed below 3.00K in the static experiment is observed in the vicinity of 4.2K in the pulsed experiment. In a pulsed field, we have always observed the same transition as in a static field at a higher temperature than in a static case. This arises from the difference in the field sweep rate.
At low temperatures, delays are observed at both the transition from the A.F. to the $M_s/2$ states and that from the $M_s/2$ to the F. states in a static field, while the delay at the upper critical field is missing in a pulsed experiment(at $2.5K<T<3.5K$ in Fig.9).
The absence of the delay at the upper critical field may come from the local heating due to the irreversible release of energy at the (delayed) lower critical field.

§5. Origin of the Large Hysteresis and Mechanism of Metamagnetic Phase Transition in $FeCl_2 \cdot 2H_2O$

In the preceding section, we have obtained experimentally the knowledge of how metamagnetic phase transformations in $FeCl_2 \cdot 2H_2O$ take place. Before discussing the mechanism of the phase changes, we define the critical fields and obtain the values from the experiment. As the present experiment is performed at temperatures well below the Néel point, we can use magnetic energies at T=0K in calculating the critical fields. We express the Hamiltonian in the A.F. state as,

$$H=-2J_0 \sum_{i,i'} S_{iz}S_{i'z} -2J_0 \sum_{j,j'} S_{jz}S_{j'z} -2J_1 \sum_{i,j} S_{iz}S_{jz} -2J_2 \sum_{i,i'} S_{iz}S_{i'z}$$

$$-2J_2 \sum_{j,j'} S_{jz}S_{j'z} -D\left(\sum_i S_{iz}^2 + \sum_j S_{jz}^2 \right) - g_{//}\mu_B H\left(\sum_i S_{iz} + \sum_j S_{jz} \right), \quad (5)$$

where, J_0 is the intrachain exchange interaction, J_1 and J_2 are the interchain exchange interactions given in Fig.3, D is the single ion anisotropy constant, H the external field applied along the easy axis(z), $g_{//}$ the g-value along the easy axis and i and j stand for the up and the down sublattices, respectively. In the calculation of the energies, the J_0 and the D terms are common to all metamagnetic phases, so that they are discarded. The small J_3 interaction along the b-axis is neglected. The calculated energies are plotted in Fig.32 as functions of the external field(the spin structure in the $M_s/2$ state is discussed later). We define as usual, H_{c1}

where the free energies in the A.F. and the $M_s/3$ states become equal and H_{c2} where $E(M_s/3)=E(M_s)$. Other two critical fields, $H_c'(E(A.F.)=E(M_s/2))$ and $H_c''(E(A.F.)=E(M_s))$ are also defined. The H_c's are represented as,

$$H_{c1}=(8|J_1|-8|J_2|)S/g_{//}\mu_B,$$

$$H_c'=(8|J_1|-4|J_2|)S/g_{//}\mu_B,$$

$$H_c''=(8|J_1|)S/g_{//}\mu_B \quad \text{and} \tag{6}$$

$$H_{c2}=(8|J_1|+4|J_2|)S/g_{//}\mu_B.$$

From Figs.24 and 25, we have

$$H_c'=39.7\pm0.5\text{kOe} \quad \text{and} \tag{7}$$

$$H_{c2}=46.7\pm0.5\text{kOe}.$$

Eq.(6) with eq.(7) gives

$$H_{c1}(\text{theor.})=(3H_c'-H_{c2})/2=36.2\text{kOe} \quad \text{and} \tag{8}$$

$$H_c''(\text{theor.})=(H_{c2}+H_c')/2=43.2\text{kOe}.$$

These are given in Fig.24. The value of H_{c2} agrees with that obtained by Narath[16], while the agreement is poor in the case of H_{c1} because Narath's value probably contains hysteretic effect. The values of H_{c1} and H_{c2} obtained by Hay and Tarrance[17] from the far-infrared experiment are a little($\sim$1kOe) smaller than the present values in both cases.

Now let us discuss origin of the anomalously large hysteresis at the metamagnetic transition in $FeCl_2 \cdot 2H_2O$ and microscopic mechanism of the phase change. First, we discuss maximum values of hysteresises in the transition points. Kanamori, Motizuki and Yosida[30] have discussed phase transitions in an antiferromagnet under an external field in the molecular field approximation. Later, Gorter and Van Peski-Tinbergen[31] have studied the problem in a similar way and shown that an antiferromagnetic state exists as a metastable state above a critical field above which it is thermodynamically unstable. We calculate in the following the threshold field below which the A.F. state is either stable or metastable. Also the threshold field for the $M_s/3$ state is calculated. Considering only the $S_z=\pm 2$ levels, the relations between the magnetization and the external field in the A.F. state are obtained to be;[30]

$$m^2=1-2x\cdot\coth(2x/t)+x^2 \quad , \qquad \text{and} \qquad (9)$$

$$h=(1-2\lambda)m+(t/2)\cdot\tanh^{-1}\{2m/(1+m^2-x^2)\}, \qquad (10)$$

where $m \equiv -(\langle S_i \rangle + \langle S_j \rangle)/2S$ is a reduced magnetization per ion, $x \equiv (\langle S_j \rangle - \langle S_i \rangle)/2S$, $\lambda \equiv (4J_0 - 4|J_2|)/(4J_0 + 8|J_1| - 4|J_2|)$, $t \equiv kT/S^2(4J_0 + 8|J_1| - 4|J_2|)$, $h \equiv g_{//}\mu_B HS/S^2(4J_0 + 8|J_1| - 4|J_2|)$, and $\langle S \rangle$ the thermal average of a spin, respectively. The m-h curve at a given temperature is obtained from eqs.(9) and (10) by eliminating the parameter x. To make a numerical calculation, we must know the values of J_0, J_1 and J_2. From eqs.(6) and (7),

$$|J_1| = 0.281 \text{cm}^{-1} \quad \text{and} \quad |J_2| = 0.046 \text{cm}^{-1}. \tag{11}$$

Taking into account the contributions of the higher levels($S_z = \pm 1, 0$) the expression for the T_N in the molecular field approximation is given by,

$$1 + 2\exp(4D/kT_N) + 2\exp(D/kT_N) = [\{8(4J_0 + 4J_2) - 64J_1\}/kT_N]\exp(4D/kT_N) + [\{2(4J_0 + 4J_2) - 16J_1\}/kT_N]\exp(D/kT_N). \tag{12}$$

The value of D is given by Hay and Torrance[17] to be,

$$D = 9.58 \text{cm}^{-1} \tag{13}$$

From eqs.(12) and (13) with $T_N = 23$K, we have

$$J_0=+0.648\text{cm}^{-1}. \tag{14}$$

Examples of m-h curves obtained from eqs.(9) and (10) are shown in Figs.33 and 34(denoted by A.F.). In the $M_s/3$ state, the following expressions are obtained;

$$m=x/3\pm\{x^2-2x\cdot\coth(2\zeta x/t)+1\}^{1/2} \quad \text{and} \tag{15}$$

$$h=\zeta x/3+(1-2\lambda)m+(t/2)\cdot\tanh^{-1}\{(-6x+18m)/(9m^2-8x^2-6mx+9)\}, \tag{16}$$

where $\zeta\equiv(4J_0+4|J_1|+2|J_2|)/(4J_0+8|J_1|-4|J_2|)$. Examples of m-h curves obtained from eqs.(15) and (16) are shown in Figs.33 and 34 (denoted by $M_s/3$). In the ferromagnetic state[30], we have

$$h=t\cdot\tanh^{-1}(m)+(1-2\lambda)m. \tag{17}$$

The threshold fields above which the A.F. and the $M_s/3$ states become unstable are determined from the inflexion points in the m-h curves and these give maximum values of delays at the transition points in an increasing field. These are plotted in Fig.35 as functions of temperature together with the experimental data obtained in an increasing pulsed field. Similar calculations were performed in the case of $CoCl_2\cdot 2H_2O$ and the result is shown in Fig.36. Comparing Fig.35 with Fig.36, we see that the observed hysteresis

in $FeCl_2 \cdot 2H_2O$ is much closer to the predicted maximum value than in the case of $CoCl_2 \cdot 2H_2O$.

Next, microscopic details of the metamagnetic transition in $FeCl_2 \cdot 2H_2O$ is discussed. At low temperatures, the Fe^{2+} spin state in $FeCl_2 \cdot 2H_2O$ is described by S=2 and a single ion anisotropy term($-DS_z^2$). In addition, the exchange fields(in the molecular field approximation) split the energy levels. The energy level scheme in the A.F. state is shown in Fig.37. As is seen in Fig.37, a spin in the down sublattice is confined almost to the $S_z=\pm 2$ levels at low temperatures in an external field and is thus approximated by a near Ising spin. In this case, we can use a nearly localized excitation model. For a spin in the up sublattice, the situation is not so simple;in this case the contribution of the $S_z=+1$ level must be considered in addition to the $S_z=\pm 2$ levels and a near Ising approximation fails. However, as the contribution of the $S_z=+1$ level is small at low temperatures, we can use a nearly localized excitation model. In the following, the nearly localized excitation model is used to describe the dynamics of the metamagnetic transition in $FeCl_2 \cdot 2H_2O$. Before discussing details of the transition, let us consider a simple case where the external field just cancels the interchain exchange fields acting on a ferromagnetic chain and the chain acts like an isolated chain. We discuss the flopping process of the isolated chain. As is pointed out by Tinkham[18], in the case of $CoCl_2 \cdot 2H_2O$, once a chain has a single spin flipped up by thermal activation to $E_0(=2J_0 \sim 24 cm^{-1})$, it is energetically down hill

for the rest of the chain to flip, domino style. The transition probability of the spin flipping is estimated to be[18],

$$w \sim 10^{7} \exp(-E_0/kT) \ \mathrm{sec}^{-1}. \tag{18}$$

For a reasonably sized crystal a few millimeters on a side, the number of spins in a chain is $\sim 10^{7}$. Then the time required for the reversal of one chain is $\sim 10^{7} \times 10^{-7} = 1$sec(for adjacent spins to a flipped spin the activation energy is zero). In the case of $FeCl_2 \cdot 2H_2O$, every spin experiences an activation energy coming from the D term. Taking the energy difference between the $S_z=-2$ and the $S_z=-1$ states(=3D) as the activation energy, the time required for the reversal of one chain is,

$$\sim 10^{7} \times 10^{-7} \exp(3D/kT) = \exp(3D/kT), \tag{19}$$

which is about 10^{4}sec at T=4.2K and is about 10^{12}sec at T=1.5K. The essential point which explains the large hysteresis in $FeCl_2 \cdot 2H_2O$ is the presence of the large single ion anisotropy and the large value of spin quantum number(S=2). It is pointed out that no hysteresis has been observed at H_{c2} in $CoCl_2 \cdot 2H_2O$ in a pulsed field[8], so the time required to reverse one chain must be smaller than $10^{-3} \sim 10^{-4}$sec. Then, the preexponential factor in eq.(18) may be larger than 10^{7} and/or there may exist a mechanism which facilitates the flopping of the chain. In any case, the time required to reverse

an isolated chain in $FeCl_2 \cdot 2H_2O$ is about exp(3D/kT) times longer than that in $CoCl_2 \cdot 2H_2O$. We proceed the discussion to the actual cases. In the transition of the A.F. to the $M_s/3$ states, 2/3 of the down chains and 1/3 of the up chains must be reversed(see Fig.3), and the external field does not cancel the interchain exchange fields at H_{c1}. Then a very long time is required in the transition. Consequently, a large hysteresis is expected at H_{c1} as is observed experimentally. The limiting field for the hysteresis at H_{c1} in the increasing case at $T \gtrsim 1K$ was calculated by Tinkham[18] to be,

$$H_{c1}+(H_{c2}-H_{c1})/2 \qquad (20)$$

Which is 38.8kOe in $CoCl_2 \cdot 2H_2O$ and is 41.5kOe in $FeCl_2 \cdot 2H_2O$. In the case or $FeCl_2 \cdot 2H_2O$ the limiting field is observed to be 39.7kOe($=H_c'$). Let us consider what happens when the hysteresis at H_{c1} becomes large until H_c'. The effective field coming from the interchain exchange interactions acting on a down spin in the A.F. state is described as, $H-H_c'$, which is zero at H_c'. So, at $H=H_c'$, the down spin chain acts like an isolated chain which is discussed previously. We can construct spin structures whose magnetization is $M_s/2$ by a simple reversal of down chains in the A.F. state. Examples of these spin structures are given in Fig.38. Kanamori[32] has discussed magnetization process in an Ising spin system. He has proposed a method to determine rigorously the lowest energy state under an external field at T=0K when exchange interactions

and symmetry of a lattice are known. Spin structure whose magnetization is $M_s/2$ is shown[32] not to be determined uniquely. In the case of $FeCl_2 \cdot 2H_2O$, the $M_s/2$ state is not a lowest energy state in the whole region of the external field, so that the spin structure is of course not determined uniquely. The spin structure(B) in Fig.38 is that proposed by Oguchi and Takano[33]. As the $M_s/2$ states are constructed by a simple reversal of down chains in the A.F. state and the down chains act like isolated chains at $H=H_c'$, the transition time of the A.F. to the $M_s/2$ states is much shorter than that for the A.F. to the $M_s/3$ states. Thus, when the hysteresis at H_{c1} becomes large with decreasing temperature, the transition from the A.F. to the $M_s/2$ states takes place at H_c' as is observed experimentally. However, as the $M_s/2$ state is not the lowest energy state, it must decay to the $M_s/3$ state. Which is also observed experimentally. The transition from the $M_s/2$ to the $M_s/3$ states is complicated: for example, in Fig.38(A), 1/3 of up chains and 2/3 of down chains must be reversed. Consequently, a long time is required for the transition. Thus, at low temperatures the $M_s/2$ state remains unchanged as is observed experimentally because of the long transition time compared with the field sweep rate. Next, we discuss the transition from the $M_s/3$ to the F. states and that from the $M_s/2$ to the F. states. In going from the $M_s/3$ and the $M_s/2$ to the F. states, we simply reverse down chains. The internal field acting on the down spins in the $M_s/3$ and the $M_s/2$ states coming from the interchain exchange interactions are described

as, $H-H_{c2}$ which is zero at H_{c2}. So, at H_{c2} the down chains act like isolated chains. In this case, the situation is similar to the case of the transition at H_c'. This is verified experimentally(for example, see Fig.24). Under a decreasing field, the transition from the F. to an intermediate states takes place essentially in a reverse of the process described above. As the transition from the $M_s/3$ to the F. states occurs with a similar speed as that from the $M_s/2$ to the F. states in an increasing case and as the $M_s/3$ state is the lowest energy state in the intermediate region, the transition from the F. to the $M_s/3$ states occurs in a decreasing field. The transition from the $M_s/3$ to the A.F. states in a decreasing case is complicated. According to Tinkham[18], a large nucleus is essential to make the transition. Thus a very long time or large hysteresis is expected in the transition. This is observed experimentally.

As is mentioned in §4, we have observed an activation energy of $20\pm2cm^{-1}$ at the transition from the A.F. to the $M_s/2$ states at H_c'. From the preceding arguments, at H_c', the down chains act like isolated chains, so that the observed activation energy corresponds to 3D in eq.(19). Comparing the value of $3D(\sim28.7cm^{-1})$ with the observed value , the agreement is fairly satisfactory.

Now, we discuss briefly the small magnetization changes observed at about 40kOe and 43kOe(Figs.8, 17, 18, 19, 21, 23 and 24). Ono and Oguchi[34] have investigated the magnetization process in $CoCl_2\cdot2H_2O$ by computer simulation and have explained small peaks

in the susceptibility at (in the present notation) H_c' and H_c'' observed by Kuramitsu, Amaya and Haseda[35]. Independently, Motokawa[36] has explained the same experiment by a model that the $M_s/3$ state is composed of domains and at the domain boundaries, the spin arrangements are irregular which make reorientations at critical fields determined by the local arrangements. He has shown that the critical fields of the spin rearrangements are restricted to H_c' and H_c'' in the case of the $M_s/3$ state. In $FeCl_2 \cdot 2H_2O$, we have observed small magnetization changes at H_c' and H_c'', so that these are explained by Ono-Oguchi and Motokawa models. It is pointed out that the small magnetization change is observed only at H_c' in $CoCl_2 \cdot 2H_2O$ in the magnetization measurement[35], while in $FeCl_2 \cdot 2H_2O$ we have observed small magnetization changes both at H_c'(Figs.18, 19-1st run and 23) and at H_c''(Figs.8, 17, 18, 21 and 23).

§6. Effect of Co^{2+} Impurity on the Metamagnetic Transition in $FeCl_2 \cdot 2H_2O$

(6-1) Experimental Results

In Fig.39, examples of recorder traces of M-H curve obtained in single crystals of $FeCl_2 \cdot 2H_2O$ containing 3.85 and 10.35 at.% Co^{2+} ions are shown. Comparing the M-H curve of pure specimen at T= 4.22K with Fig.39, we see that the transition at H_{c2} becomes broad as Co^{2+} concentration, while at H_{c1} little broadening of the transition is observed. Figs.40 and 41 show temperature dependences of H_c's and of the magnitudes of the magnetizations obtained in 3.85% Co^{2+} doped $FeCl_2 \cdot 2H_2O$, respectively. In the case of pure sample, delays at H_{c2} and H_c' are seen below 2.24K, while in 3.85% Co^{2+} doped sample, the delays are observed below 3.5K. Fig.41 shows that the $M_s/2$ state appears in 3.85% Co^{2+} doped sample at lower temperature than in the case of pure sample, i.e., the transition from the A.F. to the $M_s/3$ states takes place more easily in Co^{2+} doped sample than in pure specimen. The transition from the $M_s/2$ to the $M_s/3$ states observed in pure sample is not seen in more than 1% Co^{2+} doped specimens. In a dilute case($\sim$0.9%) an indication of the transition is seen. Concentration dependence of the $H_c(T)$ curves was investigated and the result is shown in Fig.42. With increasing Co^{2+} concentration, H_c's become weakly temperature dependent. Concentration dependences of H_{c2} and H_c' are shown in Fig.43. As the H_c's depend on temperature in the whole regions investigated, the values of H_c's are not so accurate as in the case of pure sample.

(6-2) Discussion

First, the shift of H_c's with Co^{2+} concentration is discussed. Similar effects have been studied earlier by Date, Tokura and the present author[37] in the case of $CoCl_2 \cdot 2H_2O$ containing transition metal ions. To discuss concentration dependences of H_c's quantitatively, we first calculate the free energies at the A.F., $M_s/3$, $M_s/2$ and the M_s states as functions of the concentration and the external field and next calculate the cross points of these free energies. As the present experiment was performed at low temperatures, we can use energies at T=0K. Consider a Co^{2+} ion surrounded by a unit assembly of Fe^{2+} ions shown in Fig.44(A), and by two hexagons in Fig.44(B) in the ab-plane containing the Co^{2+} ion. The critical concentration of finding only one Co^{2+} ion in the units shown in Fig.44 (A),(B) and in the two additional sites which are next nearest to the Co^{2+} ion along the c-axis, is 2.9at.%. We put the total number of ions per unit volume as N, the Co^{2+} concentration in at.% as x, the spin quantum number of Fe^{2+} as $S_0(=2)$, the Co^{2+} spin as $S(=1/2)$, the g-value of Fe^{2+} as g_0, the g-value of Co^{2+} as g, exchange interactions between Fe^{2+} and Co^{2+} as J_0', J_1' and J_2', respectively. The calculated energies are,

$$E(\text{A.F.})/N=(1-2x/100)(-2J_0S_0^2+4J_1S_0^2-2J_2S_0^2)\mp(2x/100)S_0S(2J_0'-4J_1'+2J_2'),$$

$$E(M_s/3)/N=(1/3)(1-2x/100)(-6J_0S_0^2+4J_1S_0^2+2J_2S_0^2)+(x/300)\{\mp 12J_0'S_0S$$

$$\pm 8J_1'S_0S\pm 4J_2'S_0S\}+(1/3)(1-x/100)(-S_0g_0\mu_BH)\mp(x/300)g\mu_BHS,$$

$$E(M_s/2)/N=(1-2x/100)(-2J_0S_0^2)+(x/100)(\mp 4J_0'SS_0)-(1/2)(1-x/100)g_0\mu_B HS_0$$

$$\mp(x/200)g\mu_B HS, \qquad \text{and}$$

$$E(M_s)/N=(1-2x/100)(-2J_0S_0^2-4J_1S_0^2-2J_2S_0^2)\mp(2x/100)(2J_0'S_0S+4J_1'S_0S$$

$$+2J_2'S_0S)-(1-x/100)g_0\mu_B HS_0\mp(x/100)g\mu_B HS, \qquad (21)$$

where, $\pm$ and $\mp$ represent the case of a ferromagnetic(upper signs) and of an antiferromagnetic(lower signs) couplings of Co^{2+} spins with host spins in a chain(J_0'), respectively. Then H_c's are obtained to be,

$$H_{c1}(x)=\{-(100-2x)(8J_1-8J_2)S_0^2\mp 2x(8J_1'-8J_2')S_0S\}/\{(100-x)S_0g_0\pm xgS\}\mu_B,$$

$$H_c'(x)=\{-(100-2x)(8J_1-4J_2)S_0^2\mp 2x(8J_1'-4J_2')S_0S\}/\{(100-x)S_0g_0\pm xgS\}\mu_B,$$

$$H_c''(x)=\{-(100-2x)(8J_1S_0^2)\mp 2x(8J_1'S_0S)\}/\{(100-x)S_0g_0\pm xgS\}\mu_B, \quad \text{and} \qquad (22)$$

$$H_{c2}(x)=\{-(100-2x)(8J_1+4J_2)S_0^2\mp 2x(8J_1'+4J_2')S_0S\}/\{(100-x)S_0g_0\pm xgS\}\mu_B.$$

The g-value of Co^{2+} in $CoCl_2\cdot 2H_2O$ has been obtained spectroscopically[20,21] to be $g_{//}=6.81$. $H_c'(x)$ and $H_{c2}(x)$ in eq.(22) are plotted in Fig.43 with

$$J_1'=-0.688\text{cm}^{-1}, \quad \text{and}$$

$$J_2'=-0.005\text{cm}^{-1} \tag{23}$$

for the ferromagnetic coupling(P.) of Co^{2+} spin with Fe^{2+} spin in a chain and,

$$J_1'=-0.156\text{cm}^{-1}, \quad \text{and}$$

$$J_2'=-0.128\text{cm}^{-1} \tag{24}$$

for the antiferromagnetic coupling(A.P.). As the present theory is restricted to the low concentration regions, the discrepancy between the theory and the experiment at high concentrations in Fig.43 is a natural consequence. A calculation which includes Co^{2+}-Co^{2+} pair interactions is needed to explain the concentration dependences of H_c's at high concentration regions.

Next, we discuss the dynamical problem at the critical fields of Co^{2+} doped $FeCl_2 \cdot 2H_2O$. As is described previously, we have observed a decrease of the hysteresises as Co^{2+} concentration. For example, the temperature dependent critical fields in Fig.24 become less temperature dependent with Co^{2+} concentration under the same experimental condition(Fig.42). This is explained qualitatively as follows; as the crystal structure of $CoCl_2 \cdot 2H_2O$ is isomorphous with that of $FeCl_2 \cdot 2H_2O$, Co^{2+} spin behaves as an Ising spin with S=1/2

in $FeCl_2 \cdot 2H_2O$. The time required to reverse a Co^{2+} spin is far faster than that for a Fe^{2+} spin, so that delays or hysteresises at the critical fields become small as Co^{2+} concentration.

Finally, the broadening of the transition with Co^{2+} concentration observed at H_{c2} is discussed. The broadening is observed also at H_c' while little broadening is observed at H_{c1}. Concentration dependence of the width of the transition region at H_{c2} is shown in Fig.45. Broadening of metamagnetic transition arises when the external field is rotated from the spin easy axis, and/or when temperature is decreased as in the case of $FeCl_2 \cdot 2H_2O$. If the broadenings of the H_c's in Co^{2+} doped $FeCl_2 \cdot 2H_2O$ come from a rotation of the spin easy axis with Co^{2+} concentration, H_c's must shift towards high field sides compared with those of pure sample, and the transition at H_{c1} must also become broad, contrary to the experiment(Figs.39 and 43). If the broadening comes from the delays at the critical fields as in pure sample, there must be a hysteresis comparable with the width of the transition region. Experimentally, little hysteresis at H_{c2} is observed at T=4.22K as is shown in Fig.39. Demagnetizing effect does not account for the experiment also, because the demagnetizing field shifts the critical fields to high field sides. So, we must consider other mechanism which causes the broadenings of the transitions. At present, microscopic origin of the broadening is not clear.

Acknowledgements

The author wishes to express his sincere thanks to Professor M.Date for his many stimulating discussions. Thanks are also due to Dr.M.Motokawa for his helpful discussions, to Mr.Y.Kikuchi for his helps in the static field experiment and helpful discussions, to Mr.K.Tada of Research and Development Laboratories, Sumitomo Electric Industries, Ltd. for his helps in constructing the 90kOe superconducting solenoid and to Professor Y.Yokozawa for his continual stimulations. The numerical calculation was performed by using FACOM230-25 computer in R.I.A.E., Hokkaido University.

References

1). L.Néel: Ann Phys.(France) 5 (1936) 232.

2). N.J.Poulis, J.van den Handel, J.Ubbink, J.A.Poulis and C.J.Gorter: Phys. Rev. 82 (1951) 552.

3). L.Néel: CR Acad. Sci.(France) 242 (1956) 1549.

4). M.Date and K.Nagata: J. appl. Phys. 34 (1963) 1038.

5). I.S.Jacobs: J. appl. Phys. 32 (1961) 61S.

6). F.Keffer and H.Chow: Phys. Rev. Letters 31 (1973) 1061.

7). D.L.Mills: Phys. Rev. Letters: 20 (1968) 18.

8). M.Motokawa and M.Date: J. Phys. Soc. Japan 20 (1965) 465.

9). H.Kobayashi and T.Haseda: J. Phys. Soc. Japan 19 (1964) 765; A.Narath: J. Phys. Soc. Japan 19 (1964) 2244.

10). I.S.Jacobs and P.E.Lawrence: Phys. Rev. 164 (1967) 866.

11). C.Starr, F.Bitter and A.R.Kaufmann: Phys. Rev. 58 (1940) 977.

12). M.Ball, W.P.Wolf and A.F.G.Wyatt: Phys. Letters 10 (1964) 7.

13). B.E.Keen, D.Landau, B.Schneider and W.P.Wolf: J. appl. Phys. 37 (1966) 1120.

14). G.T.Rado: Phys. Rev. Letters: 23 (1969) 644.

15). J.C.Wright, H.W.Moos, J.H.Colwell, B.W.Mangum and D.D.Thornton: Phys. Rev. B3 (1971) 843.

16). A.Narath: Phys. Rev. 139 (1965) A1221.

17). K.A.Hay and J.B.Torrance,Jr.: Phys. Rev. B2 (1970) 746.

18). M.Tinkham: Phys. Rev. 188 (1969) 967.

19). T.Oguchi: J. Phys. Soc. Japan 20 (1965) 2236.

20). M.Date and M.Motokawa: Phys. Rev. Letters 16 (1966) 1111.

21). J.B.Torrance,Jr., and M.Tinkham: Phys. Rev. 187 (1969) 587, 595.

22). K.Ôno, A.Ito and T.Fujita: J. Phys. Soc. Japan 19 (1964) 2119; R.Alben: J. Phys. Soc. Japan 26 (1969) 261; R.J.Birgeneau, W.B.Yelon, E.Cohen and J.Makovsky: Phys. Rev. B5 (1972) 2607.
23). B.Morosin and E.J.Graeber: J. chem. Phys. 42 (1965) 898.
24). M.Motokawa and M.Date: J. Phys. Soc. Japan 23 (1967) 1216.
25). G.B.Scott, M.Springford and J.R.Stockton: J. Phys. E1 (1968) 925.
26). K.Strnat and L.Bartimay: J. appl. Phys. 38 (1967) 1305.
27). S.Foner and E.J.McNiff,Jr.: Rev. sci. Instrum. 39 (1968) 171.
28). K.Okuda and M.Date: J. Phys. Soc. Japan 27 (1969) 839.
29). This work was performed at Department of Physics, Faculty of Science, Osaka University, and a part of which has been reported earlier; K.Katsumata, M.Motokawa and M.Date: Phys. Soc. of Japan 1968 Annual Meeting, Osaka, April 1968, 5PM8.
30). J.Kanamori, K.Motizuki and K.Yosida: Busseiron Kenkyu(in Japanese) 63 (1953) 28.
31). C.J.Gorter and T.van Peski-Tinbergen: Physica 22 (1956) 273.
32). J.Kanamori: Progr. theor. Phys.: 35 (1966) 16.
33). T.Oguchi and F.Takano: J. Phys. Soc. Japan 19 (1964) 1265.
34). I.Ono and T.Oguchi: Phys. Letters 38A (1972) 39.
35). Y.Kuramitsu, K.Amaya and T.Haseda: J. Phys. Soc. Japan 33 (1972) 83.
36). M.Motokawa: J. Phys. Soc. Japan 35 (1973) 1315.
37). M.Date, S.Tokura and K.Katsumata: reported at the Meeting of Phys. Soc. of Japan in Oct. 1968, 5AE9.

Figure Captions

Fig.1. Crystal structure of $FeCl_2 \cdot 2H_2O$.

Fig.2. Orientation of the α, β principal axes of the susceptibility tensor in the ac-plane. The γ-axis coincides with the b-axis.

Fig.3. Arrangements of the magnetic moments in the A.F.(a), $M_s/3$(b) and M_s(c) states of $FeCl_2 \cdot 2H_2O$. Here $\oplus$ and $\mathbf{O}$ mean magnetic moments point parallel and antiparallel to the α-axis, respectively. The external field is assumed to lie along the $+\alpha$-axis.

Fig.4. Field deviation along the coil axis in the 90kOe superconducting solenoid.

Fig.5. Schematic diagram of an automatic M-H curve recorder.

Fig.6. An example of recorder traces of M-H curve obtained in the present system.

Fig.7. Dependence of recorder output on sample weight in the present system.

Fig.8. Examples of photographs of dM/dH signals obtained in an increasing pulsed field at T=8.0K(a), T=6.4K(b) and at T=4.2K(c).

Fig.9. Temperature dependences of the critical fields obtained in an increasing pulsed field($T<8K$). Here ⊙ represents the transition field associated with a decrease in magnetization. The magnitudes of the decreased magnetizations observed near 3K are very small.

Fig.10. Temperature vs. critical fields in an increasing pulsed field($T>8K$).

Fig.11. Temperature dependence of the magnitude of the magnetization change at 40kOe observed in an increasing pulsed field. If we assume that the magnetization decreases with temperature as, $M(T)\propto\exp(-E_0/kT)$, then $M(T)/M(4.2K)=\exp[(E_0/4.2k)(t-1)/t]$, where $t\equiv T/4.2$. In this figure, the values of E_0 to fit the experiment are given.

Fig.12. Examples of photographs of dM/dH signals obtained at $T=4.2K$ in a duration of a pulsed field, $H_{max.}=40.5kOe$(a), $H_{max.}=47.8kOe$(b) and $H_{max.}=54.3kOe$(c), where $H_{max.}$ means the maximum field produced in the pulsed field coil. The spikes seen at $H\sim0$ in the increasing cases are not the dM/dH signals.

Fig.13. $H_{max.}$ vs. critical fields obtained in an increasing and a decreasing pulsed field at $T=4.2K$.

Fig.14. Critical fields vs. $H_{max.}$ obtained in a duration of the pulsed field at T=3.20K.

Fig.15. Critical fields vs. $H_{max.}$ under an increasing and a decreasing pulsed fields at T=1.98K.

Fig.16. Sample dependences of the temperature vs. critical field curve($H_c(T)$) in $FeCl_2 \cdot 2H_2O$.

Fig.17. Examples of recorder traces of M-H curves obtained in a slowly increasing field and at various temperatures. M-H curves are displayed vertically for clarity and the base lines are shown in the figure.

Fig.18. Examples of M-H curves obtained in a slowly decreasing field and at various temperatures. Base lines for the respective curve are shown.

Fig.19. Dependence of the transition from the A.F. to the $M_s/3$ states on a process of field sweep.

Fig.20. Hysteresises at the transition point of the A.F. to the $M_s/3$ states when the external field is decreased from the M_s state(upper) and when decreased from the $M_s/3$ state(lower).

Fig.21. M-H curves in the 1st and the 2nd runs obtained in an increasing field at T=3.00K.

Fig.22. Transitions of the intermediate states($M \sim M_s/2$) to a state of low net moment at T=2.00K and at T=3.00K when the external field is decreased from the intermediate states.

Fig.23. M-H curve obtained in a decreasing field(dH/dt=60 Oe/sec) at T=2.24K.

Fig.24. Temperature dependences of the critical fields in $FeCl_2 \cdot 2H_2O$ obtained under slowly varying fields. Here 1 and 2 stand for the 1st and the 2nd runs, respectively.

Fig.25. Temperature vs. magnitudes of the magnetizations at the intermediate and the F. states of $FeCl_2 \cdot 2H_2O$. Here + represents the magnetization observed under a fixed external magnetic field.

Fig.26. Examples of time dependences of magnetizations at the transition from the A.F. to the $M_s/3$ states(upper), where the smooth curve represents $M(t)=1.42-1.06\exp(-t/522)$, at the transition from the $M_s/2$ to the $M_s/3$ states(middle), where the smooth curves represent, $M(t)=1.42+0.65\exp(-t/34$ for T=3.00K and $M(t)=1.42+0.70\exp(-t/892)$ for T=2.75K and at the transition from the A.F. to the $M_s/2$ states(lower), where the smooth curves represent $M(t)=2.13-1.85\exp(-t/208)$ for T=2.00K, $M(t)=2.13-1.87\exp(-t/337)$ for T=1.91K and $M(t)=2.13-1.87\exp(-t/1345)$ for T=1.74K, respectively.

The external field is increased from zero to the values shown in the figure with a speed of 60 Oe/sec.

Fig.27. Temperature dependences of the rise time of the A.F. to the $M_s/2$ states and of the decay time of the $M_s/2$ to the $M_s/3$ states under fixed external fields.

Fig.28. Dependences of the decay time of the $M_s/2$ to the $M_s/3$ states (upper) and of the rise time of the A.F. to the $M_s/2$ states(lower) on the external field.

Fig.29. Magnetic field dependences of τ at the transition from the A.F. to the $M_s/2$ states obtained from the observed M-H curves. The pulsed field data are also shown.

Fig.30. Magnetic field vs. τ at the transition from the $M_s/2$ to the M_s states obtained from the observed M-H curves.

Fig.31. Field dependences of τ at the transition from the $M_s/3$ to the A.F. states obtained from the observed M-H curves.

Fig.32. Free energies vs. external field in the A.F., $M_s/3$, $M_s/2$ and M_s states of $FeCl_2 \cdot 2H_2O$.

Fig.33. Calculated m-h curves in the A.F., $M_s/3$ and F. states of $FeCl_2 \cdot 2H_2O$ at T=5.36K in the molecular field approximation.

Fig.34. Relations between m and h in the molecular field theory in the A.F., $M_s/3$ and F. states of $FeCl_2 \cdot 2H_2O$ at T=14.7K.

Fig.35. Temperature dependences of the calculated maximum possible values of the critical fields in $FeCl_2 \cdot 2H_2O$ in an increasing field case. Experimental data obtained in an increasing pulsed field are also shown. Here $H_{c1}^{th.}(0)$ and $H_{c2}^{th.}(0)$ mean the thermodynamic critical fields at $T \ll T_N$.

Fig.36. Calculated maximum possible values of the critical fields vs. temperature in $CoCl_2 \cdot 2H_2O$ in an increasing field case. The pulsed field data shown in this figure are those obtained by Motokawa and Date.[8)]

Fig.37. Single ion energy level diagram of Fe^{2+} in the A.F. state of $FeCl_2 \cdot 2H_2O$ at T=0K. Energies are in units of cm^{-1}.

Fig.38. Examples of the arrangements of magnetic moments in the $M_s/2$ state which are constructed by a simple reversal of down chains in the A.F. state. This figure shows as in the case of Fig.3, the projection of the magnetic moments on the ab-plane.

Fig.39. Examples of M-H curves obtained in Co^{2+} doped $FeCl_2 \cdot 2H_2O$.

Fig.40. Temperature dependences of H_c's in 3.85% Co^{2+} doped $FeCl_2 \cdot 2H_2O$.

Fig.41. Temperature vs. magnetizations in the intermediate and the F. states obtained in 3.85% Co^{2+} doped $FeCl_2 \cdot 2H_2O$.

Fig.42. Concentration dependence of $H_c(T)$ curves in $FeCl_2 \cdot 2H_2O$:Co^{2+} specimens. Dotted lines represent the $H_c(T)$ curves in pure $FeCl_2 \cdot 2H_2O$.

Fig.43. Co^{2+} concentration vs. H_c' and H_{c2} in $FeCl_2 \cdot 2H_2O$. Where the full and the dotted lines are the theoretical ones(see the text).

Fig.44. A Co^{2+} ion surrounded by unit assemblies of Fe^{2+} ions in $FeCl_2 \cdot 2H_2O$.

Fig.45. Co^{2+} concentration dependence of the width of the transition region at H_{c2} in $FeCl_2 \cdot 2H_2O$.

Fig. 1.

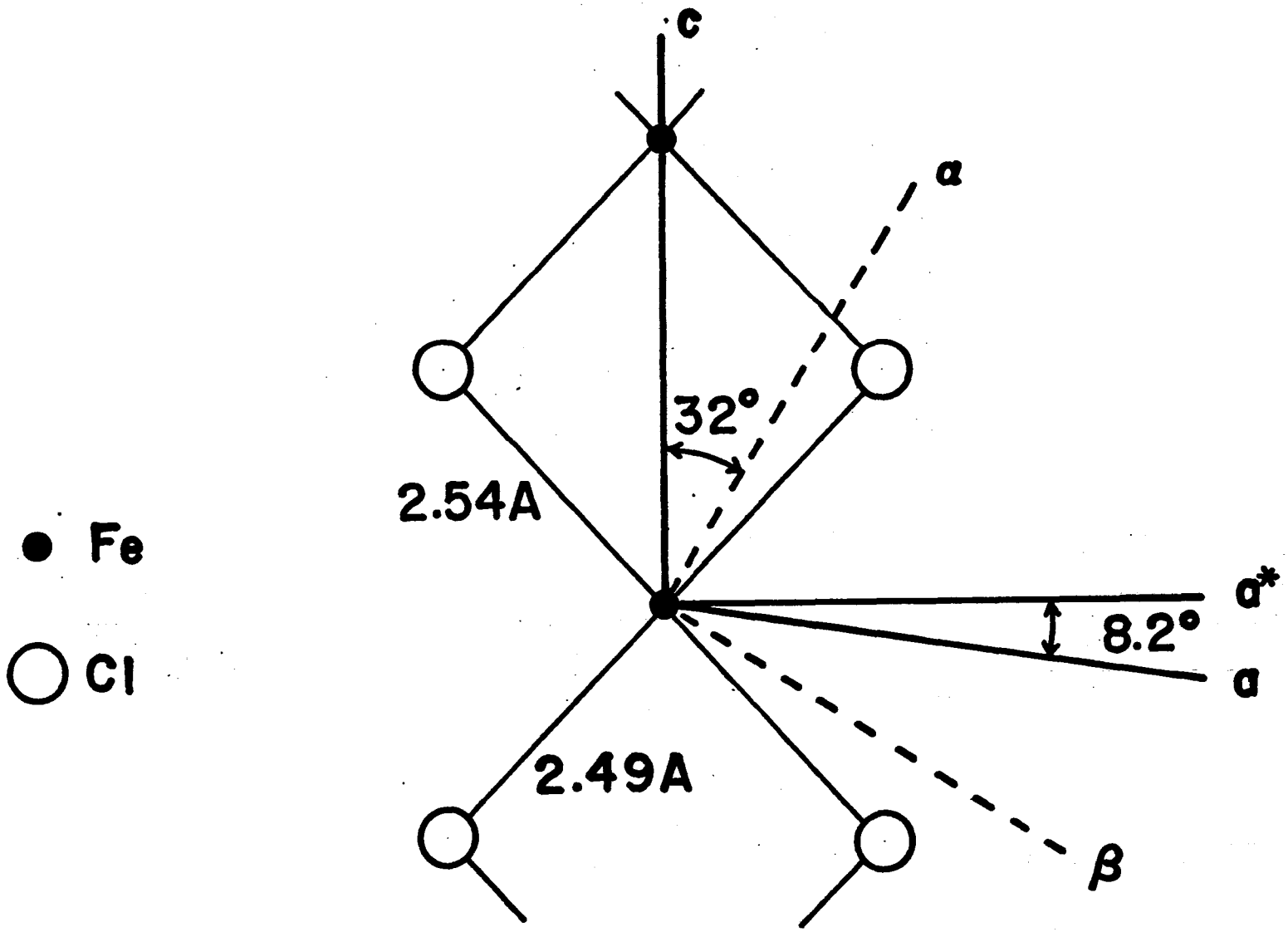

Fig. 2.

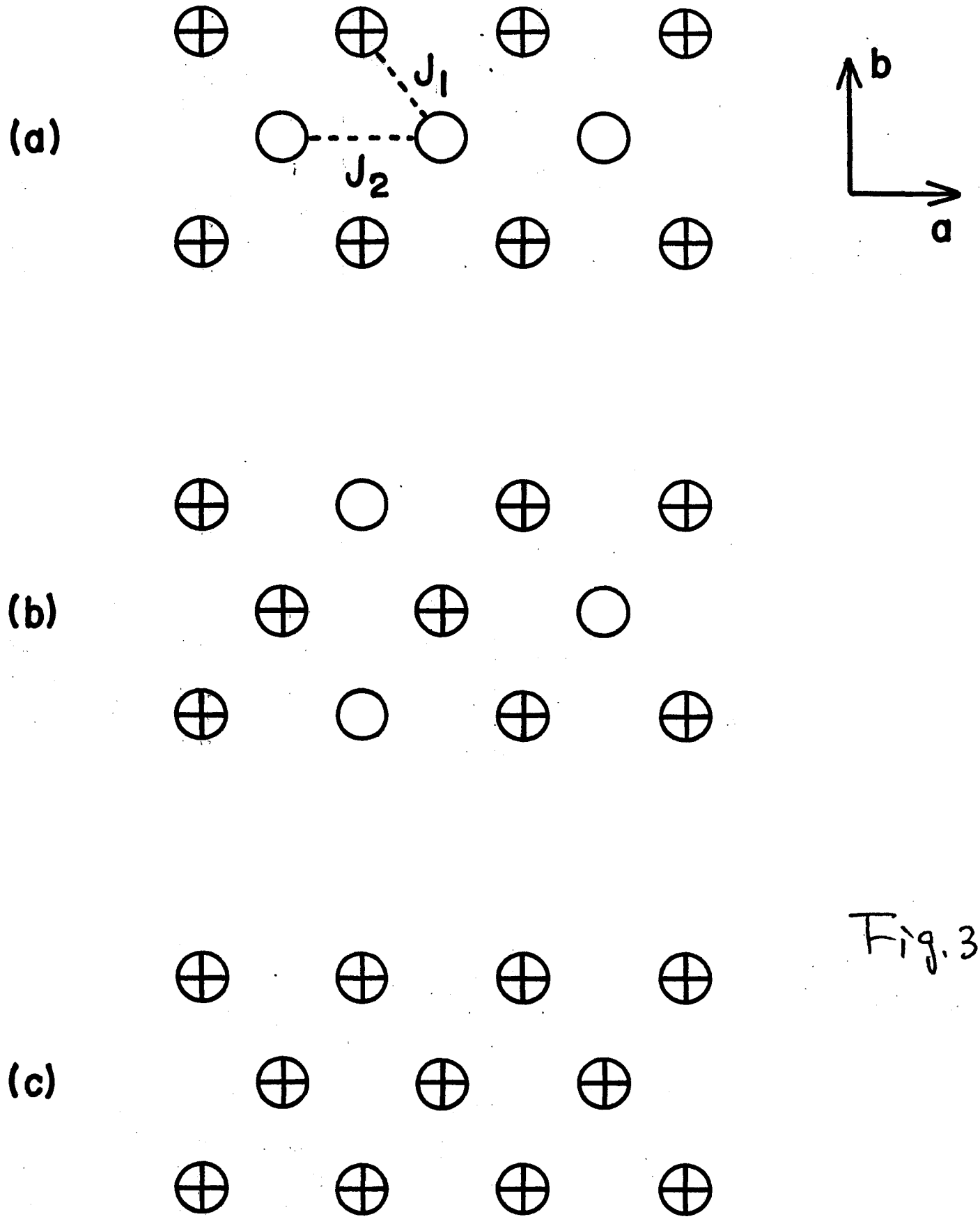

Fig. 3.

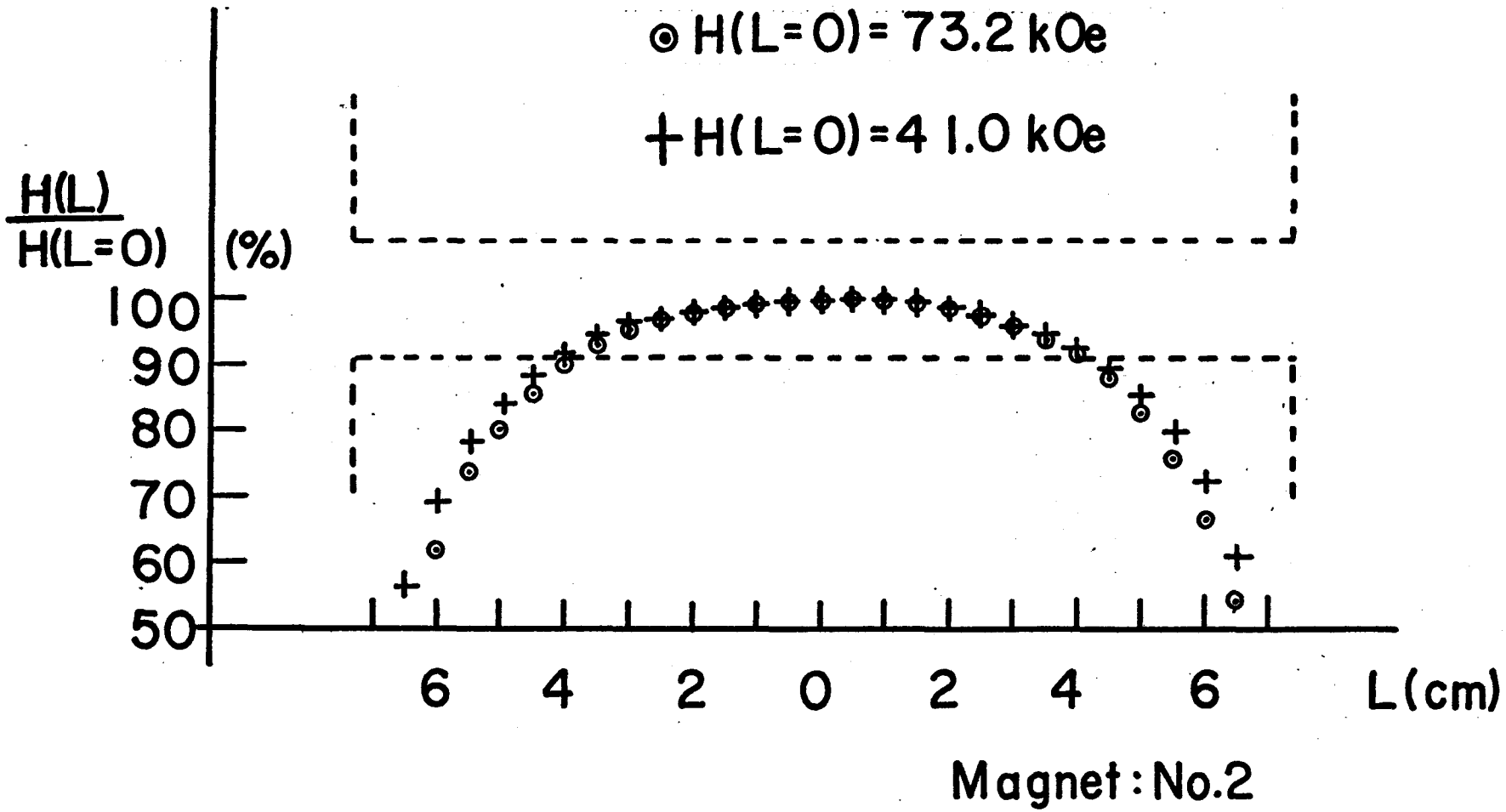
⊙ H(L=0)= 73.2 kOe
+ H(L=0)=4 1.0 kOe
H(L)/H(L=0) (%)
100
90
80
70
60
50
6
4
2
0
2
4
6
L(cm)
Magnet : No.2

(25)

Fig. 4.

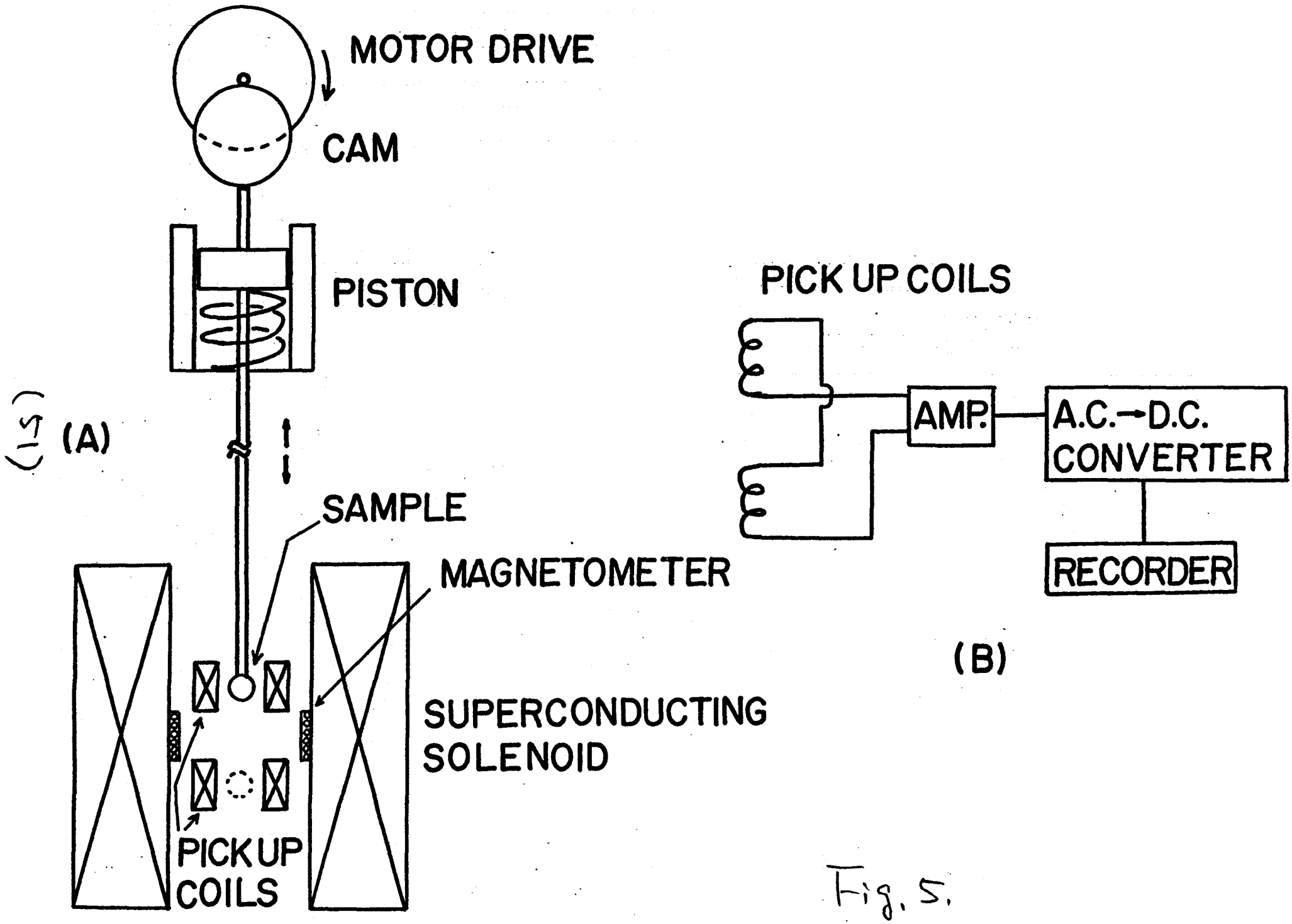
MOTOR DRIVE
CAM
PISTON
(A)
SAMPLE
MAGNETOMETER
SUPERCONDUCTING SOLENOID
PICK UP COILS
PICK UP COILS
AMP.
A.C.→D.C. CONVERTER
RECORDER
(B)

Fig. 5.

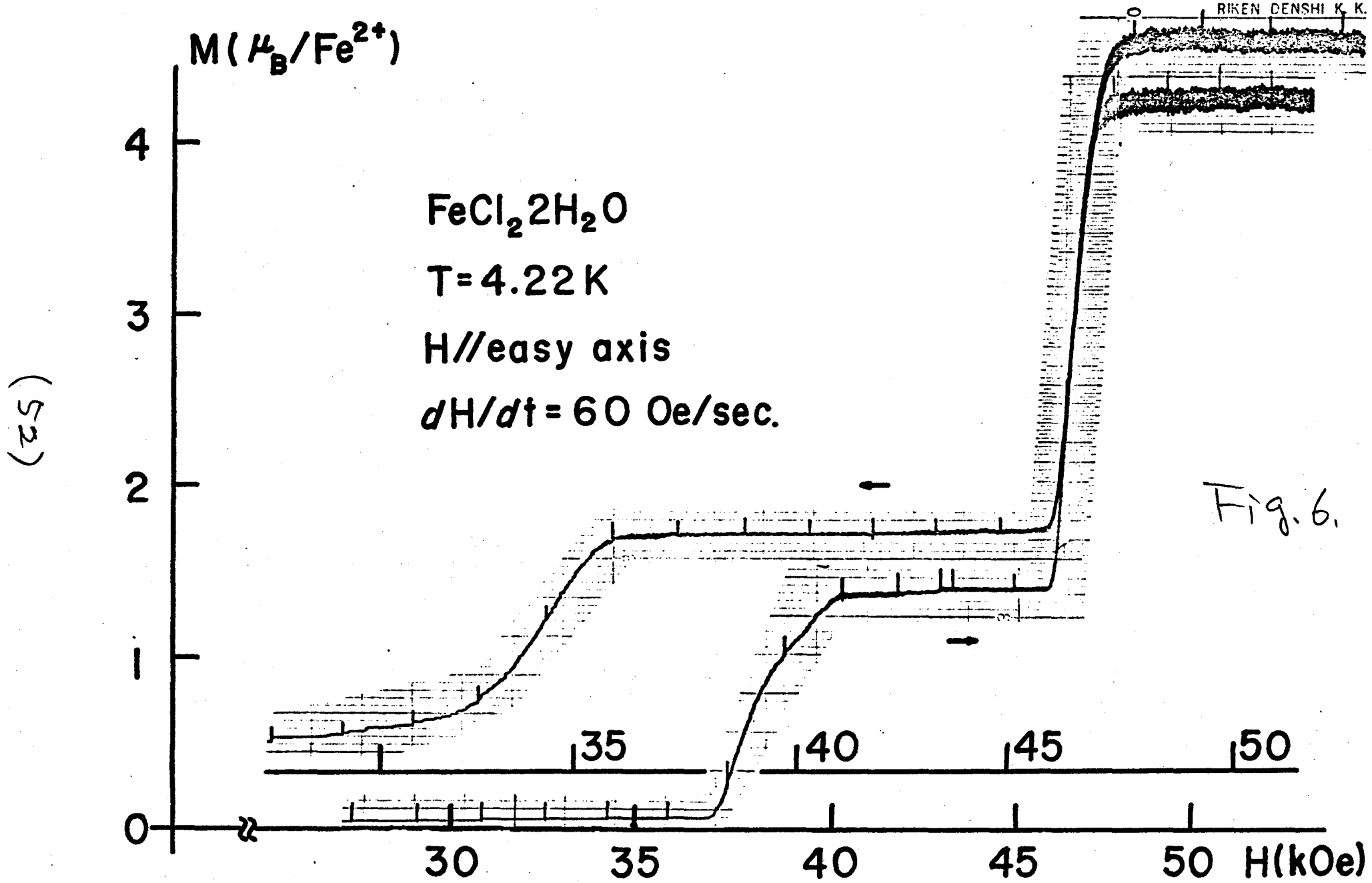
RIKEN DENSHI K. K.
M(μ_B/Fe^{2+})
$FeCl_2 2H_2O$
T=4.22K
H//easy axis
dH/dt = 60 Oe/sec.
4
3
2
1
0
30
35
40
45
50
H(kOe)

Fig. 6.

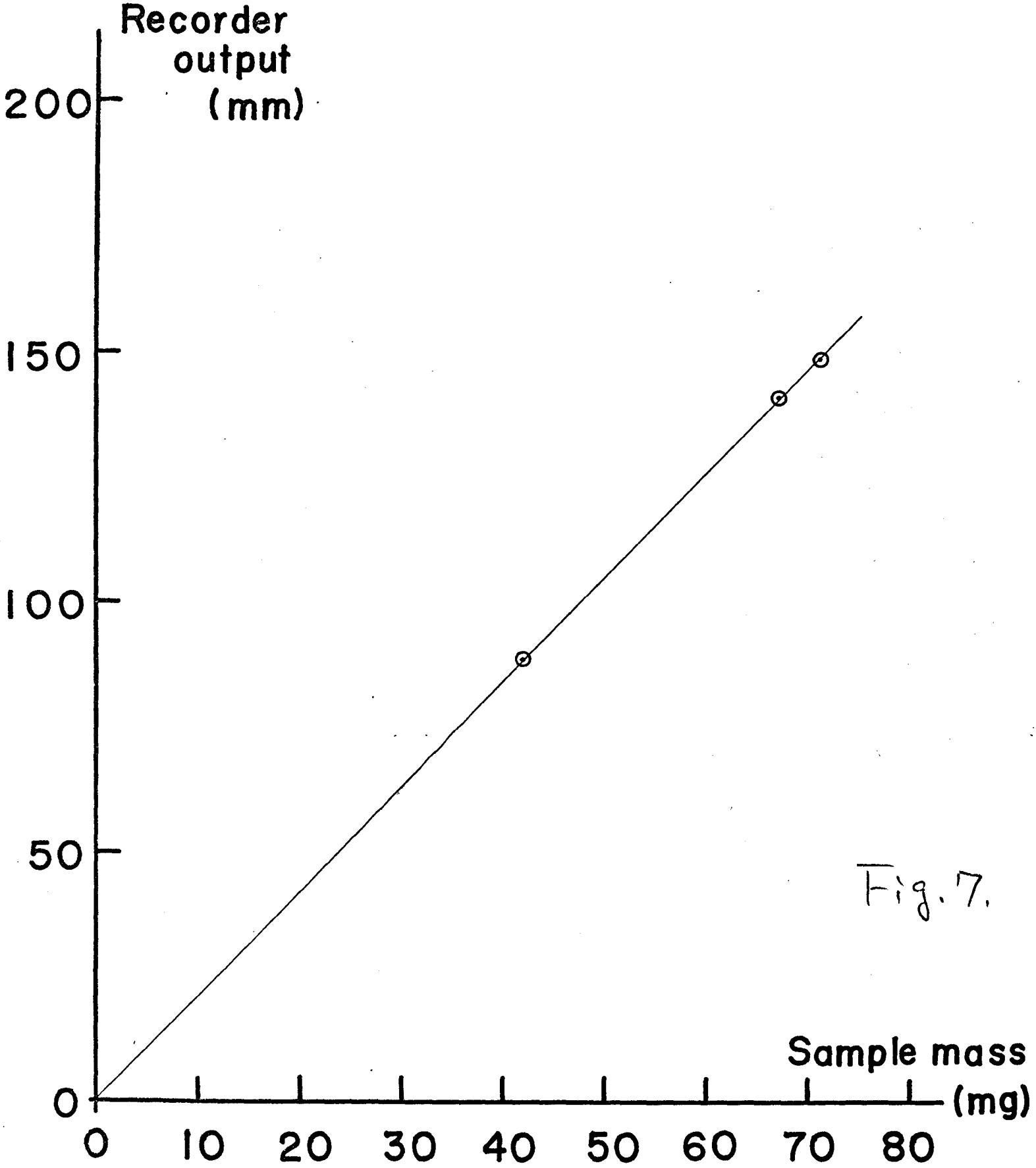
Recorder output (mm)
200
150
100
50
0
Sample mass (mg)
0
10
20
30
40
50
60
70
80

Fig. 7.

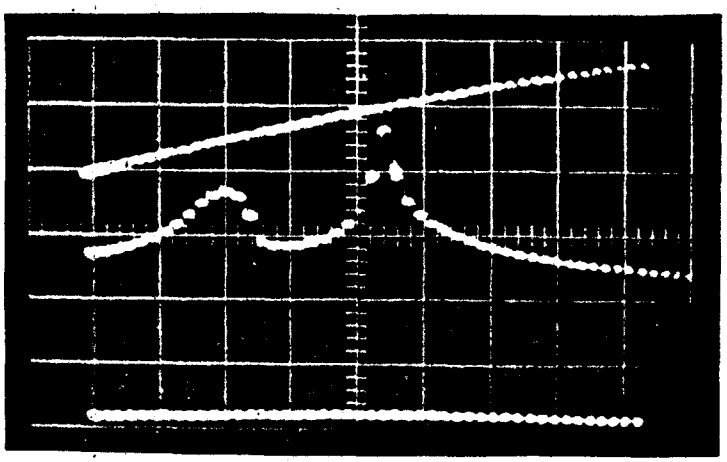

(a)

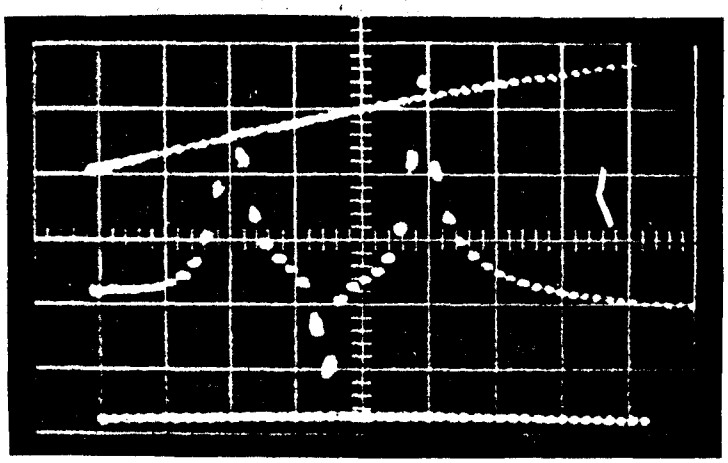

(b)

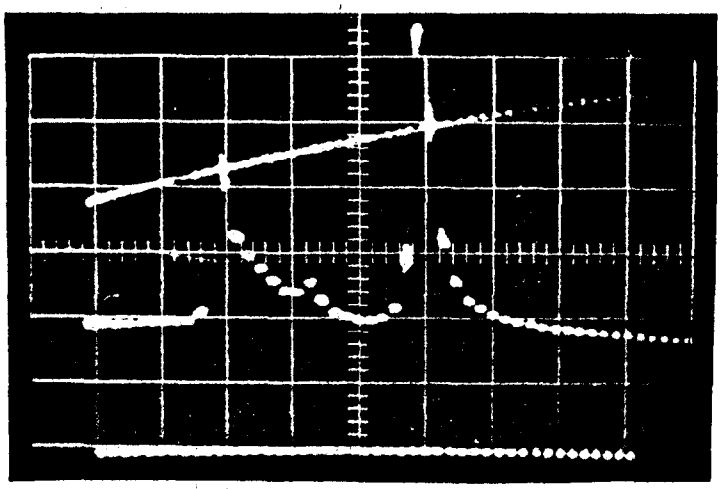

(c)

Fig. 8.

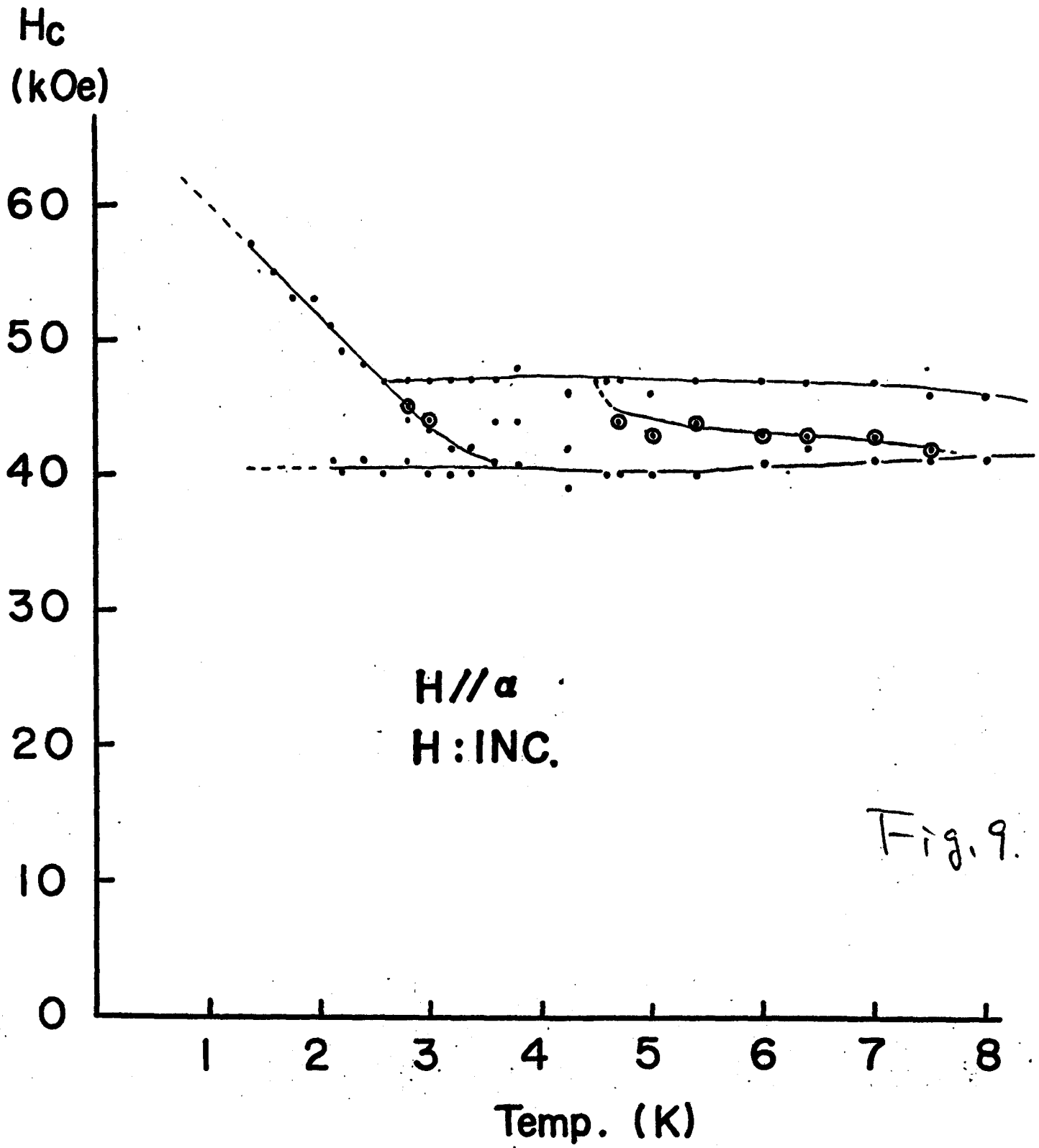

Fig. 9.

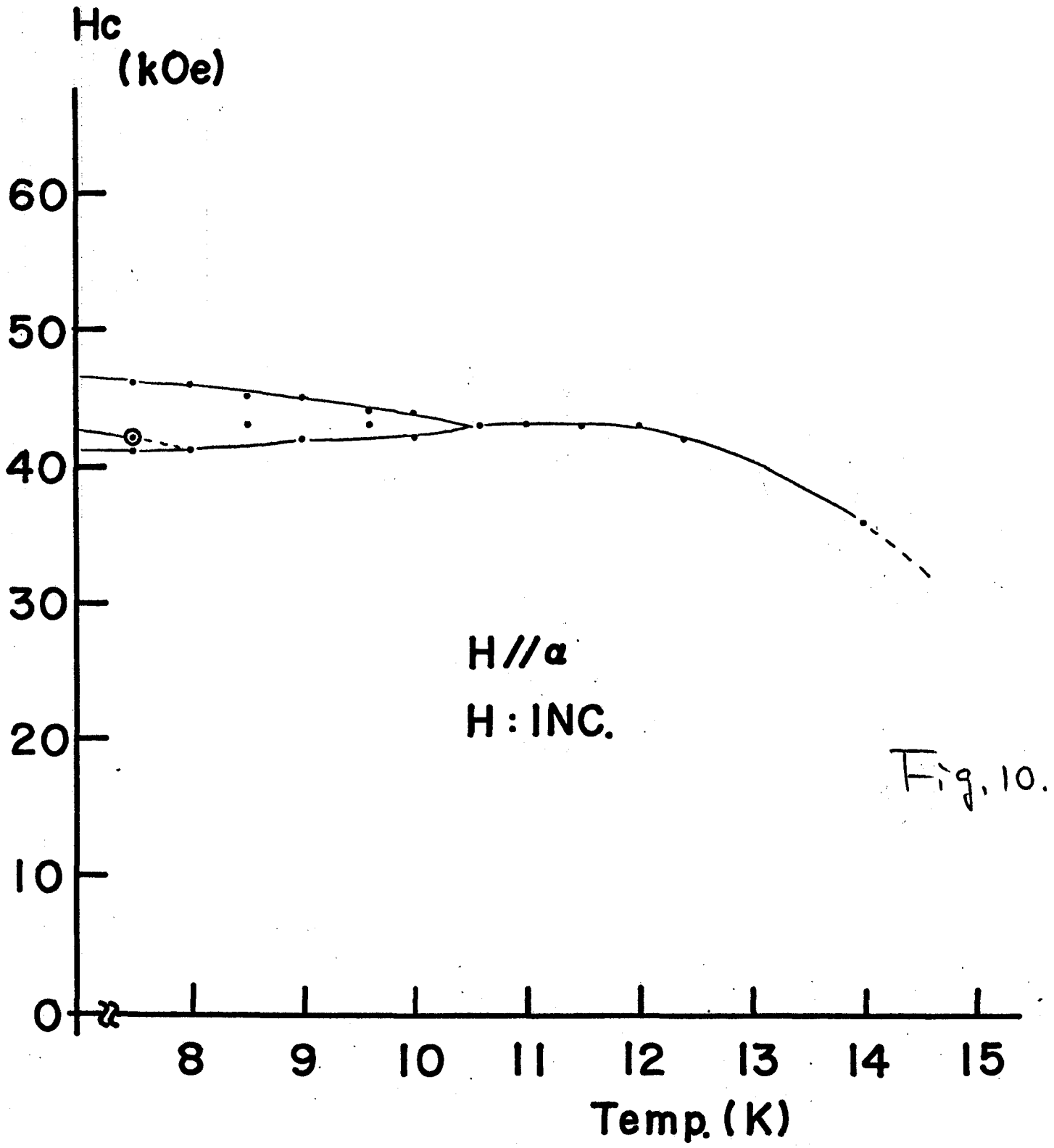

Fig. 10.

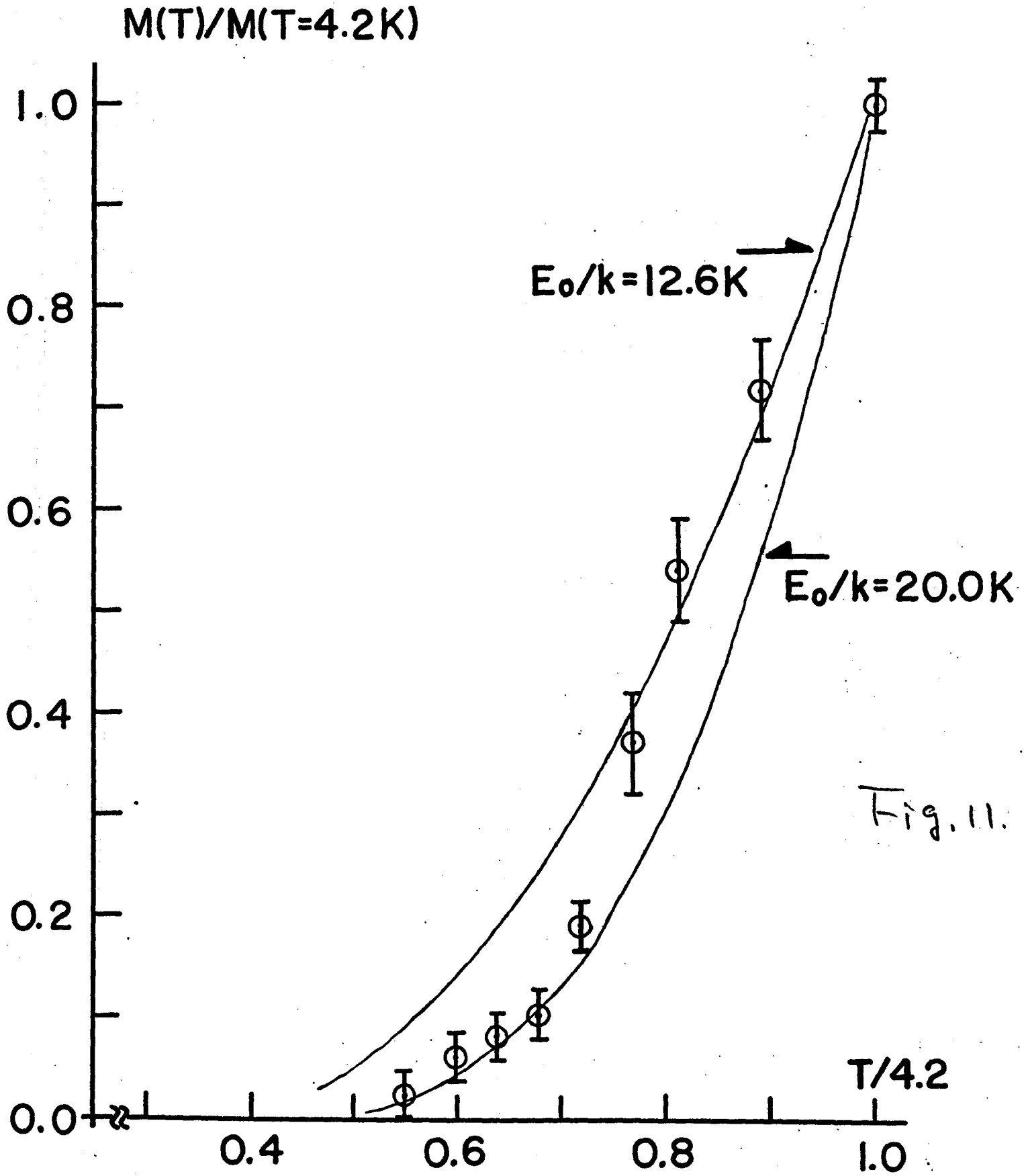

Fig. 11.

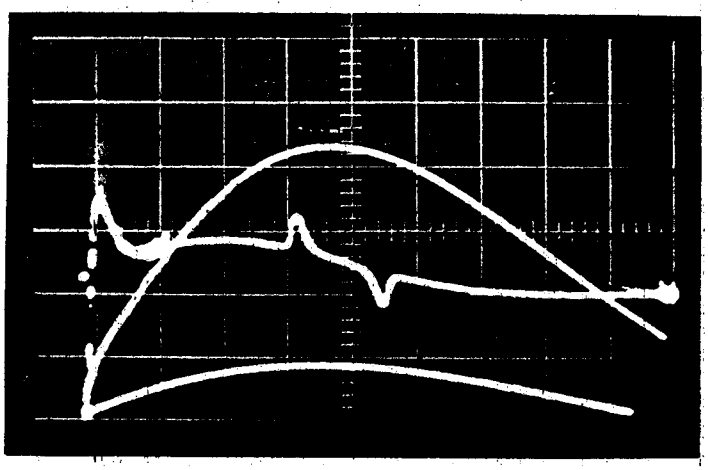

(a)

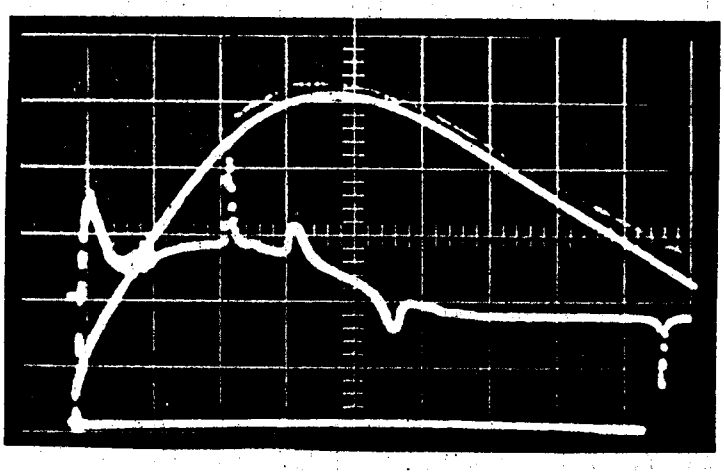

(b)

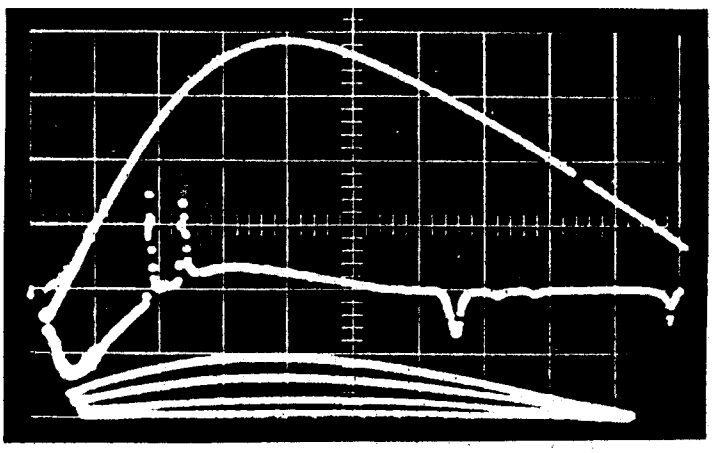

(c)

Fig. 12.

Fig. 13.

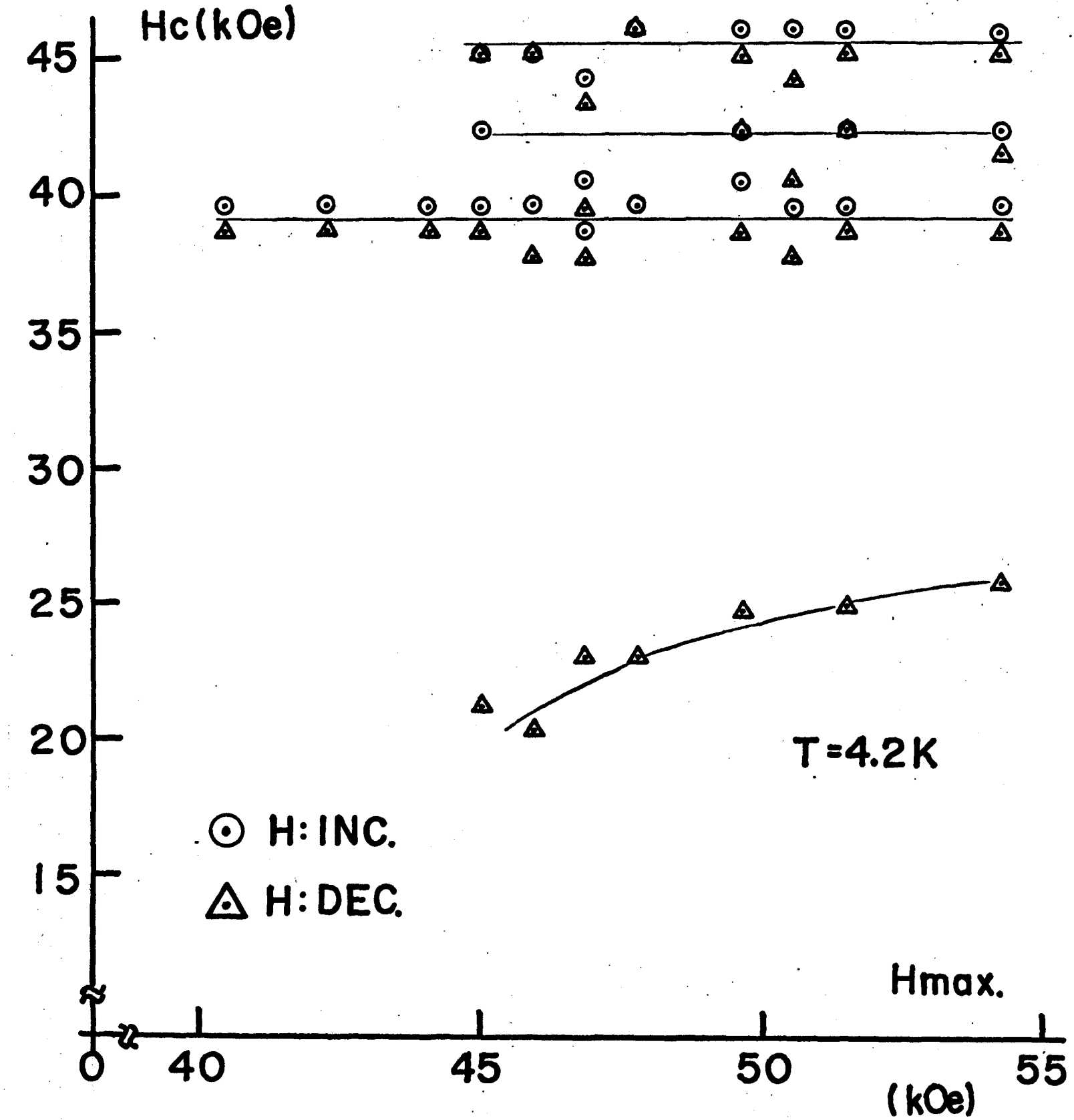

Fig. 14.

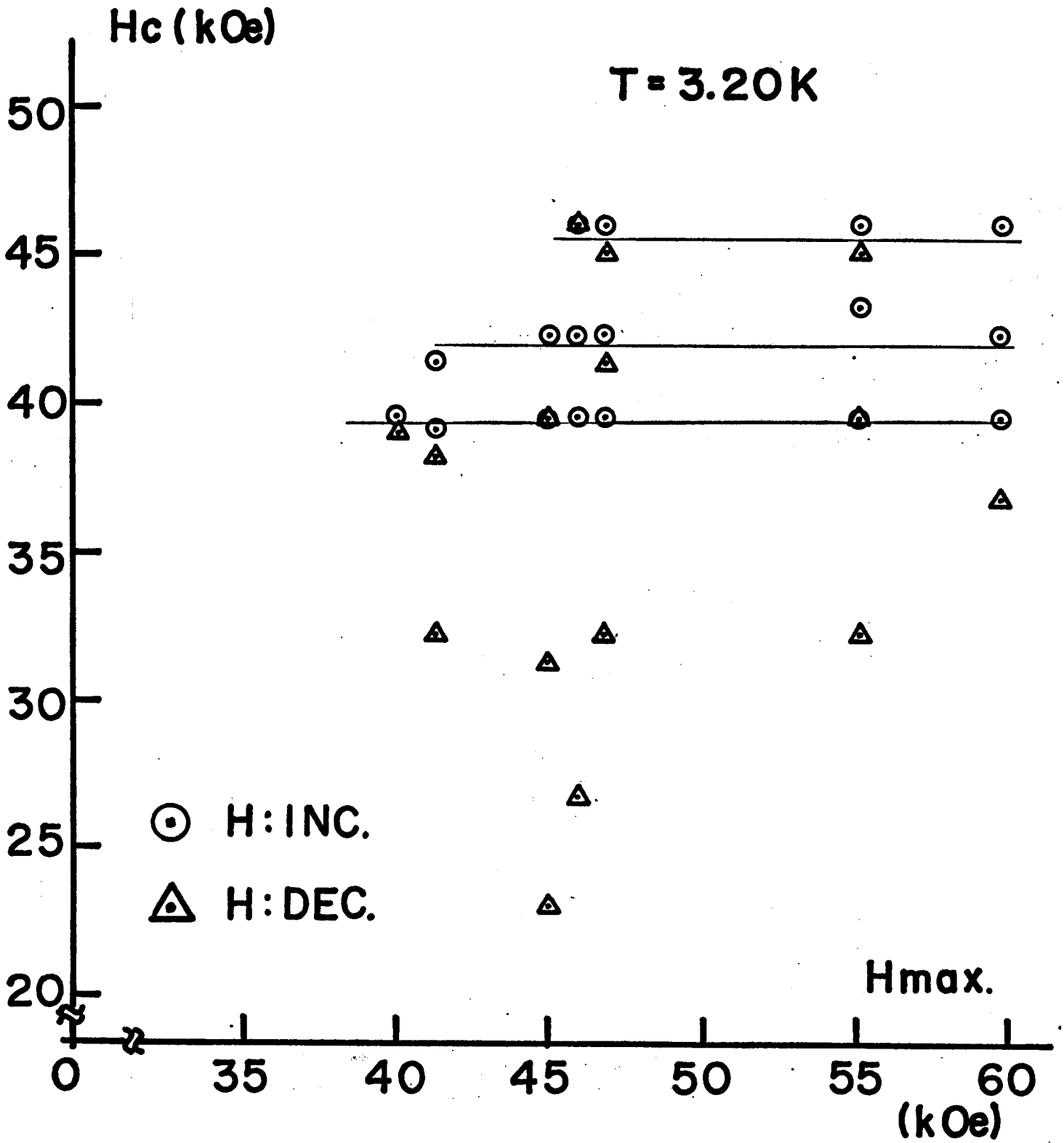
Hc (kOe)
T = 3.20K
50
45
40
35
30
25
20
H: INC.
H: DEC.
Hmax.
0
35
40
45
50
55
60
(kOe)

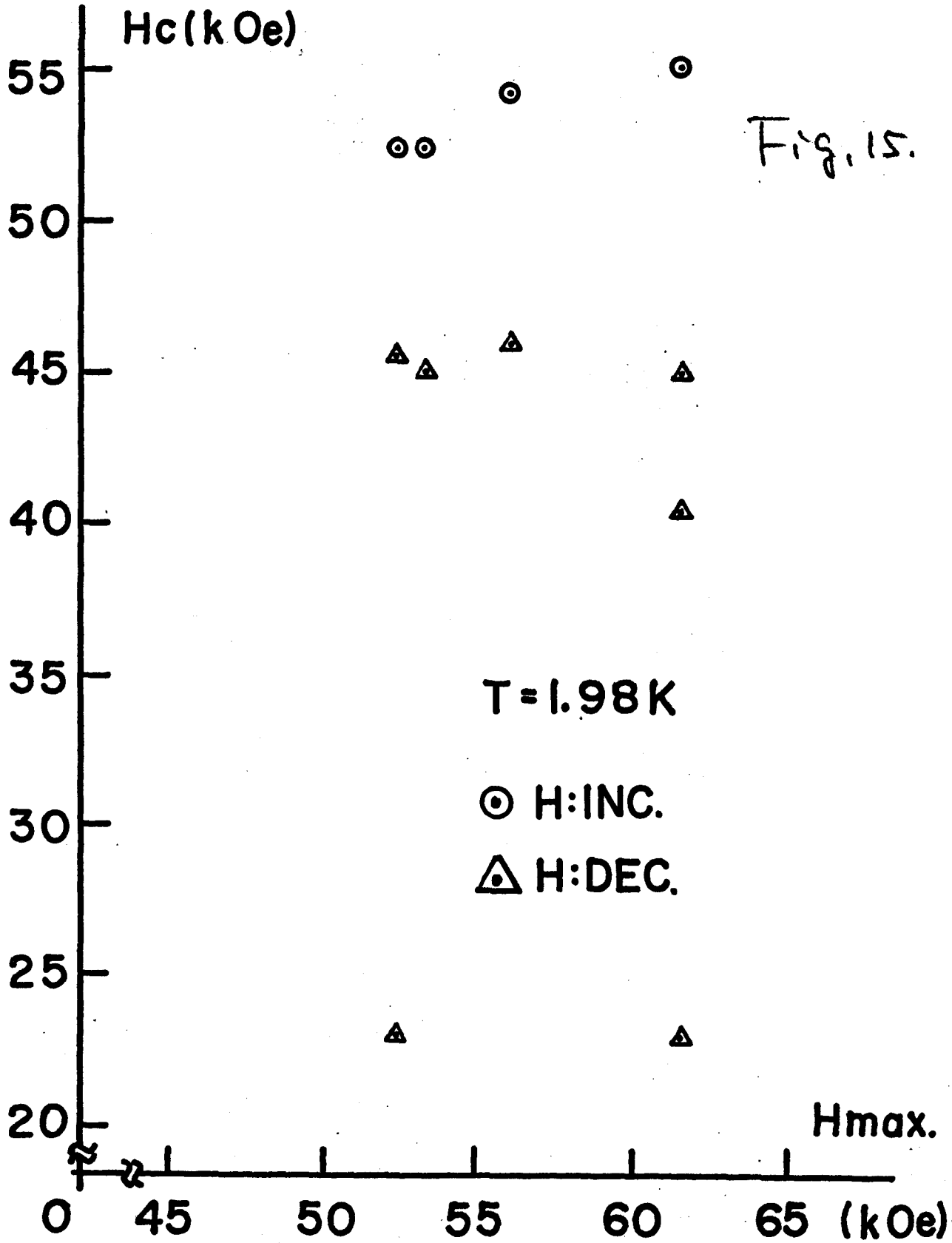
Hc(kOe)
55
50
45
40
35
30
25
20
T=1.98K
⊙ H:INC.
△ H:DEC.
Hmax.
0
45
50
55
60
65 (kOe)

Fig. 15.

Fig. 16.

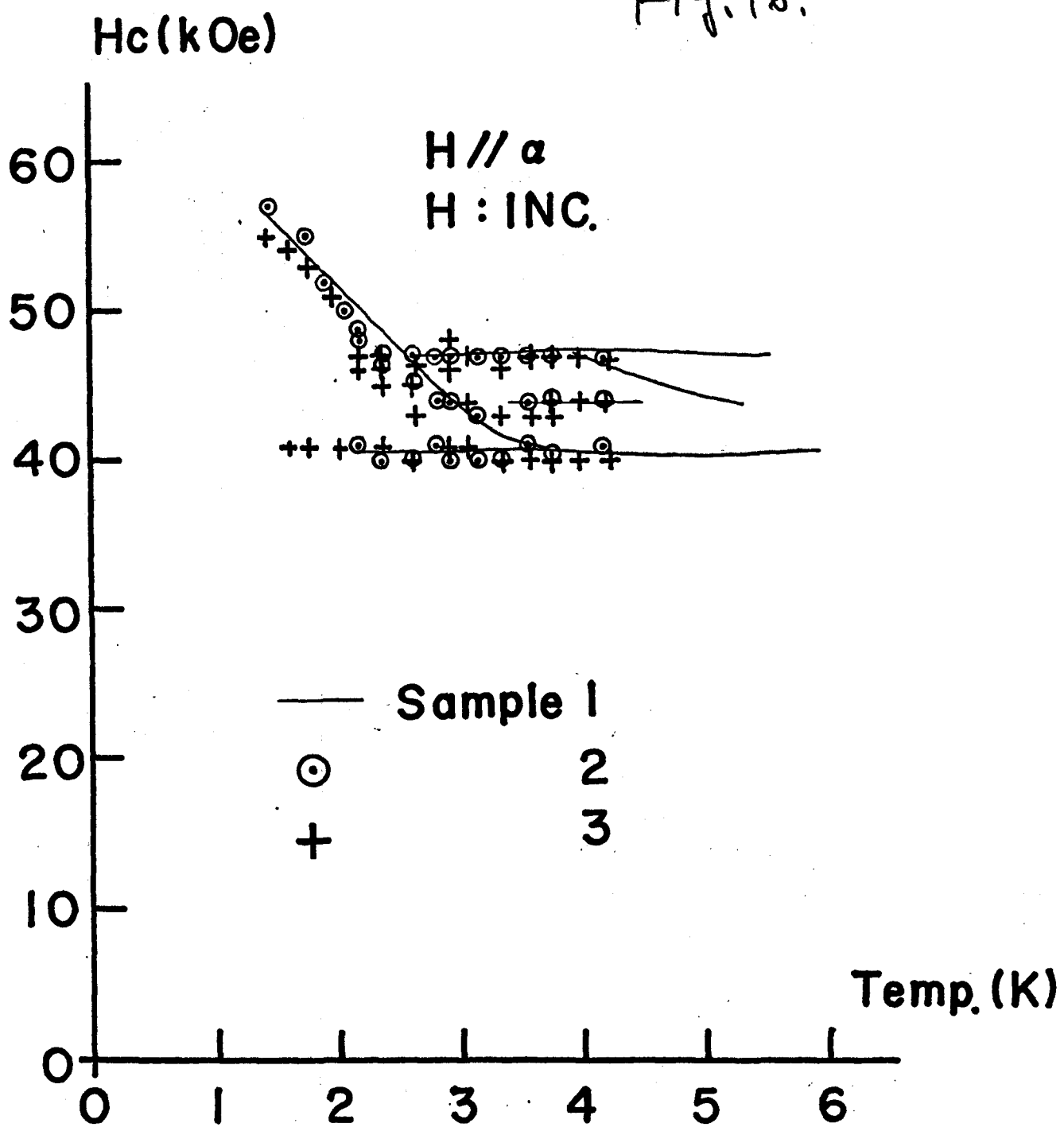

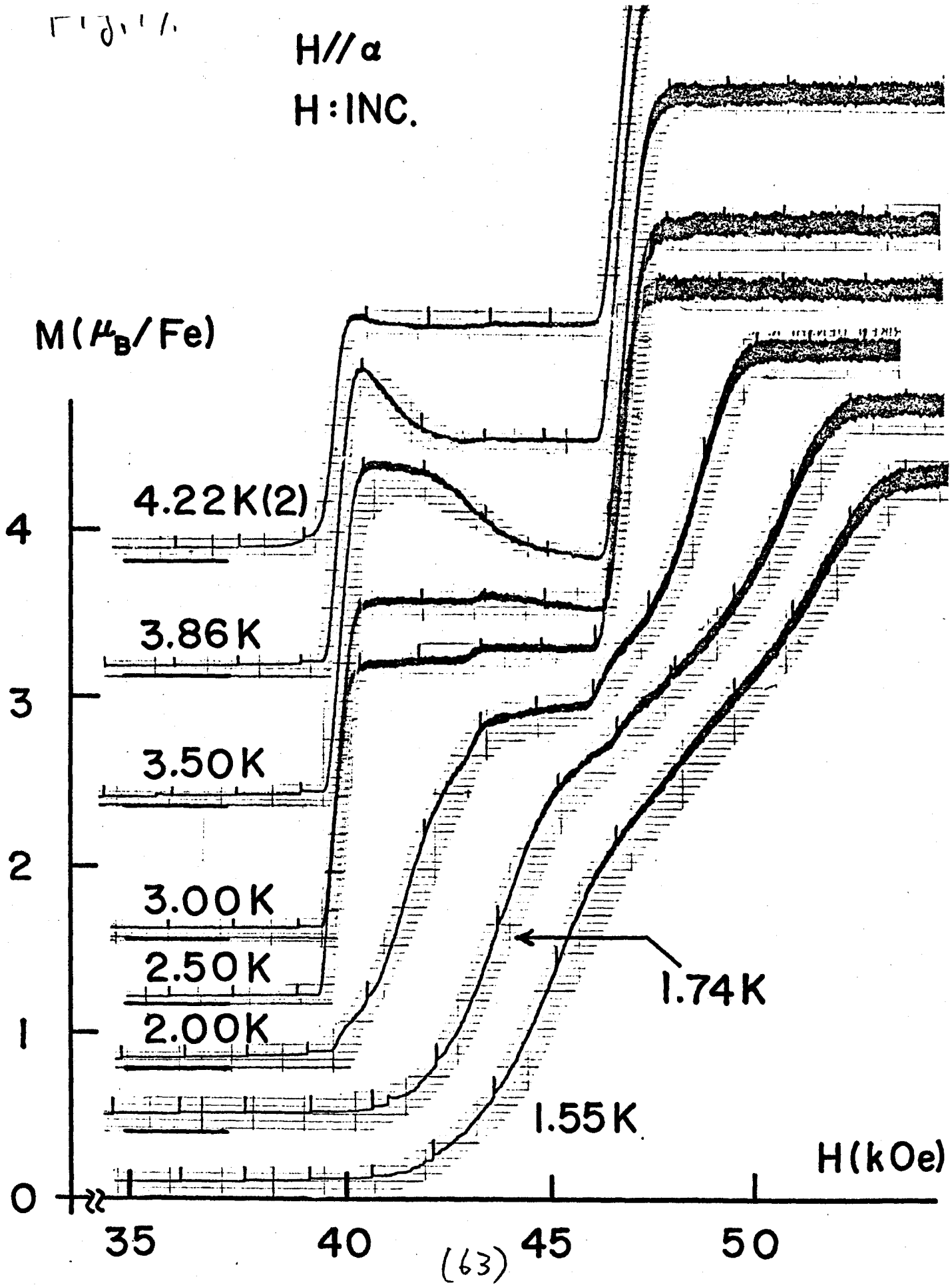
H//a
H:INC.
M(μB/Fe)
4.22K(2)
3.86K
3.50K
3.00K
2.50K
2.00K
1.74K
1.55K
H(kOe)
0
1
2
3
4
35
40
45
50

Fig. 18.

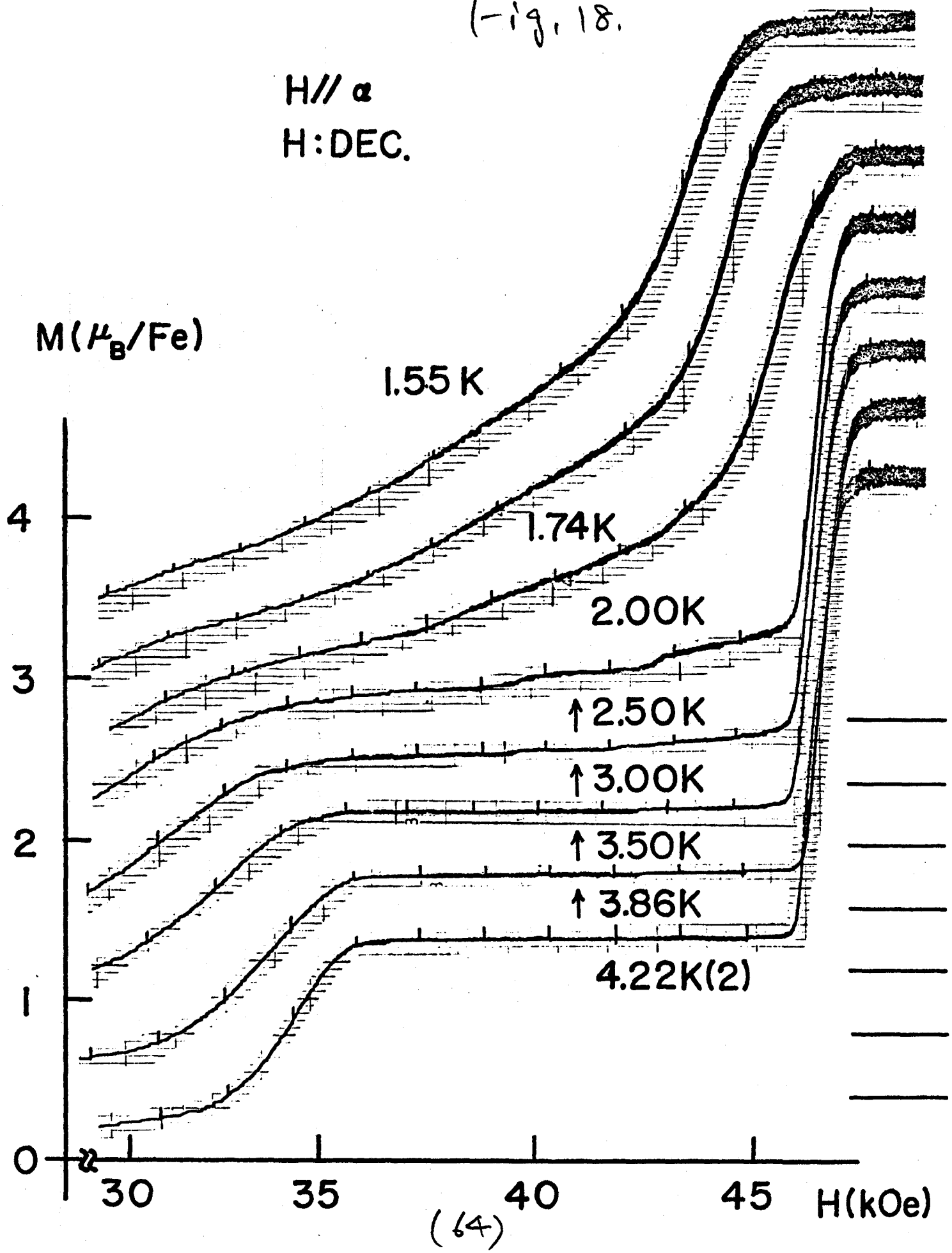
H// a
H:DEC.
M(μB/Fe)
1.55 K
1.74K
2.00K
↑2.50K
↑3.00K
↑3.50K
↑3.86K
4.22K(2)
4
3
2
1
0
30
35
40
45
H(kOe)

Fig. 19.

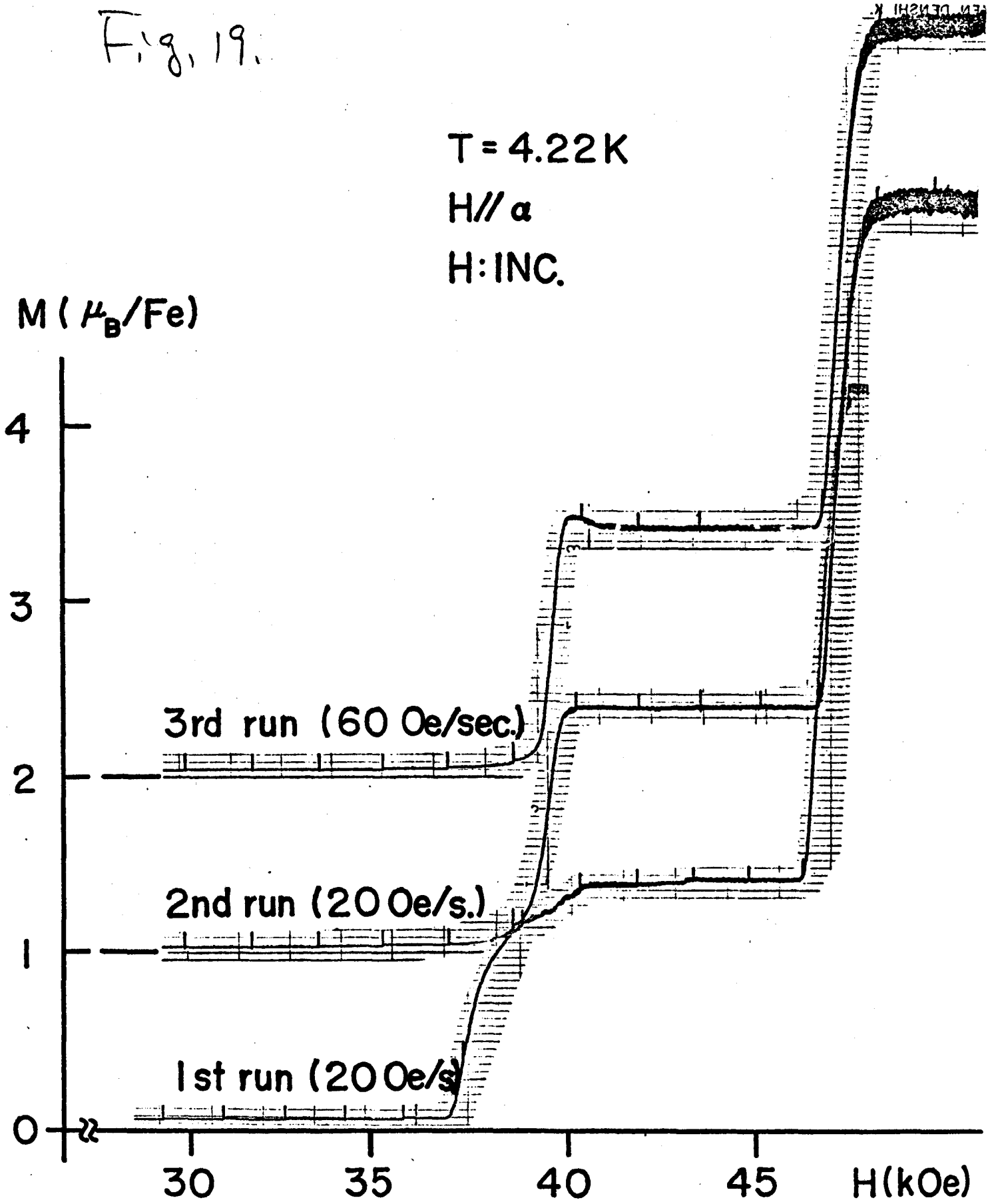
T = 4.22K
H// a
H: INC.
M (μ_B/Fe)
4
3
2
1
0
3rd run (60 Oe/sec.)
2nd run (20 Oe/s.)
1st run (20 Oe/s)
30
35
40
45
H(kOe)

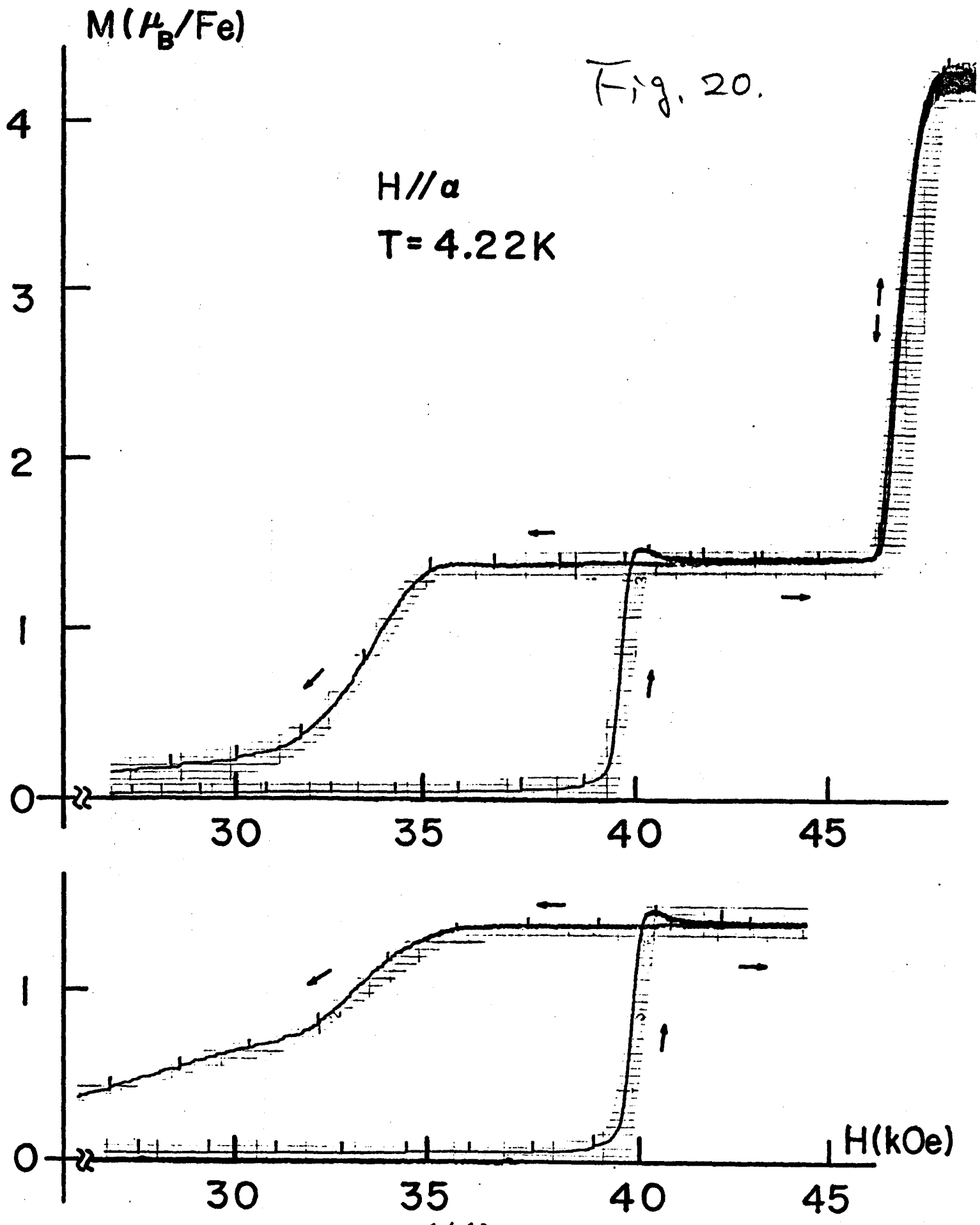

Fig. 20.

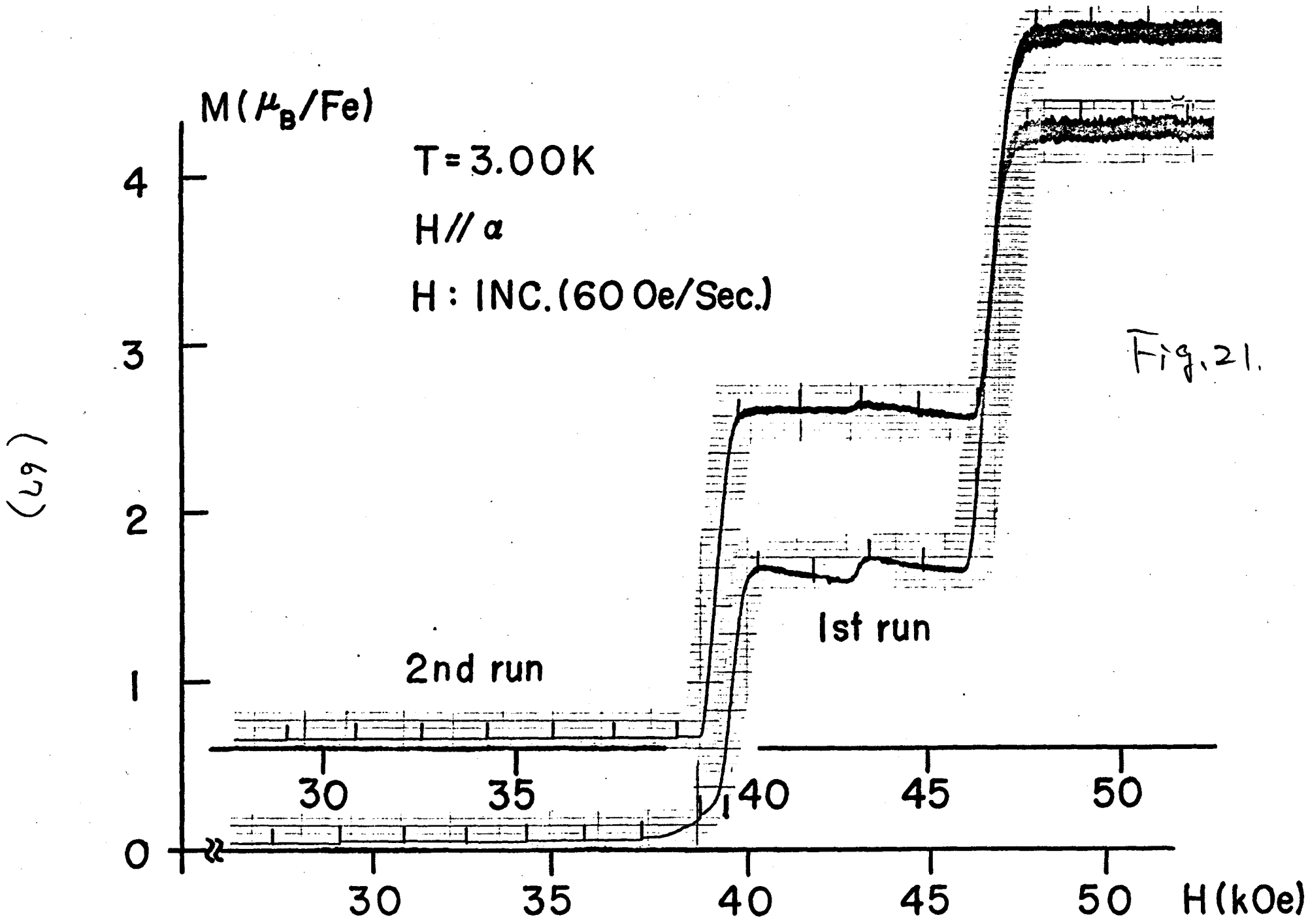
M(μB/Fe)
T=3.00K
H//α
H : INC.(600e/Sec.)
1st run
2nd run
0
1
2
3
4
30
35
40
45
50
H(kOe)

Fig. 21.

Fig. 22.

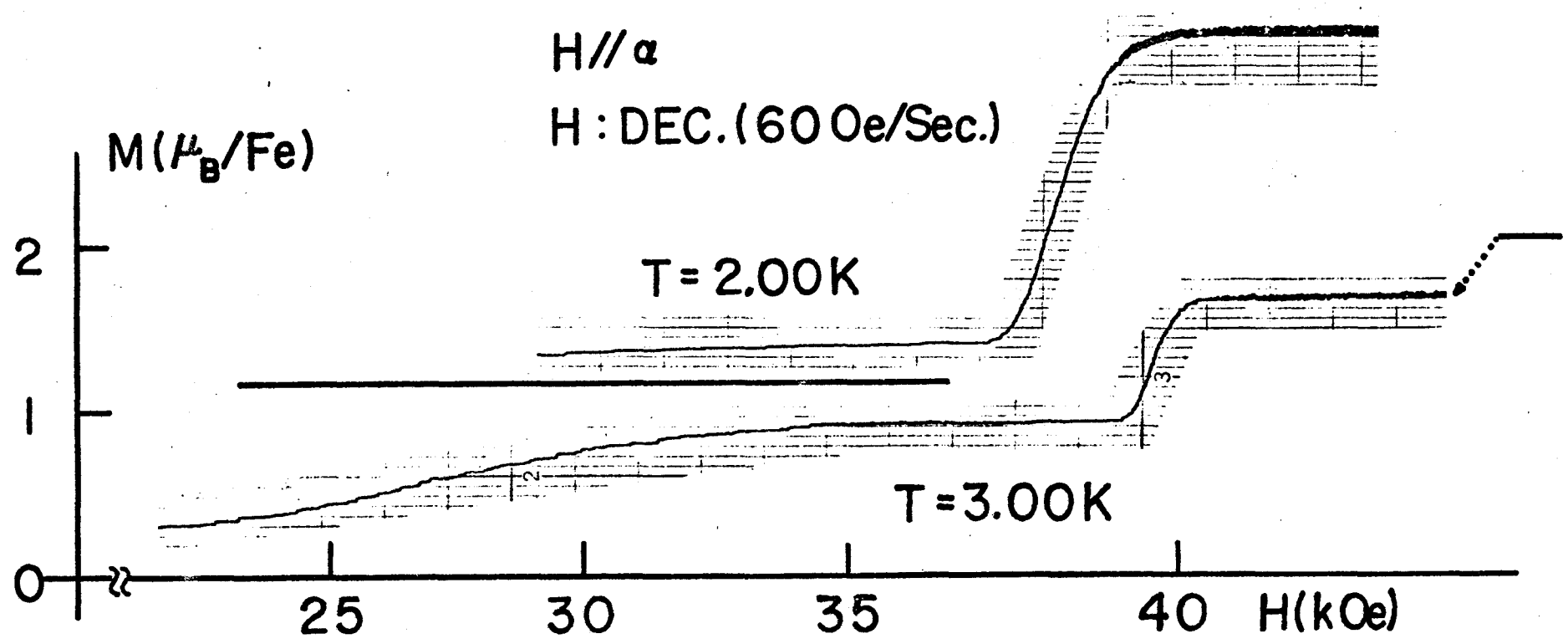

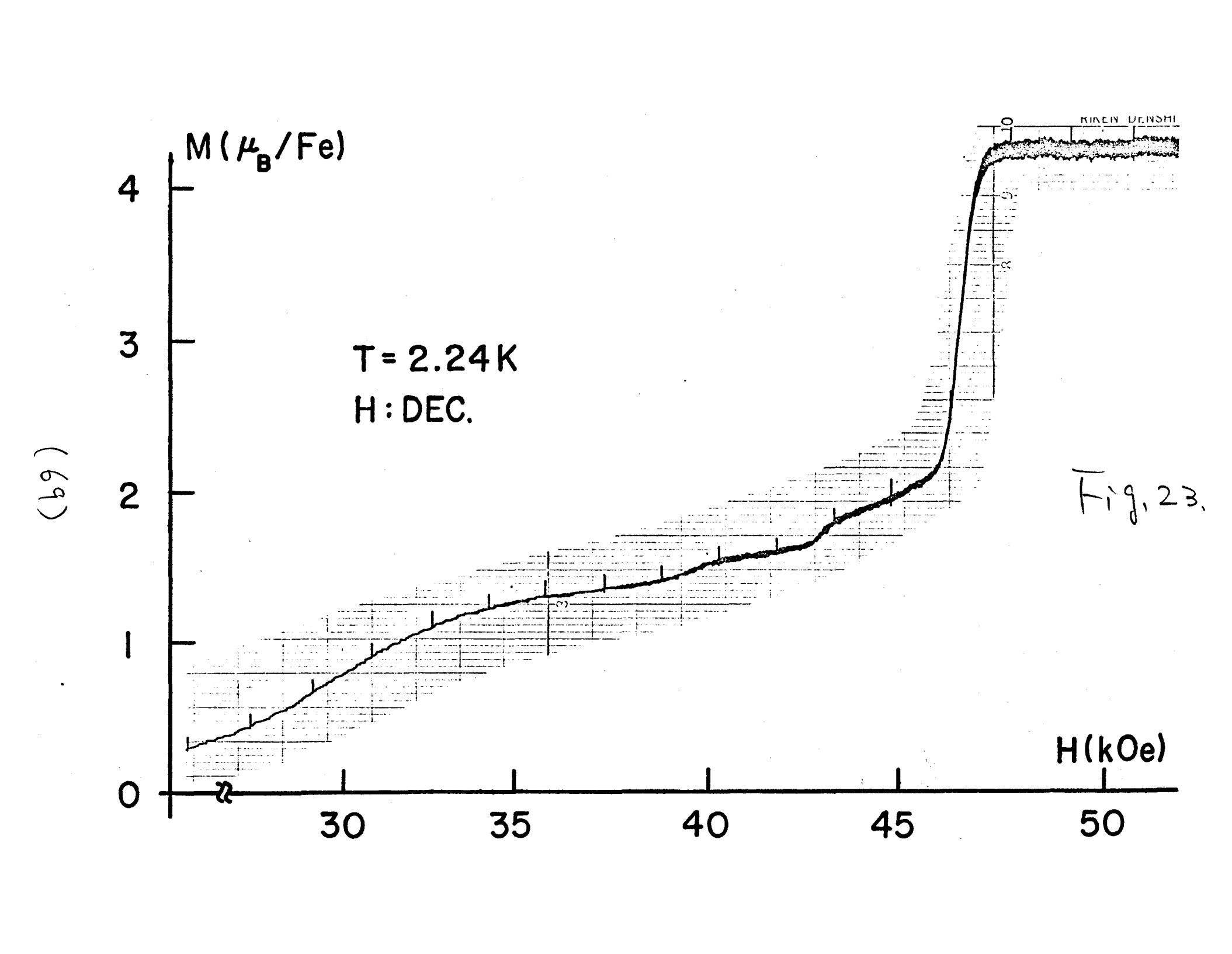

Fig. 23.

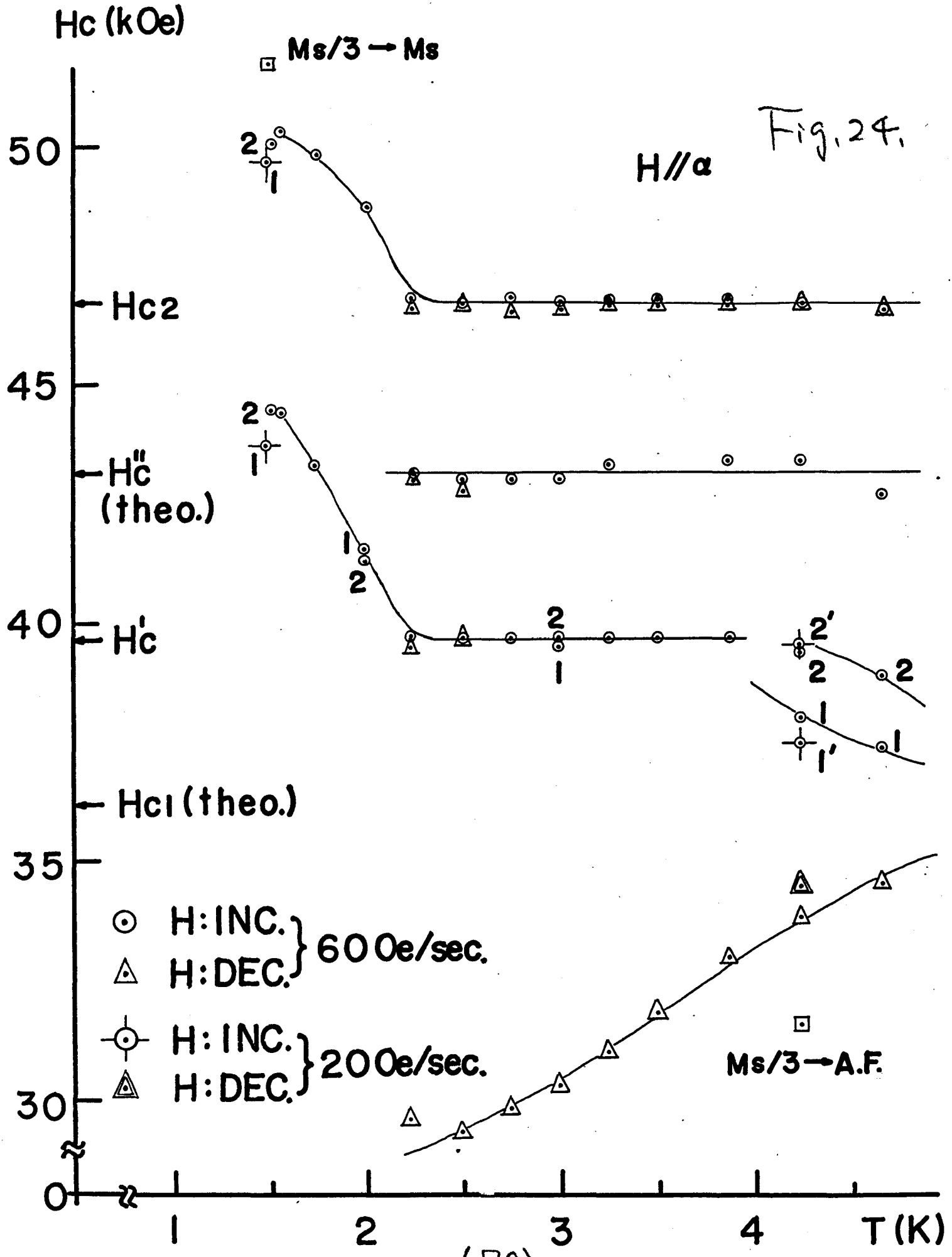
Hc (kOe)
Ms/3 → Ms
Fig. 24.
H//a
50
45
40
35
30
0
Hc2
Hc" (theo.)
Hc'
Hc1 (theo.)
H: INC.
H: DEC.
600e/sec.
H: INC.
H: DEC.
200e/sec.
Ms/3 → A.F.
1
2
3
4
T (K)

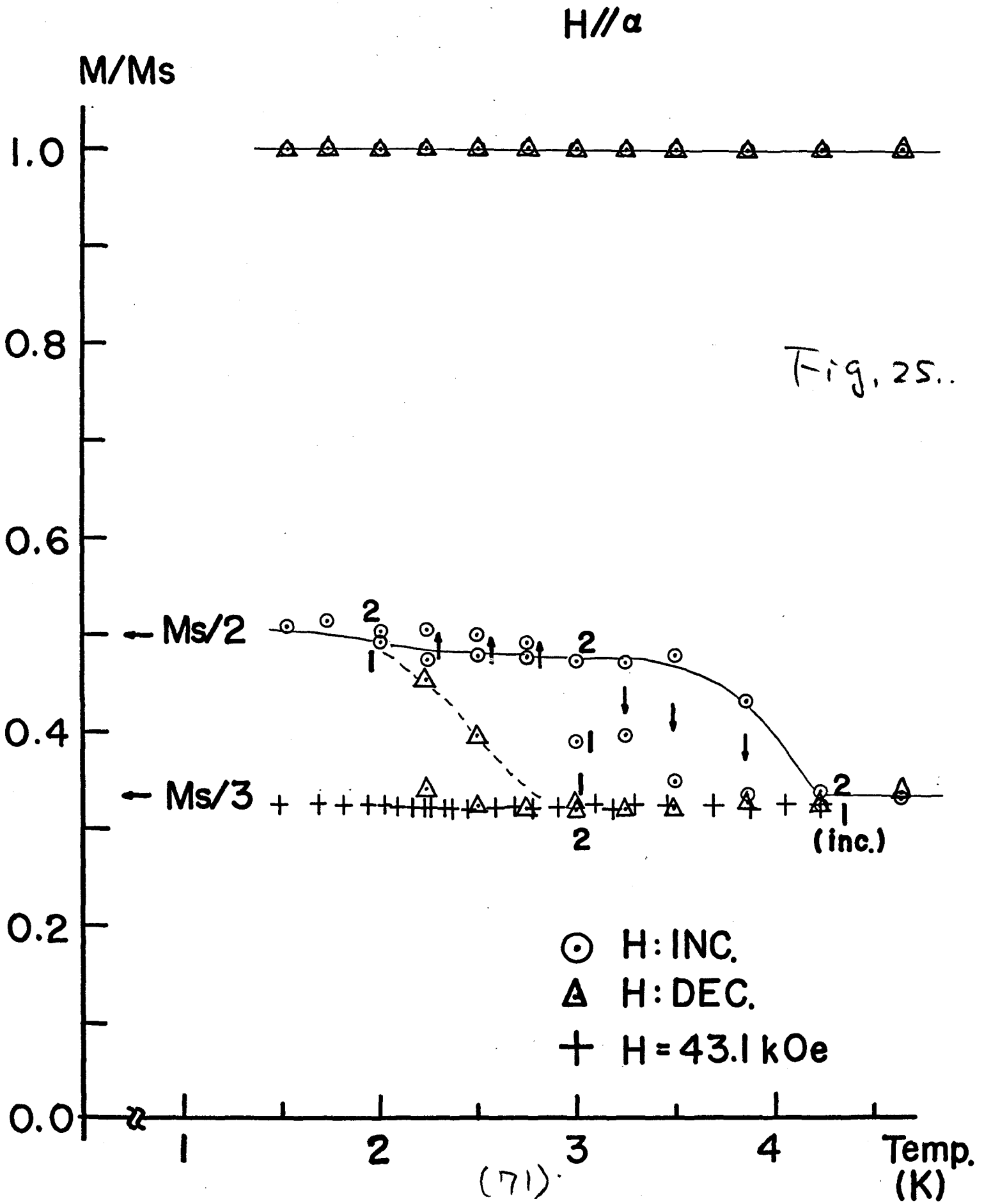
H//a
M/Ms
1.0
0.8
0.6
0.4
0.2
0.0
Ms/2
Ms/3
1
2
3
4
Temp.
(K)
(inc.)
⊙ H: INC.
Δ H: DEC.
+ H = 43.1 kOe

Fig, 25..

Fig. 26.

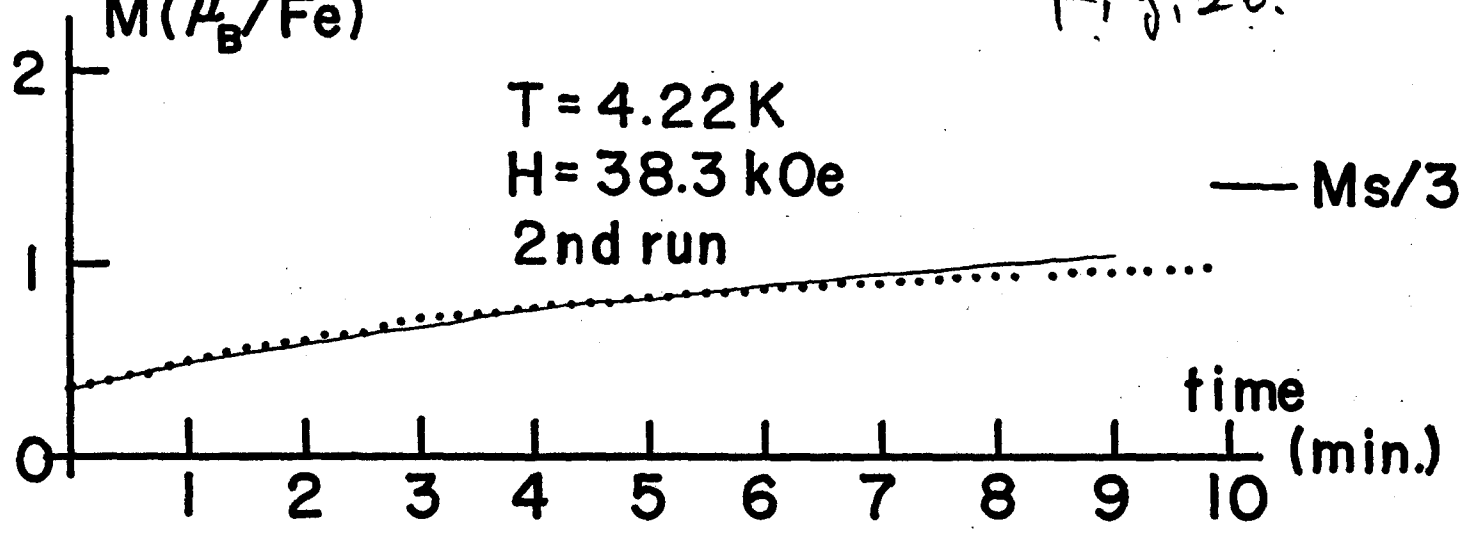
M(μB/Fe)
2
1
0
T = 4.22 K
H = 38.3 kOe
2nd run
Ms/3
time
(min.)
1 2 3 4 5 6 7 8 9 10

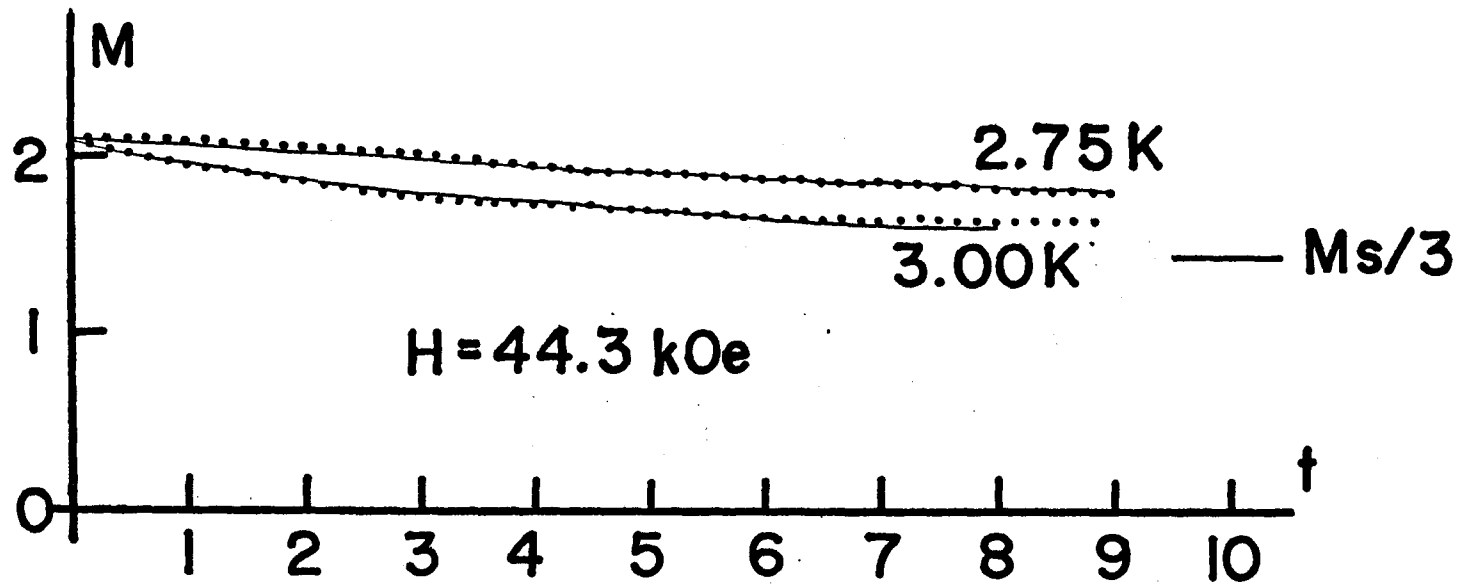
M
2
1
0
2.75 K
3.00 K
Ms/3
H = 44.3 kOe
t
1 2 3 4 5 6 7 8 9 10

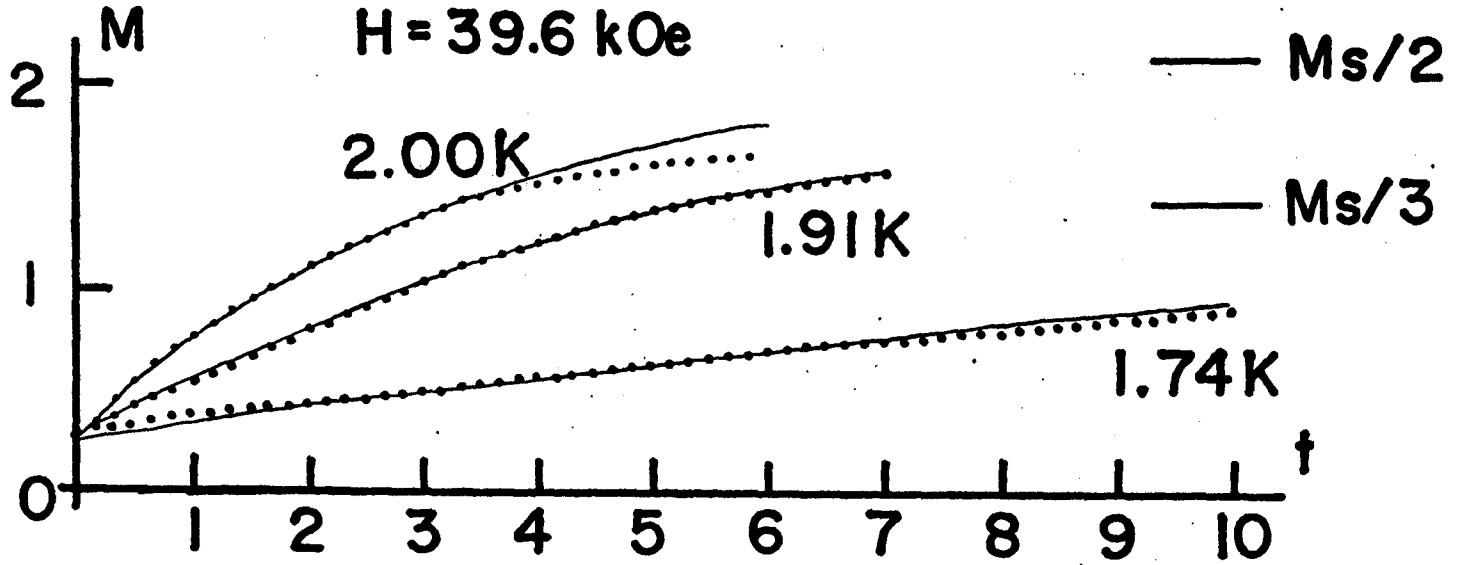
M
H = 39.6 kOe
Ms/2
Ms/3
2
1
0
2.00 K
1.91 K
1.74 K
t
1 2 3 4 5 6 7 8 9 10

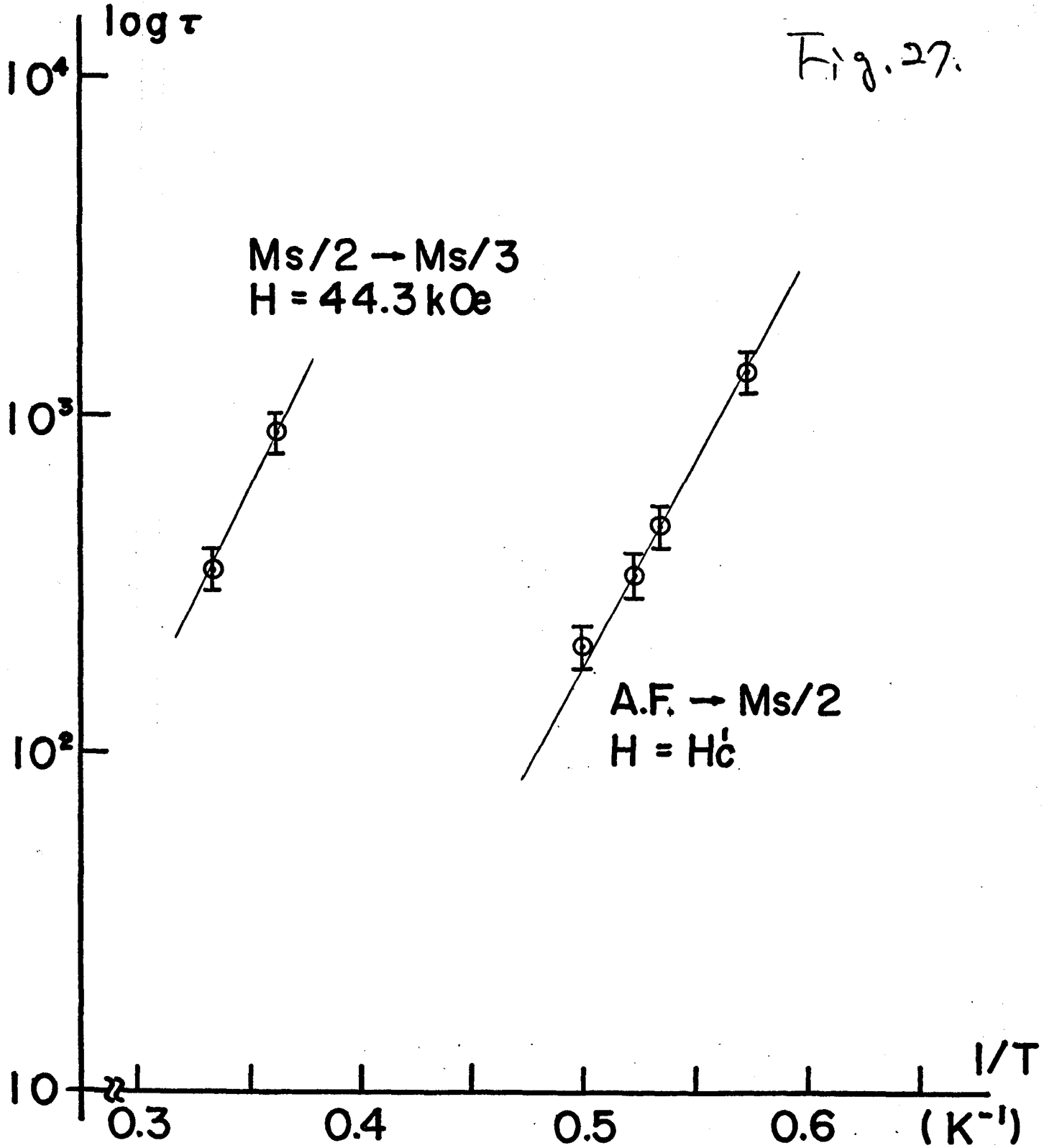

Fig. 27.

Fig. 28.

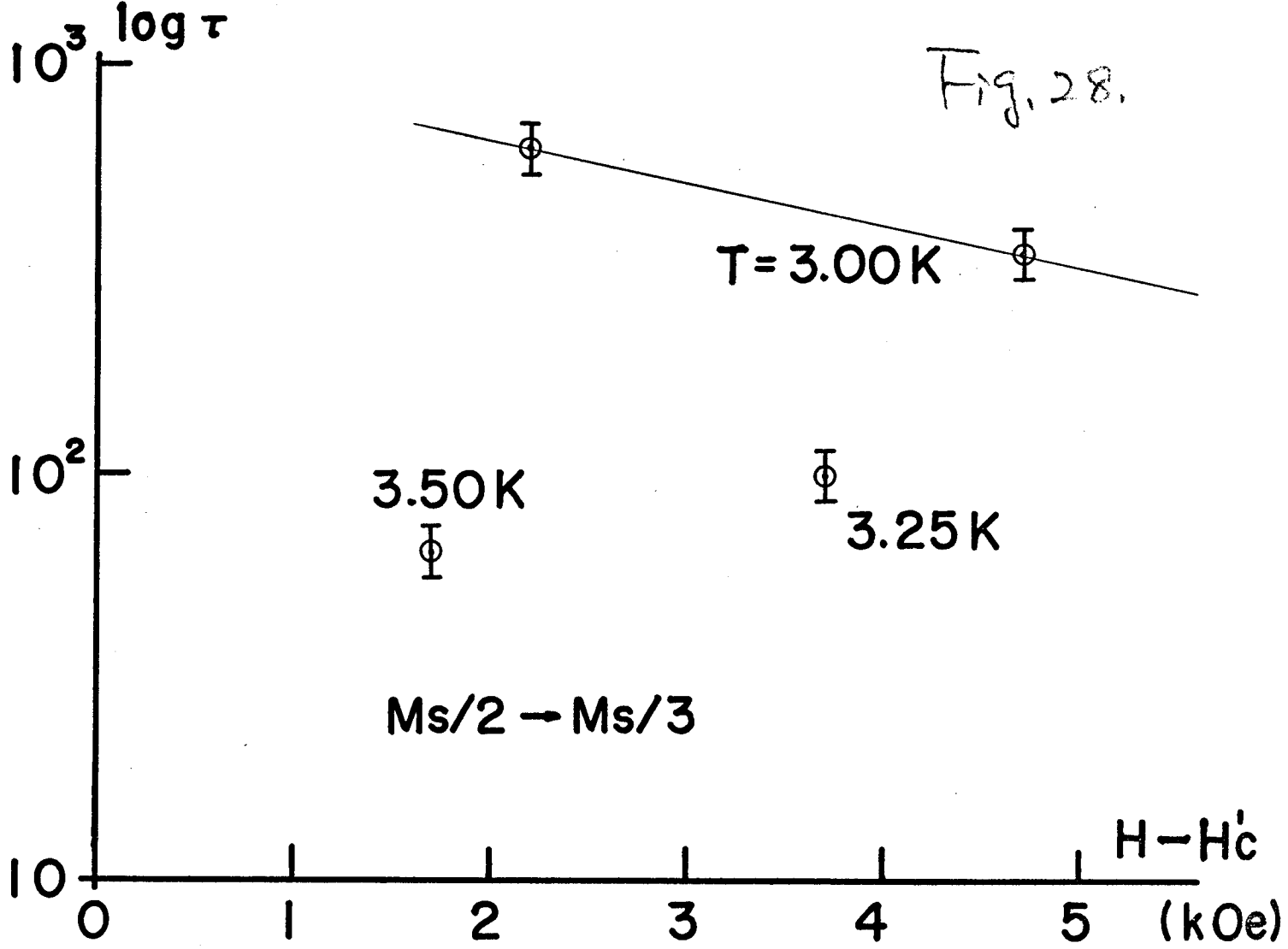
log τ
10³
10²
10
T = 3.00 K
3.50 K
3.25 K
Ms/2 → Ms/3
H − Hc'
0
1
2
3
4
5
(kOe)

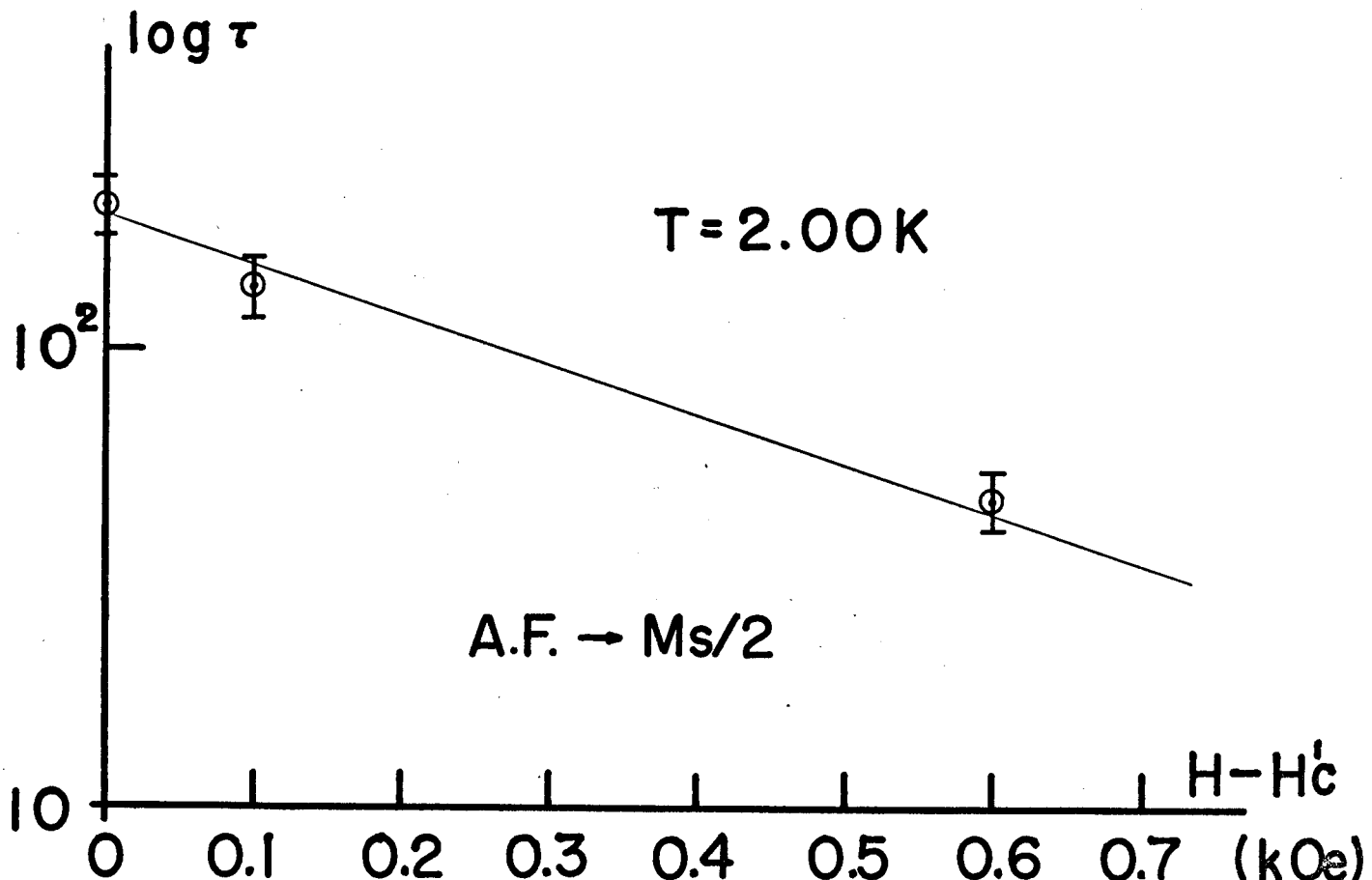
log τ
T = 2.00 K
10²
10
A.F. → Ms/2
H − Hc'
0
0.1
0.2
0.3
0.4
0.5
0.6
0.7
(kOe)

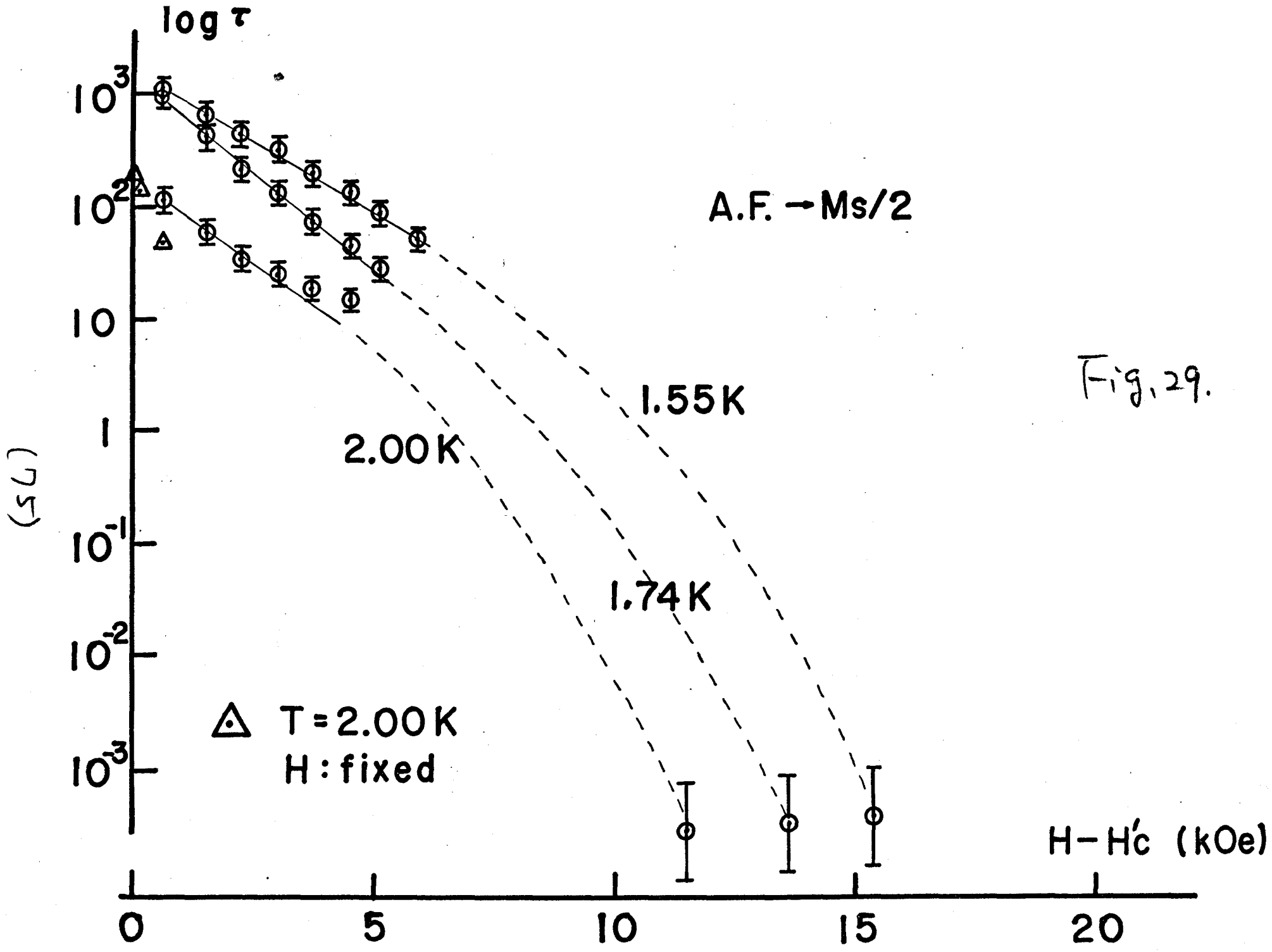
log τ
10^3
10^2
10
1
10^-1
10^-2
10^-3
(sec)
A.F. → Ms/2
1.55K
2.00K
1.74K
T = 2.00K
H : fixed
H − Hc (kOe)
0
5
10
15
20

Fig. 29.

(94)

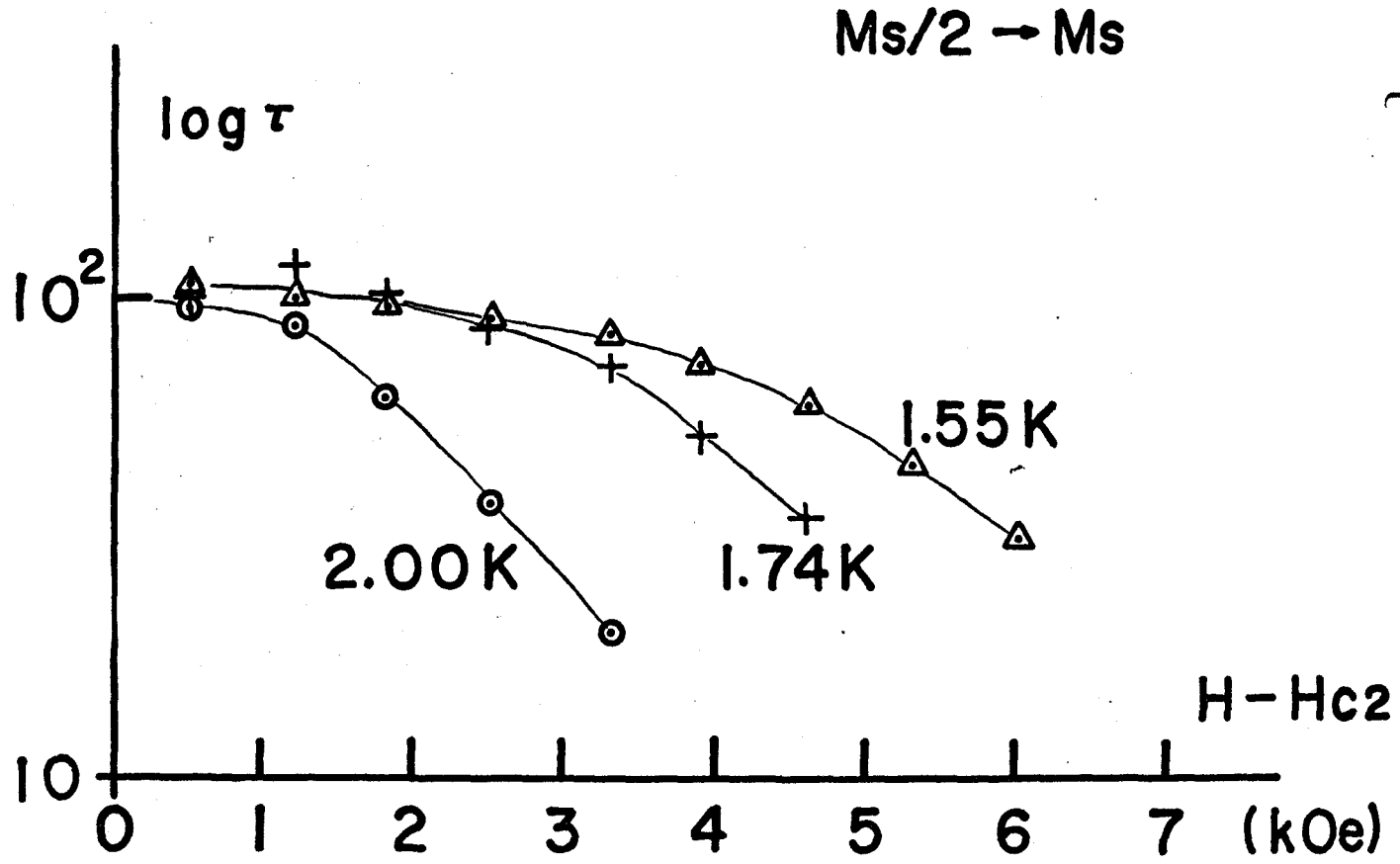

Fig. 30.

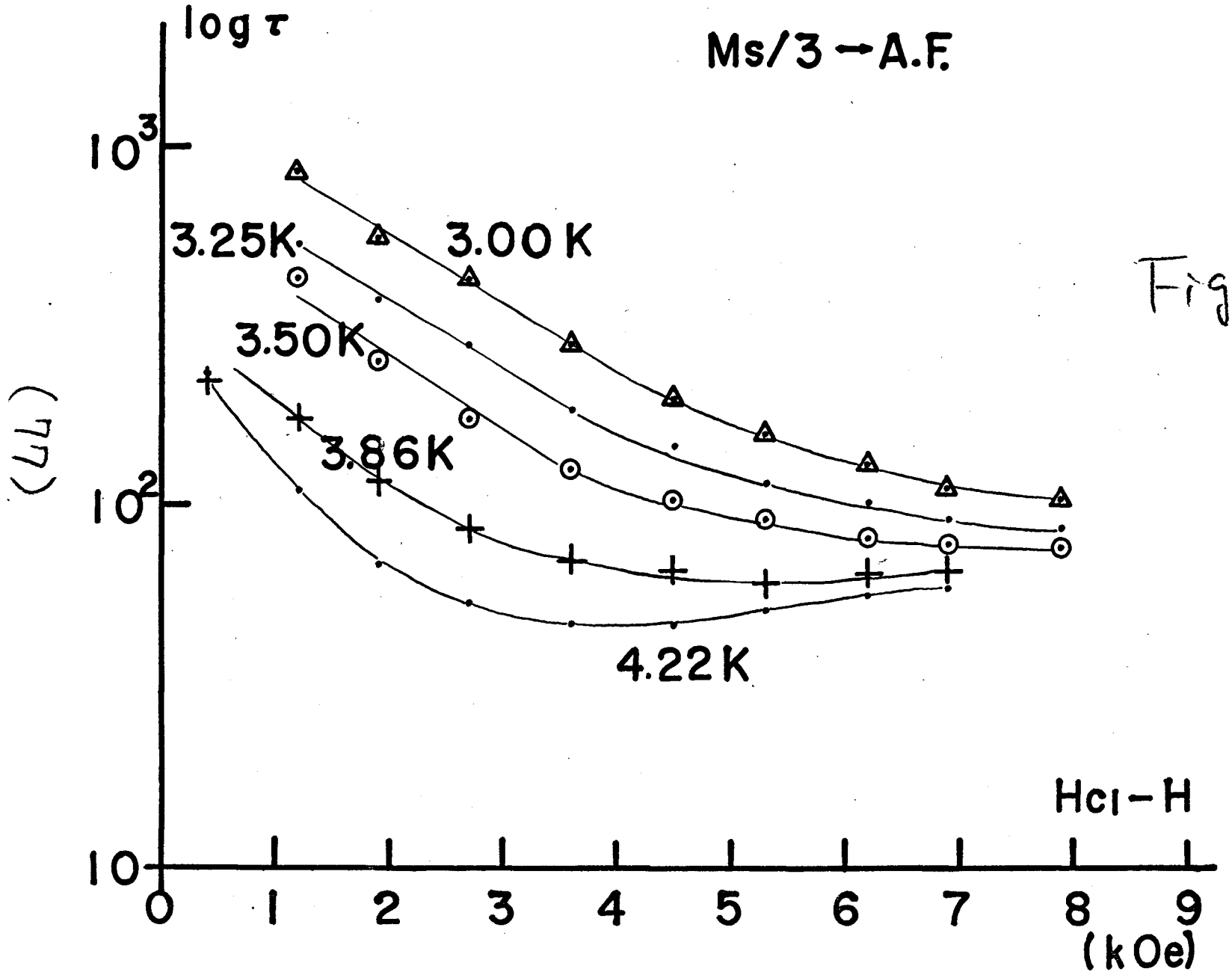
log τ
Ms/3 → A.F.
10^3
10^2
10
(μs)
3.25K
3.00K
3.50K
3.86K
4.22K
Hc1 - H
0
1
2
3
4
5
6
7
8
9
(kOe)

Fig. 31.

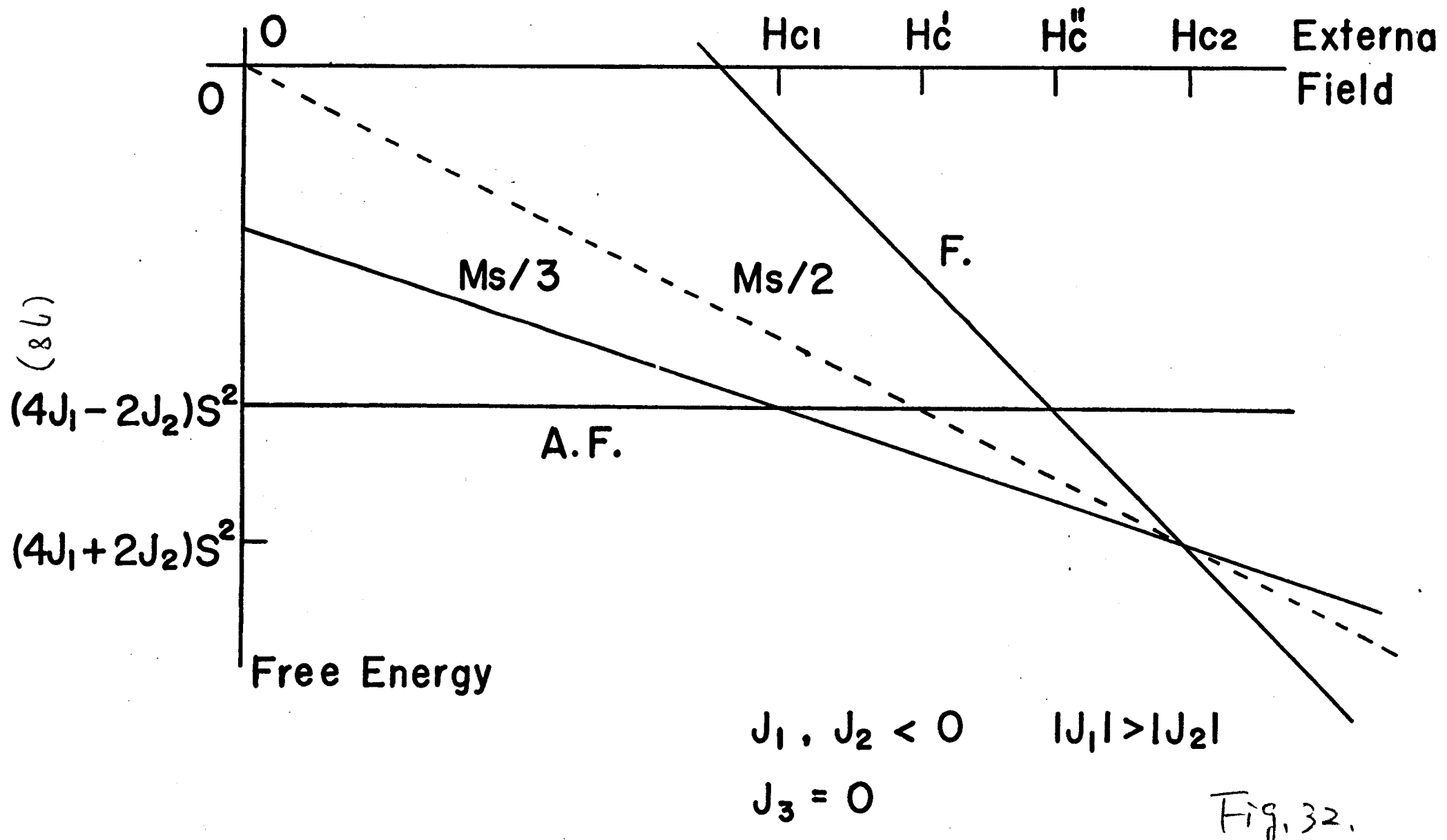
O
Hc1
Hc'
Hc''
Hc2
External Field
O
Ms/3
Ms/2
F.
(8L)
$(4J_1 - 2J_2)S^2$
A.F.
$(4J_1 + 2J_2)S^2$
Free Energy
$J_1, J_2 < 0$
$|J_1| > |J_2|$
$J_3 = 0$

Fig. 32.

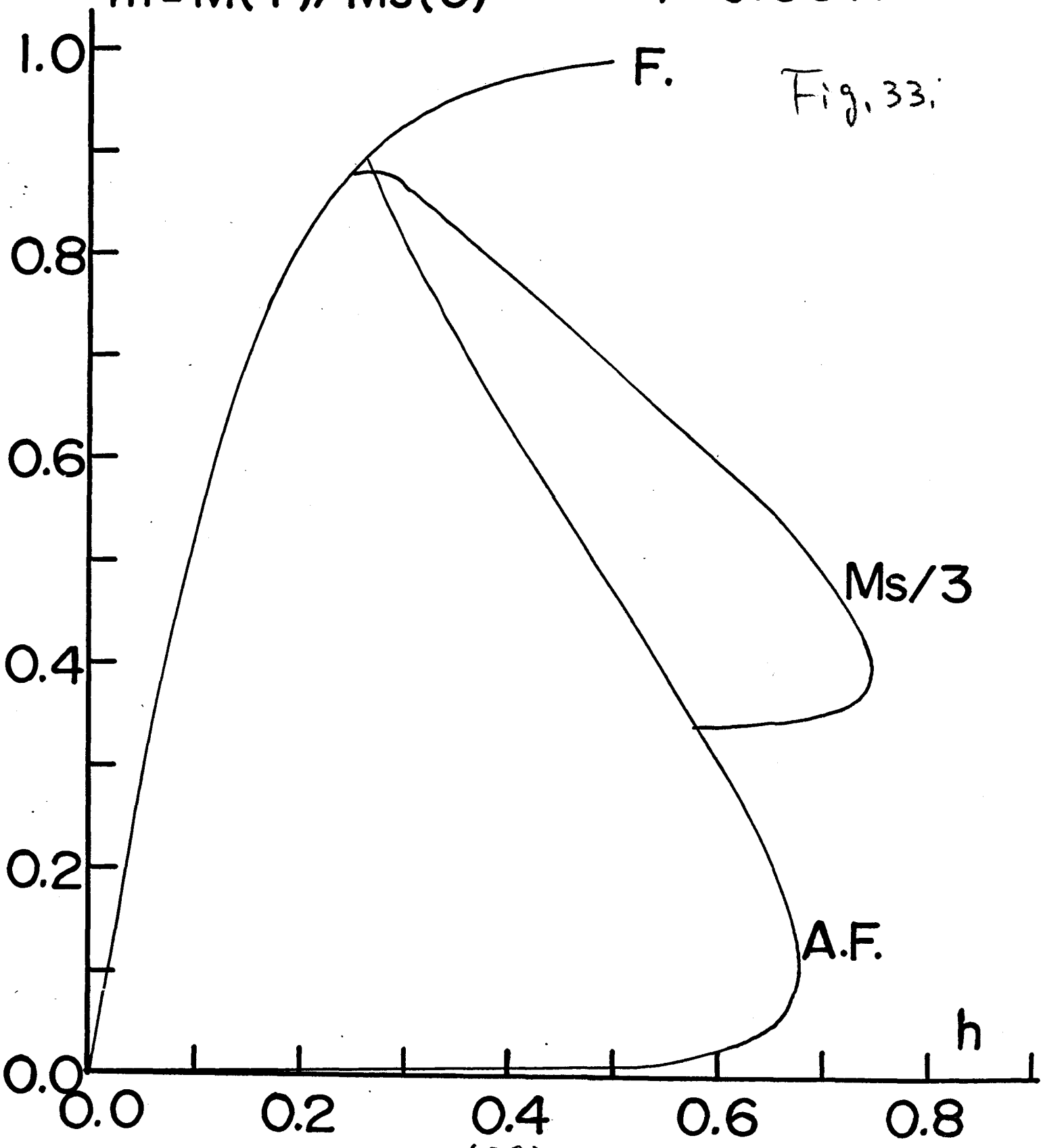

Fig. 33.

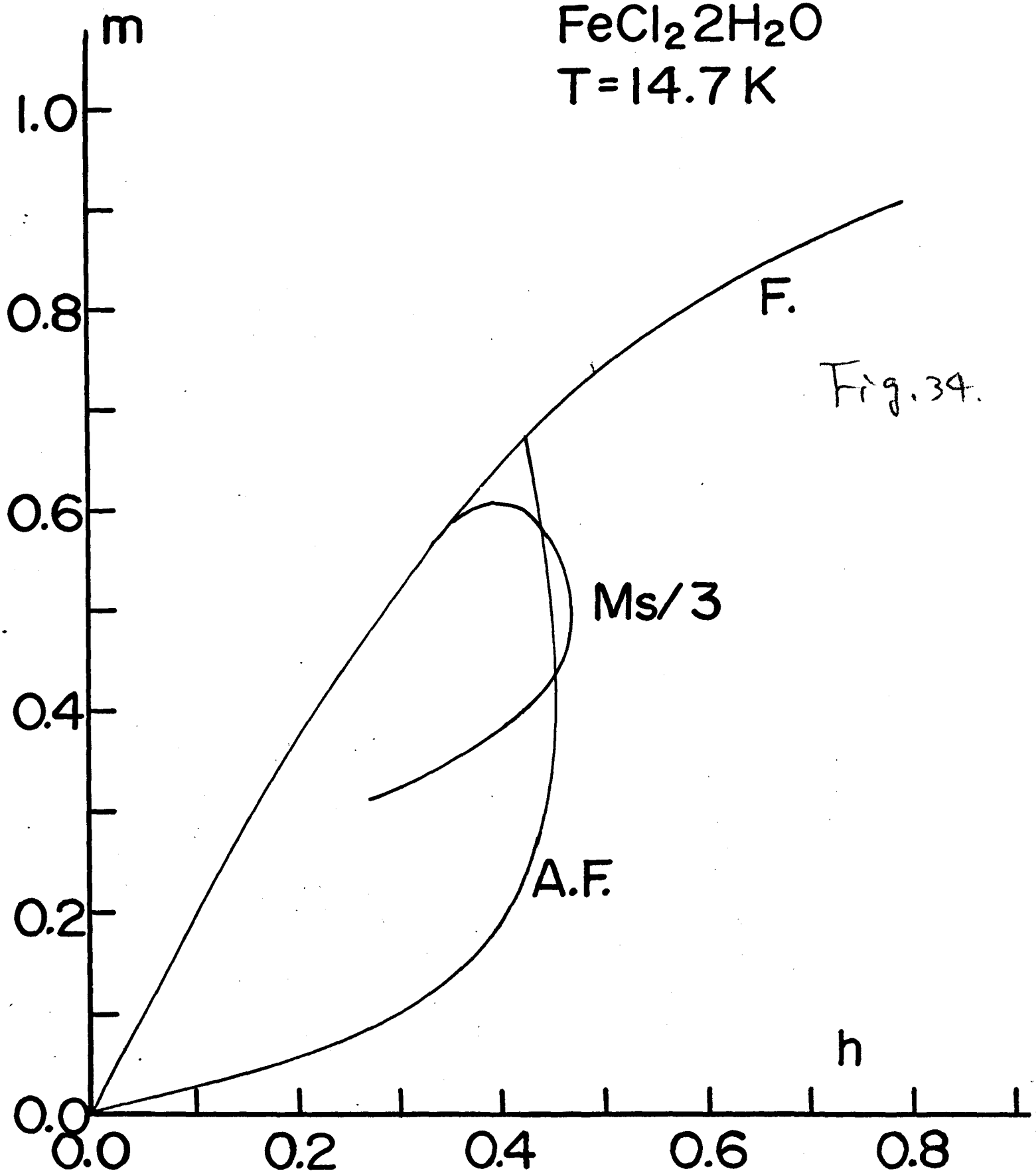

Fig. 34.

Fig. 35.

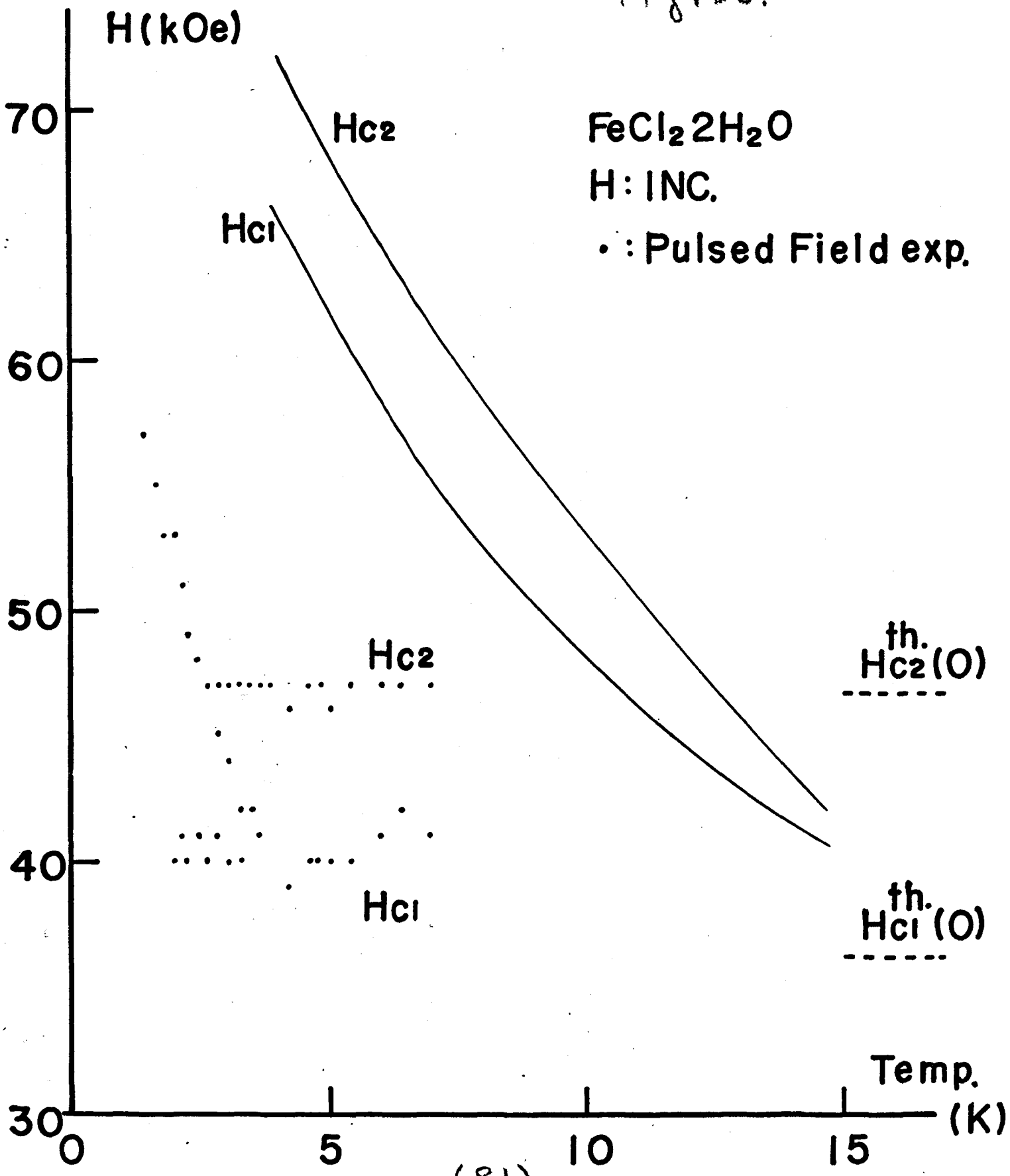
H(kOe)
70
60
50
40
30
0
5
10
15
Temp.
(K)
Hc2
Hc1
FeCl2 2H2O
H: INC.
• : Pulsed Field exp.
Hc2
Hc1
th.
Hc2(0)
th.
Hc1(0)

Fig. 36.

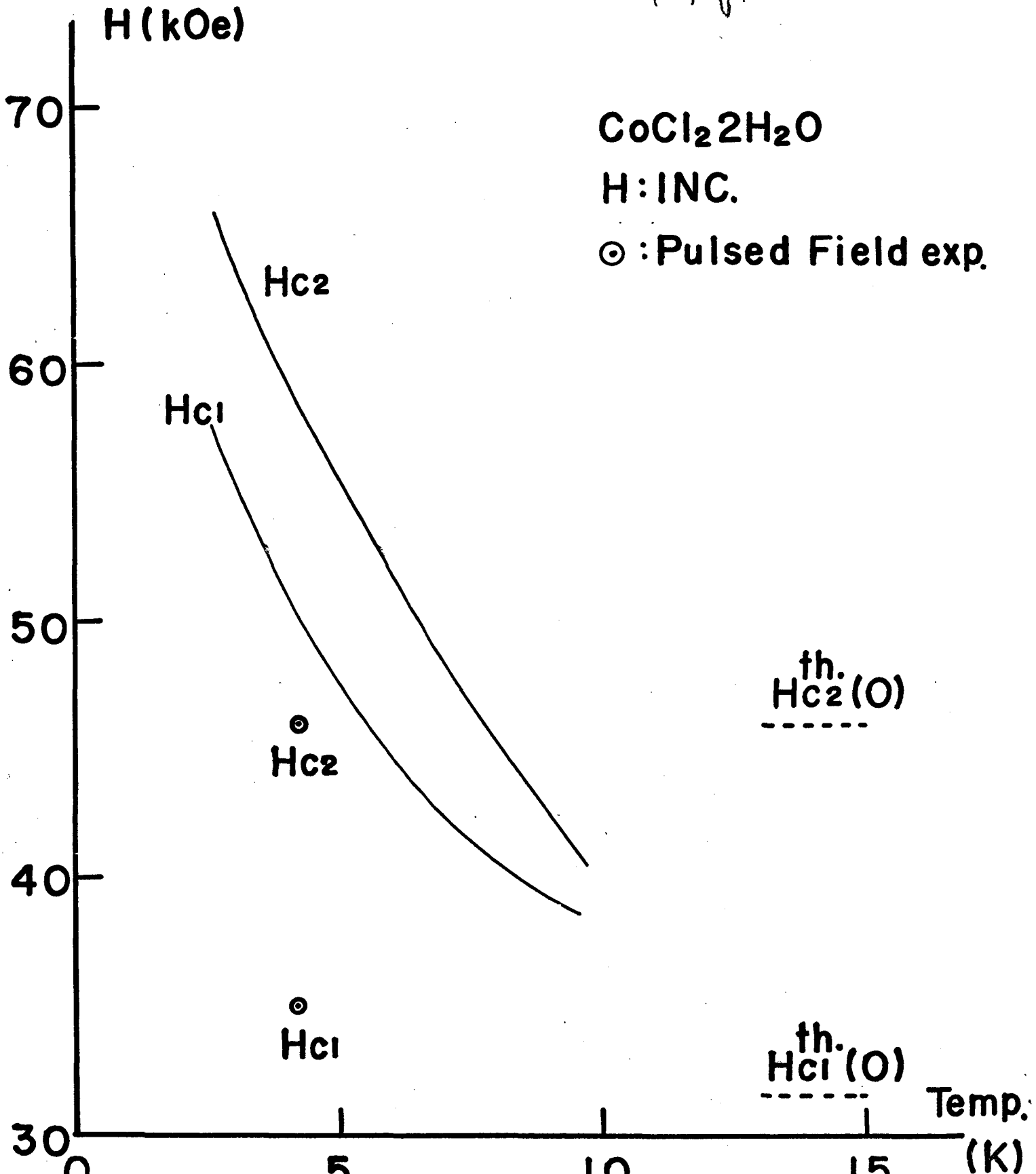
H(kOe)
70
60
50
40
30
0
5
10
15
Temp.
(K)
$CoCl_2 2H_2O$
H: INC.
⊙: Pulsed Field exp.
Hc2
Hc1
⊙ Hc2
⊙ Hc1
$H_{c2}^{th.}(0)$
$H_{c1}^{th.}(0)$

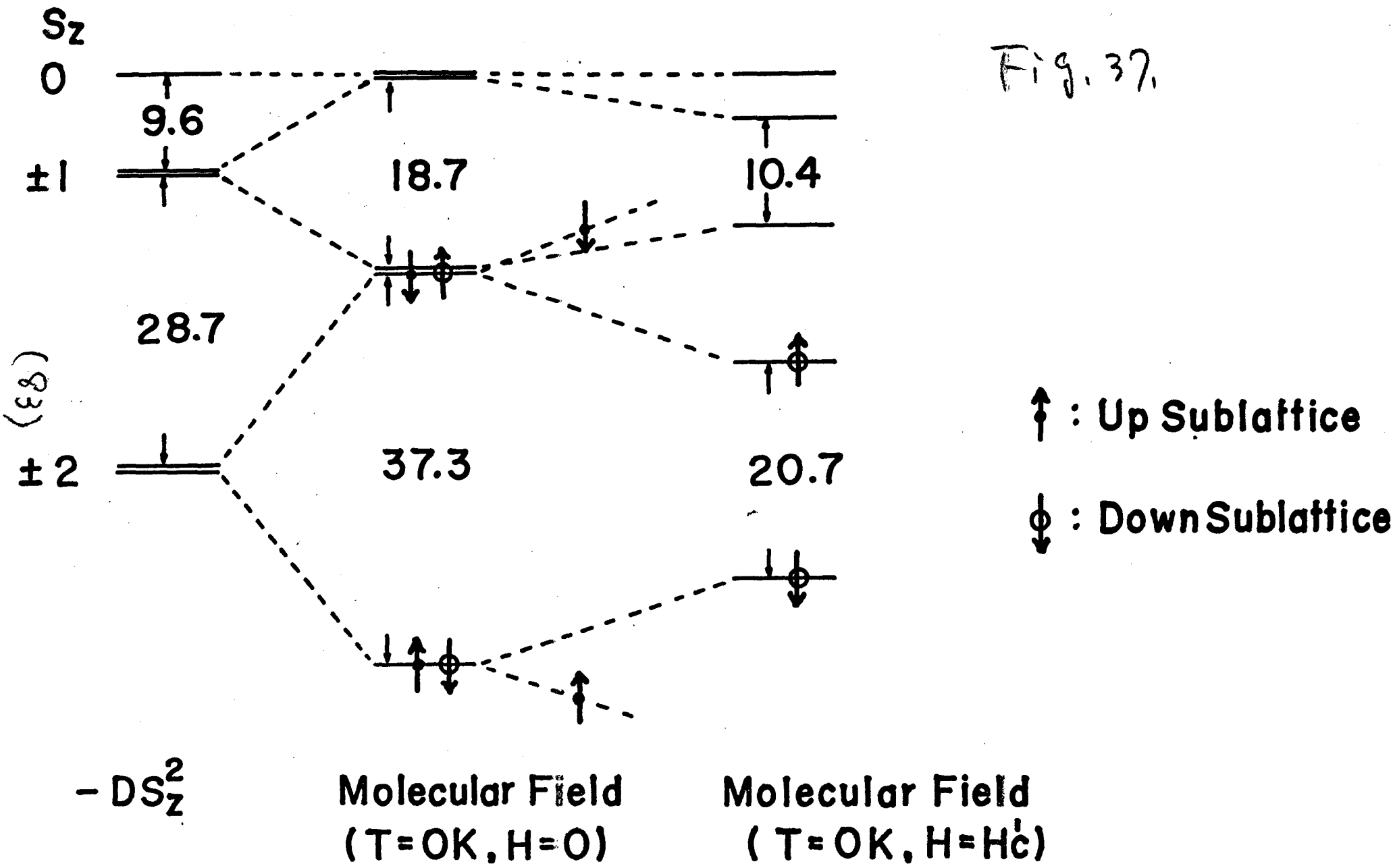
Sz
0
9.6
±1
18.7
10.4
28.7
(cm⁻¹)
±2
37.3
20.7
: Up Sublattice
: Down Sublattice
$-DS_z^2$
Molecular Field
(T=OK, H=0)
Molecular Field
(T=OK, H=Hc)

Fig. 37.

Fig. 38.

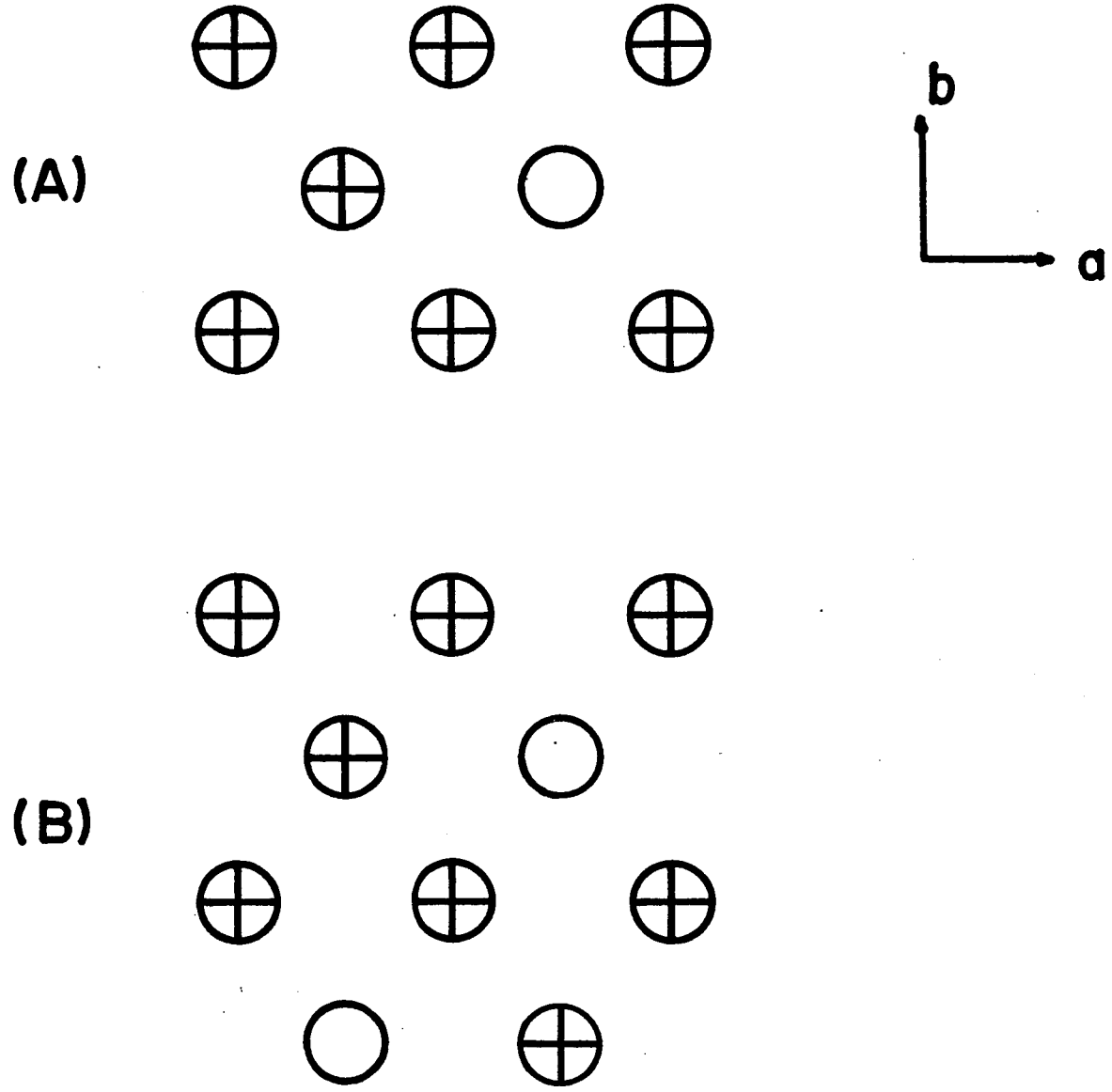

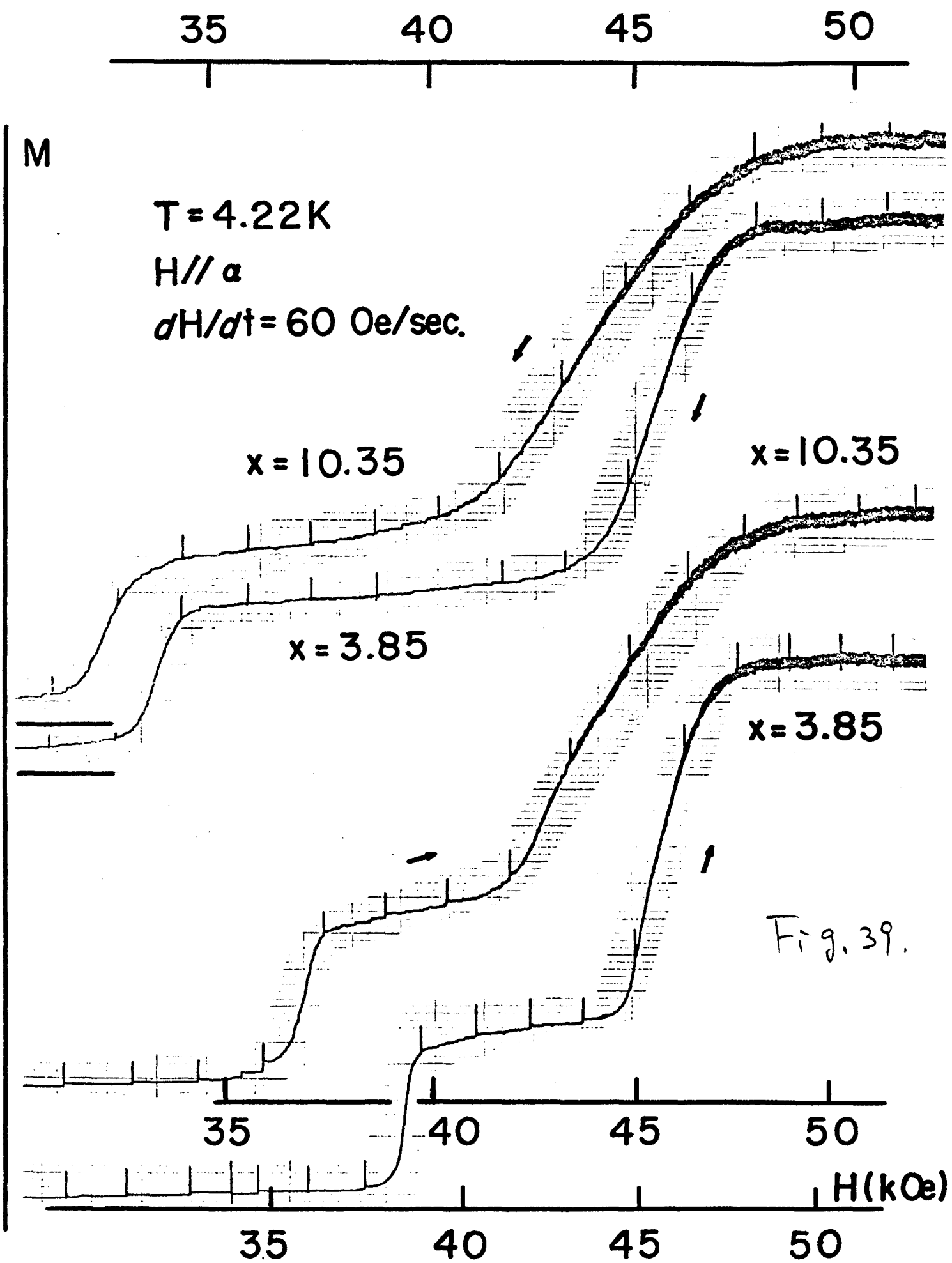
35
40
45
50
M
T = 4.22K
H // a
dH/dt = 60 Oe/sec.
x = 10.35
x = 3.85
x = 10.35
x = 3.85
35
40
45
50
H(kOe)
35
40
45
50

Fig. 39.

Fig. 40.

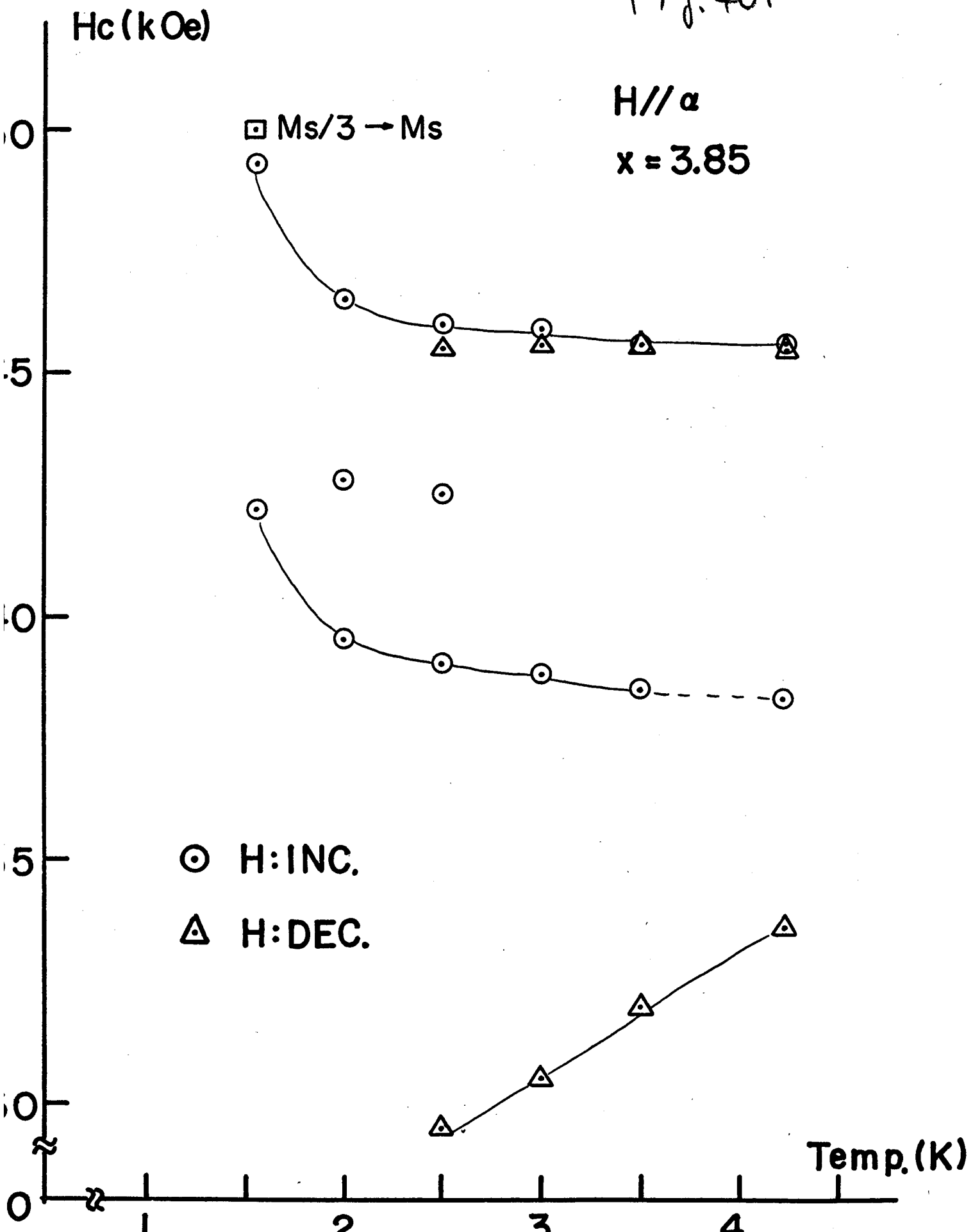

Fig. 41.

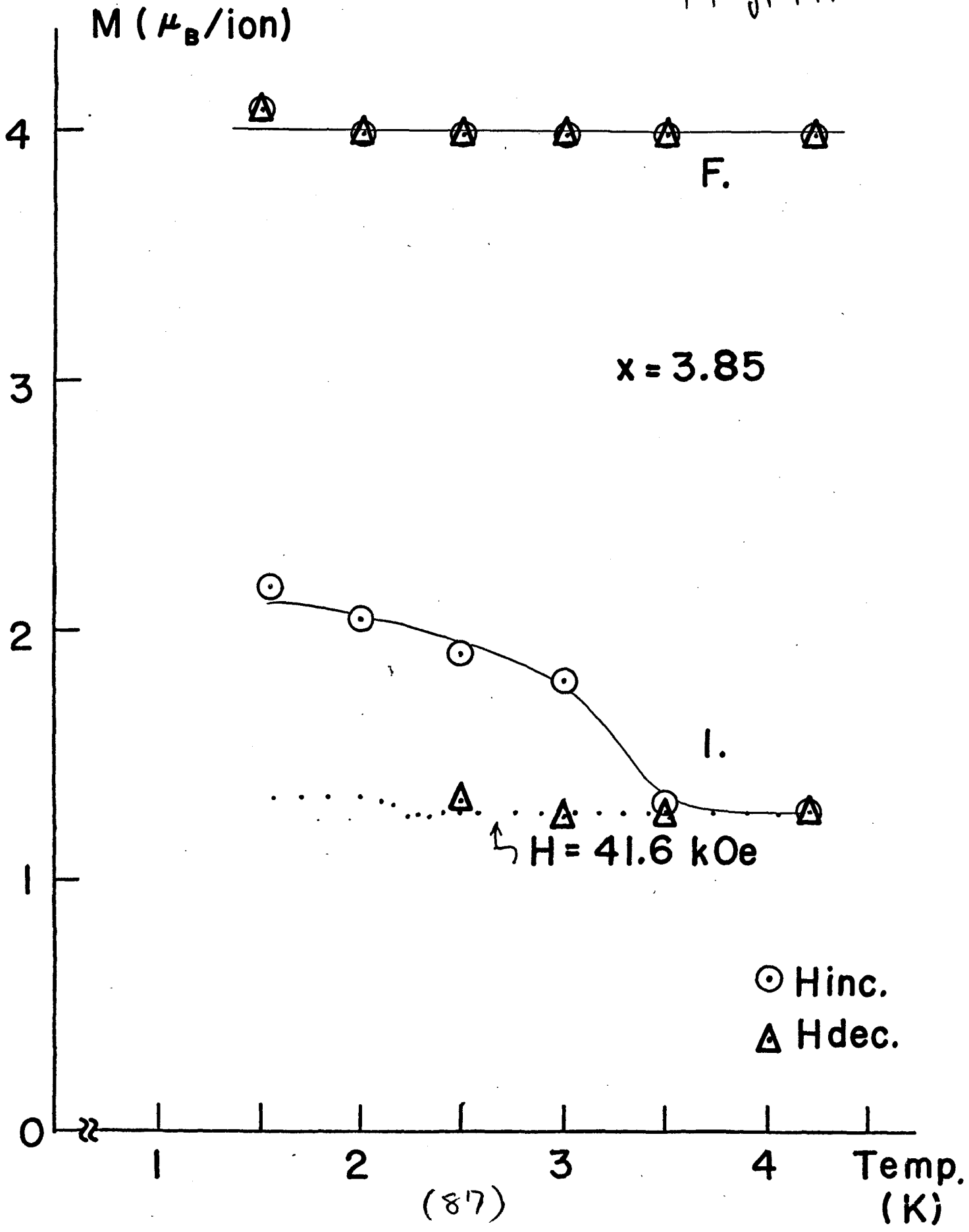

Fig. 42.

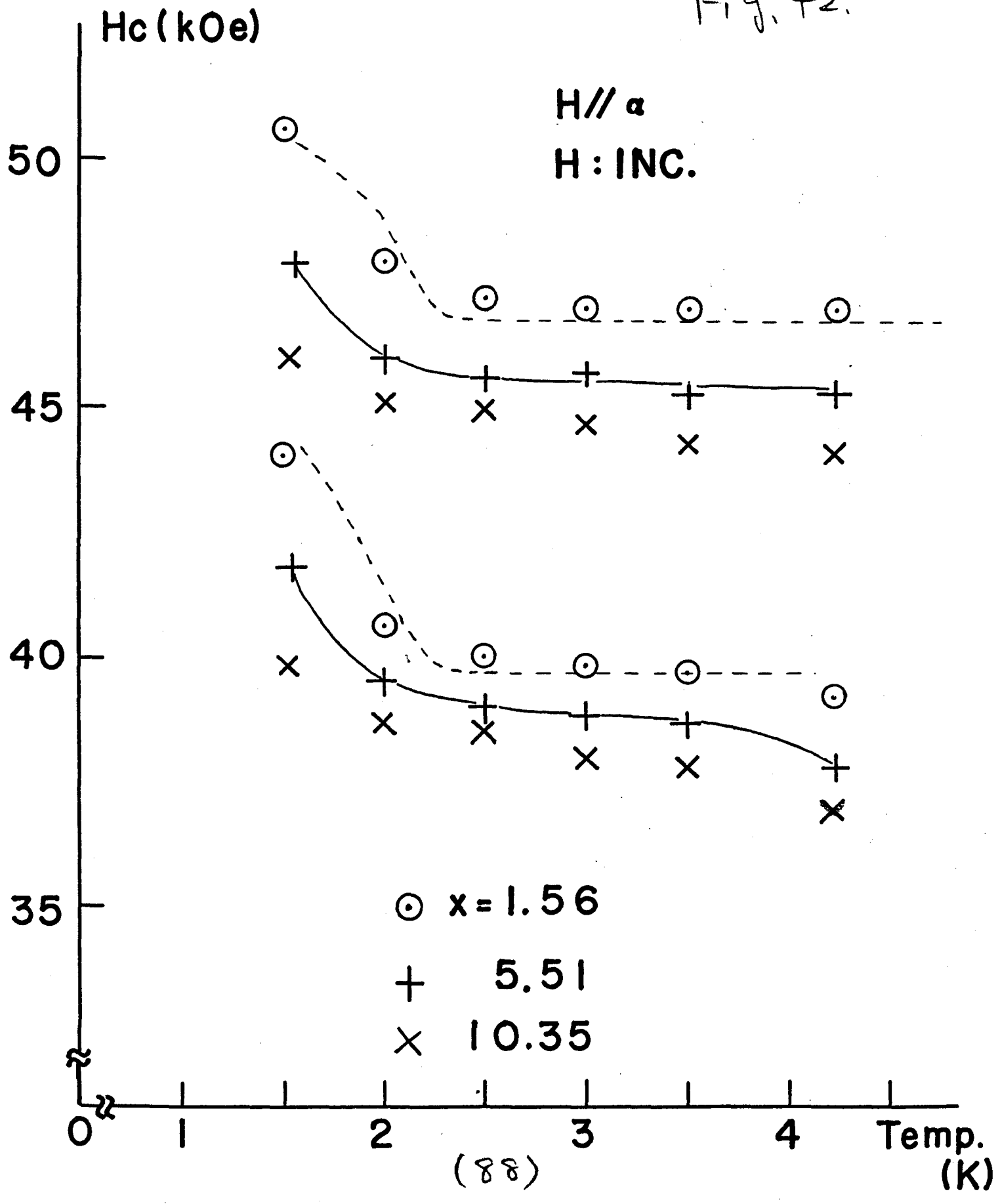

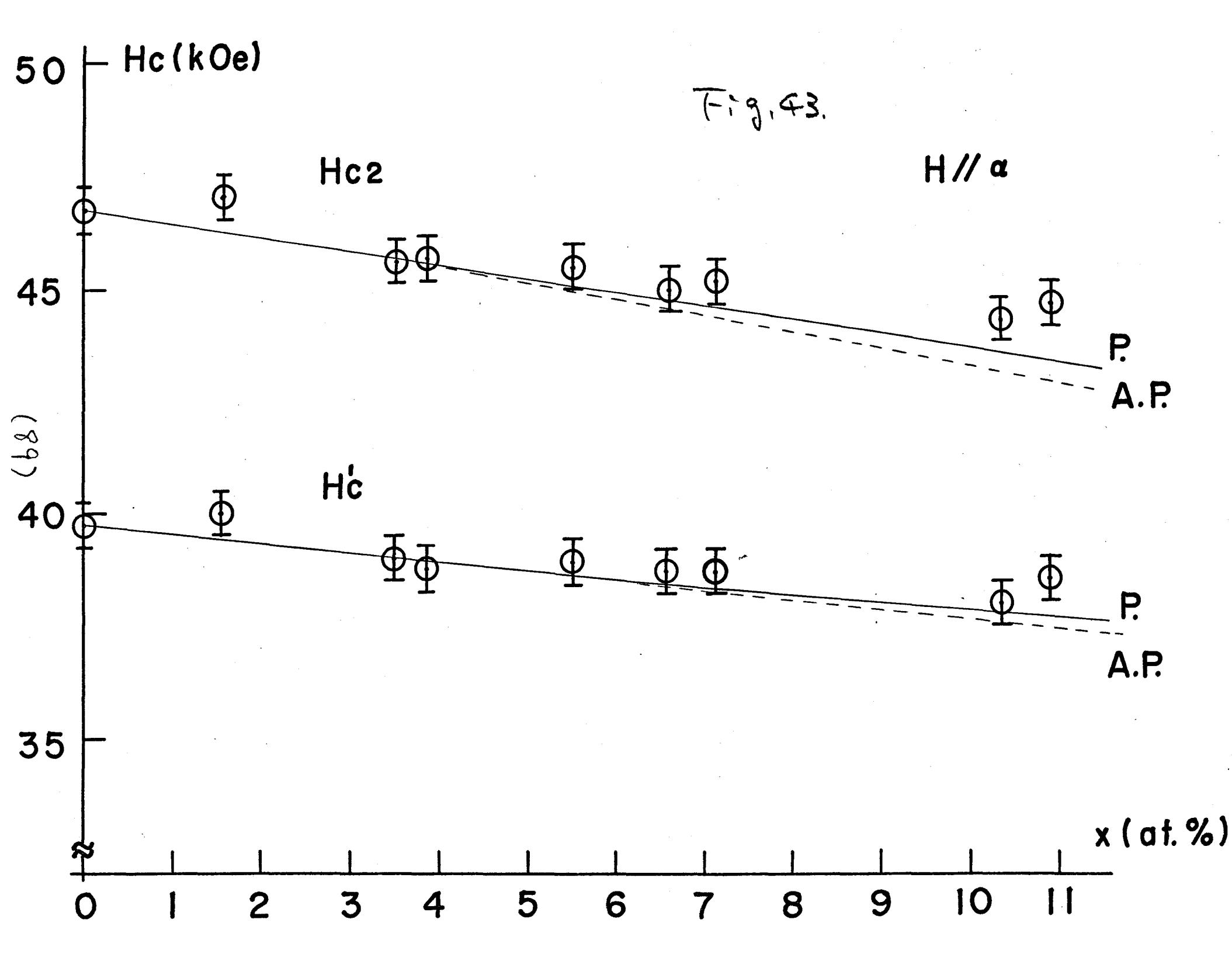

Fig. 43.

Fig. 44.

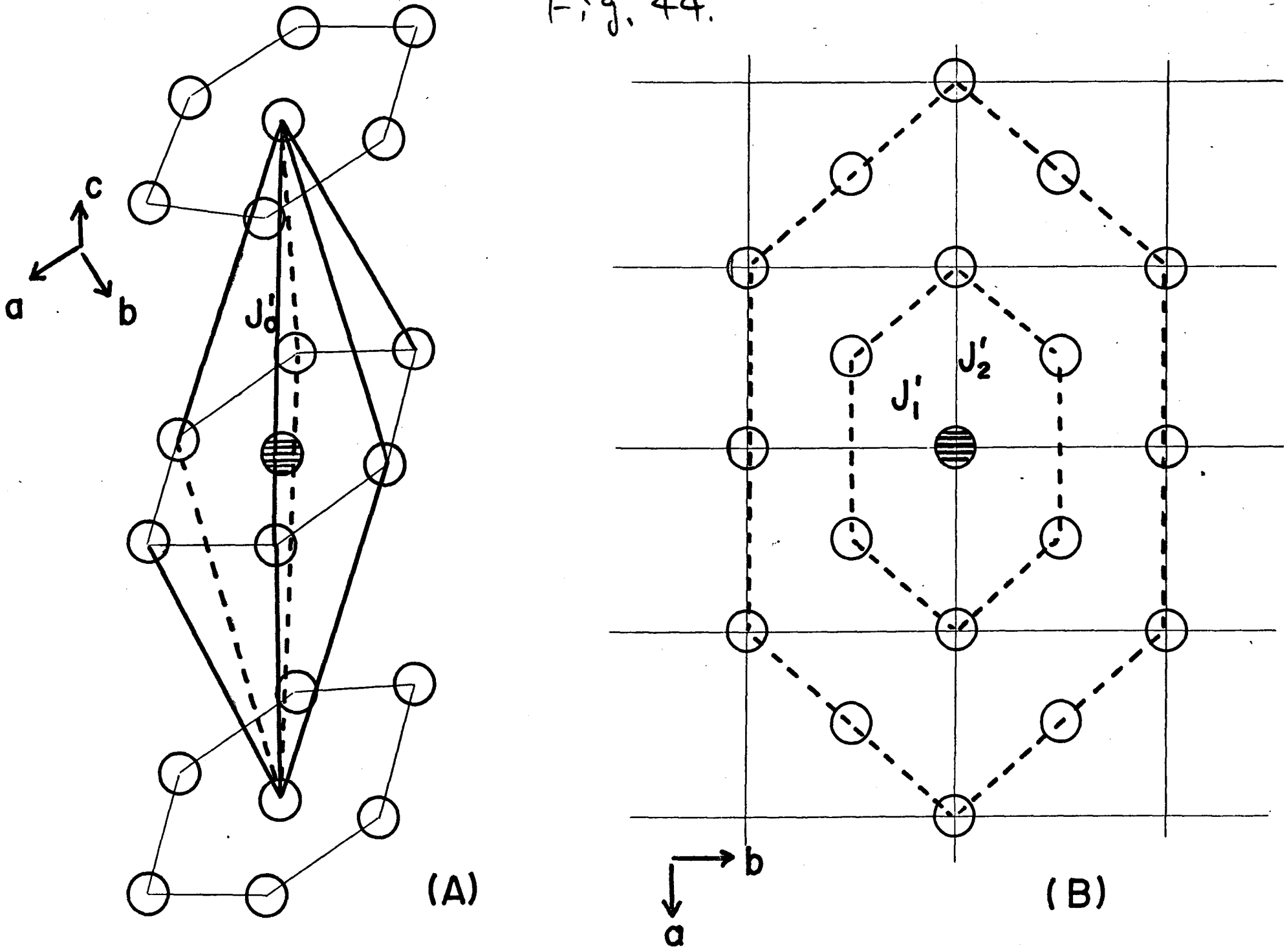

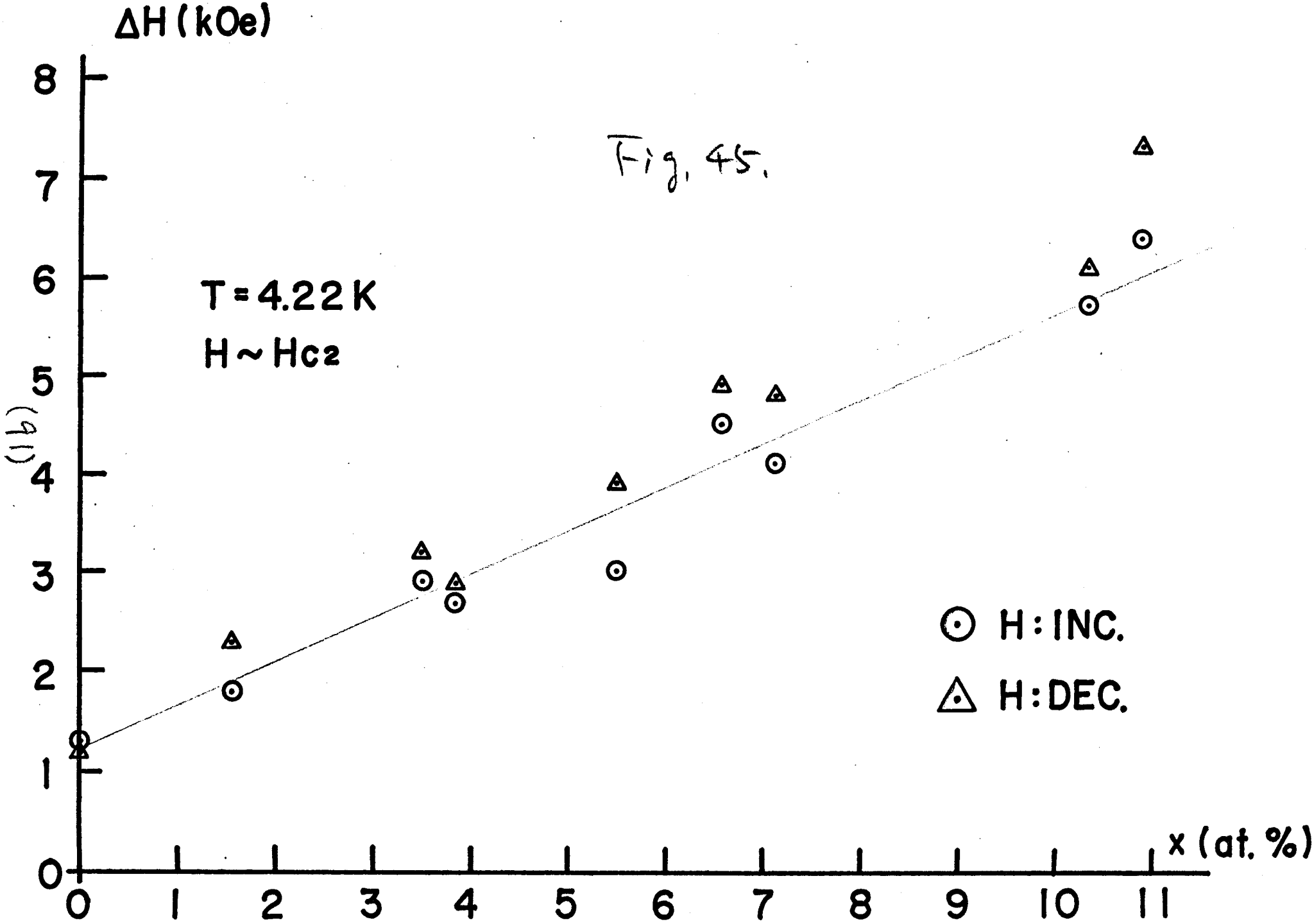

Fig. 45.

(91)